Geochemistry and Au Mineralization within the Kakagi-Rowan Lakes Greenstone Belt: A Study of the Angel Hill Gold Zone.

Scott Robert Secord

A thesis submitted to the Faculty of Graduate Studies in partial fulfillment of the requirements for the degree of Master of Science

Department of Geology

Lakehead University
Thunder Bay, Ontario
May 2011

Abstract

The Angel Hill Gold Zone of the West Cedartree Gold Project has been exposed over 300 meters along the internal contact of ultramafic and gabbroic rocks within the Kakagi Sill. The sill lies within the Kakagi-Rowan Lakes greenstone belt and has intruded the mafic metavolcanic rocks of the Snake Bay Formation and the felsic to intermediate metavolcanic rocks of the Emm Bay Formation. The Snake Bay Formation consists of pillowed and massive basalts and fine-grained tuffs. The Emm Bay Formation stratigraphically overlies the Snake Bay Formation and consists of tuffs and tuff breccias. Trace element geochemistry and primitive mantle normalised plots suggest that both the rocks of the Kakagi Sill and the Snake Bay Formation are comprised of metasomatsed island arc tholeiite basalts whereas the rocks of the Emm Bay Formation are characterised of a back island arc affinity.

The Angel Hill Gold Zone occurs as extensive carbonate and quartz flooding within a zone of brittle deformation termed the master fault. A distinguishing feature of the gold zone is the presence of extensive fuchsite alteration forming large mats up to 20 meters wide. Mineralization in the Angel Hill Gold Zone consists of free gold and sylvanite occurring as inclusions within and rimming pyrite grains, as well as precipitated along small fractures in quartz. Associated mineralization includes pyrite as well as galena and sphalerite. Textural relationships and stable isotope analyses of carbonate ($\delta^{18}O$ 13.6 to 17.9 ‰), quartz ($\delta^{18}O$ 8.8 to 13.1 ‰), pyrite ($\delta^{34}S$ -0.8 to 1.0 ‰), sphalerite ($\delta^{34}S$ 1.3 to 5.4 ‰), and galena ($\delta^{34}S$ 5.9 to 7.3 ‰) suggest multiple episodes of brittle deformation and fluid influx within a protracted lode gold system. The combination alteration assemblages and stable isotope characteristics suggest that the Angel Hill Gold Zone formed as a result of listwanite metasomatism with input of fluids from both magmatic and metamorphic sources. These fluids propagated as a result of the brittle faulting that occurred due to a competency contrast between the ultramafic footwall and the gabbro hangingwall during regional deformation.

Acknowledgements

Those who know me, even a little bit, know that I take a lot of time and even more patience. This project was one of the hardest things I have ever had to do, from fending off the invading hordes of ticks to trying to comprehend oxygen isotope fractionation; I could never have attempted (let alone completed) it without the help of numerous people. While there are far too many people to mention each of them by name there a few key individuals I would like to personally thank for assistance above and beyond the call of duty.

First and foremost I need to thank Dr. Peter Hollings, supervisor of the year, or at least should be for putting up with me for so long. His patience is unmatched as is his dedication to his students. Secondly I cannot begin to thank enough Dean R. Cutting P. Geo (the project geologist of the West Cedartree Gold Project) for his tutelage, mentorship, and field support; I have learned more from him than both he and I give him credit for. I think I finally became a bush man during this whole thing and that would not have happened without learning it from the best-John Robinson (though next time he should teach me about how a fawn sneezes before teaching me about the terror of bear attacks). Kyle Goertzen, my loyal field assistant, I have never met a person before whose sole source of sustenance was cigarettes and energy drinks, but he was always there when I needed him. Grayme Anthony was president of Houston Lake Mining (HLM) during my tenure there and he was instrumental in organising the project and securing funding, and without him none of this would be possible.

The faculty of geology at Lakehead University were beyond helpful during this research project, however, there are a few key members I would like to thank who were not only as patient with my incessant questions but also treated me as if I were their own student. Dr. Mary Louise Hill visited the West Cedartree Gold project twice over the course of two field seasons and provided excellent field support for mapping, sampling, and structural interpretation. She also orchestrated a field trip for me and another geologist from the project with the resident geologist from the Kenora office of the MNDM, Craig Ravnaas, to investigate the Cameron Lake-Pipestone Lake shear zone. I also need to thank Dr. Andrew "DC" Conly. He was always there to help no matter how inane or lengthy the question, especially through my "what's a stable isotope?" phase.

Craig Ravnaas, the regional geologist from the Kenora office of the MNDM, as mentioned earlier, was involved in organising and providing access and the boat for the Cameron Lake-Pipestone Lake shear zone field trip hosted by Dr. Hill.

I cannot possibly thank enough Anne Hammond at Lakehead University for second to none thin section and sample preparation. Kristine Carey, the administrative assistant in the geology office was always more than helpful with my pesky requests and dealing with all my ridiculousness. Whole rock and trace element geochemistry analyses were performed by Geolabs in Sudbury; they were always quick and reliable.

My dabble into stable isotope geochemistry was, at least to me, a seemingly impossible task. It certainly would have been if it were not for Dr. Mostafa Fayek and Dr. Rong Liu in the SIMS lab at the University of Manitoba. They had both hosted me for a week and assisted me with my analyses and interpretation.

I need to thank my family; they supported me from day one and helped me out along the way whenever I needed it. Maura, Benny, Johnny, Marc, Adam, Jay Seals, Gabe, Larissa, Corey, and Simon you were all influential in my time at Lakehead and I will forever be in your debt for everything you all have done for me.

I would like to also thank the financial contributors to this project. This was a joint research project between Lakehead University and HLM with funding from HLM and a NSERC Collaborative Research Development grant.

I would like to personally thank Dr. Stephen Piercey for his thorough review and critique of this study. I greatly appreciated the time and effort he put in to generate very constructive comments and revisions.

Lastly, I cannot possibly ever thank enough Kylie Cronin for helping me along every step of the way.

Thanks to everyone, Scotty.

Table of Contents

List of Figures

List of Tables

Chapter 1:
Introduction

1.1 Objective

The objective of this thesis was to characterise the Angel Hill Gold Zone of the West Cedartree Gold Project located in the Kakagi-Rowan Lakes greenstone belt south of Sioux Narrows, Ontario. This involved creating a detailed map at the property scale, in conjunction with petrologic and petrographic analyses to investigate the lithological characteristics and relationships of the host rock assemblages. Trace element and radiogenic isotope geochemistry were used to determine tectonic relationships and to add to the very limited data sets available for these rocks. The Angel Hill Gold Zone was further analyzed using a scanning electron microscope to investigate the details of gold mineralization and alteration. A secondary ion mass spectrometer was used to determine in situ stable isotope characteristics of gold bearing phases.

1.2 The West Cedartree Gold Project

Houston Lake Mining Inc.'s (HLM) West Cedartree Gold Project (WCGP) encompasses eight contiguous properties within the Kakagi-Rowan Lakes greenstone belts in the Lake of the Woods region of Northwestern Ontario (Fig. 1.1). There are four known gold occurrences on these properties, each hosted within a different lithology. They are the McLennan Gold Zone, hosted in mafic metavolcanic rocks; the Dogpaw Zone, hosted in sheared gabbro; the Dubenski Zone, hosted in sheared felsic metavolcanic rocks and the Angel Hill Gold Zone (AHGZ), recently discovered by HLM, which contains samples grading 2.97 g/t Au over 106400 tonnes (Fig. 1.1). The AHGZ is hosted in an altered olivine-pyroxenite adjacent to the contact with a gabbro unit of the

Kakagi Sill. The AHGZ represents an example of Archean lode gold (orogenic gold or mesothermal vein-type) mineralisation. Many aspects of the AHGZ occurrence have yet to be defined or characterized, including the type and style of mineralisation, the nature of alteration and constraints on ore bearing fluids, as well as detailed petrologic, tectonic, and geochemical characterisation of the host rocks from the Kakagi-Rowan Lakes greenstone belt.

1.3 Location and Accessibility

The West Cedartree Gold Project is 1,674 hectares in size and is located in the Kenora Mining District of Ontario about 70 kilometres southeast of Kenora and approximately 15 kilometres southeast of Sioux Narrows, Ontario (Fig. 1.1). Access to the property is via the Cameron Lake Road off Highway 71 which traverses the northern portions of the property. The Cameron Lake road is a restricted access road and special permitting is required from the Ministry of Natural Resources for access. The Angel Hill Gold Zone is found at kilometre eight along the Cameron Lake Road where it has been exposed over 300 metres by mechanical trenching along a roughly north north-east trending zone. Access to the southern portions of the property is possible by boat from Crow (Kakagi) Lake. Eastern portions of the WCGP are accessed by boat from Cedartree Lake either portaging in from Crow Lake or from the Cedartree River. The property is bounded to the north by Dogpaw Lake, to north-east by Flint Lake, to the east by the Cedartree River, to the south-east by Cedartree Lake, and to the south by Crow (Kakagi) Lake (Fig. 1.1). The western boundary of the property runs roughly north-south through kilometre 6 of the Cameron Lake Road (Fig. 1.1).

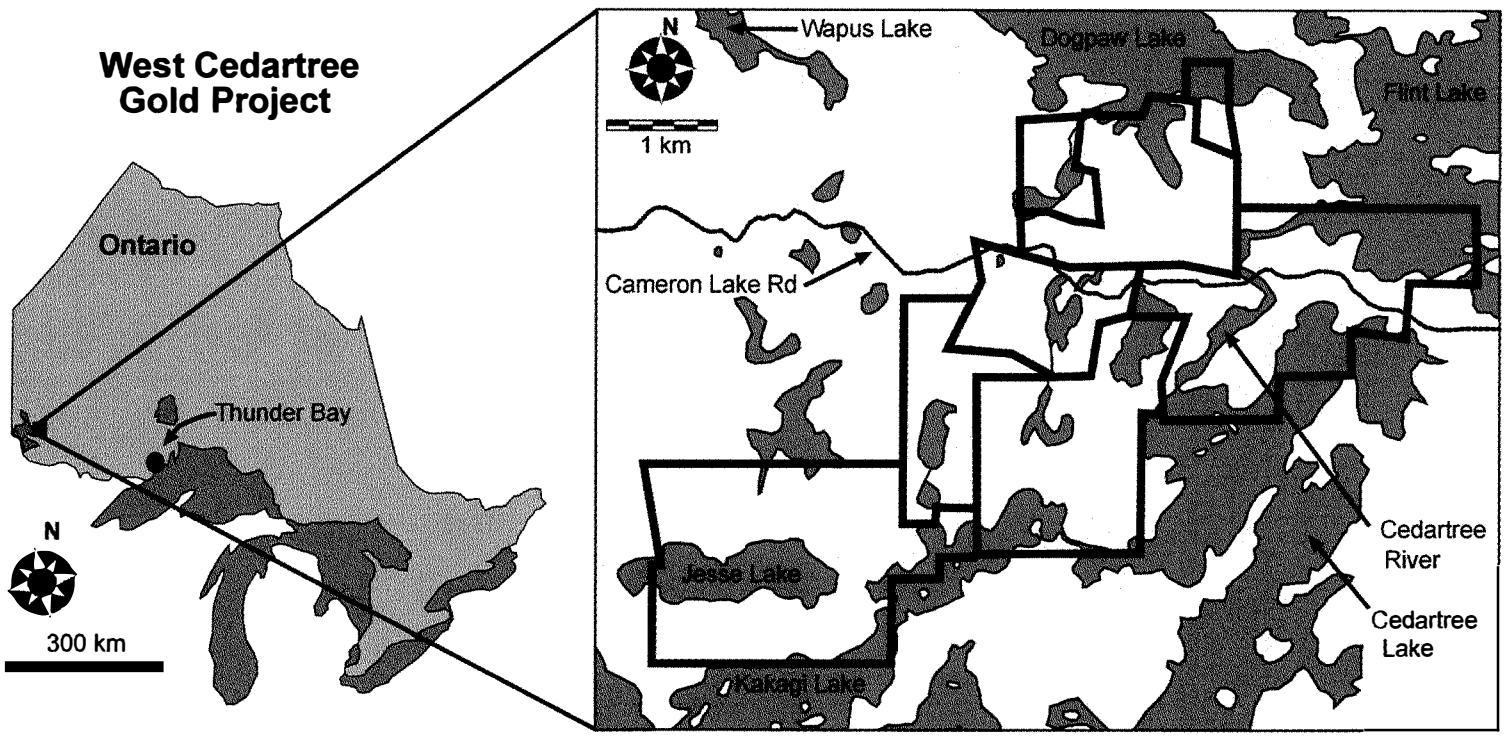

Figure 1.1. Property map of the West Cedartree Gold Project: (1) Gold Sun Property; (2) Jesse North Property; (3) West Cedartree Property; (4) McLennan Property; (5) Dogpaw West Property; (6) Dogpaw Property; (7) North Block Property; (8) Dubenski Property.

1.4 Property History

Gold exploration in the West Cedartree and Dog Paw areas has occurred since the 1800s which has led to the development of several mines including the Gold Panner Mine on Caviar Lake and the Flint Lake mine, in 1899 and 1901, respectively (Davies and Morin, 1976). Exploration at the WCGP started in 1944 with G. E. McLennan who staked a group of nine claims next to the Noranda Dog Paw Lake claims. The McLennan properties were then optioned by Sylvanite Gold Mines Ltd. in 1945, where the presence of visible gold identified in a quartz carbonate vein prompted drilling, trenching and sampling on the property (Davies and Morin, 1976). In 1983, along with seven other claims to the south, the Sylvanite option was taken over by Welcome North Mines Ltd. (Cutting and Anthony, 2005). In 1984 Falconbridge took over the options on the McLennan property, which were subsequently purchased in 1997 by Houston Lake Mining Ltd. (Cutting and Anthony, 2005). HLM began stripping the Angel Hill Zone in 2002 and by 2003 diamond drilling of the AHGZ had commenced. Angel Hill South was stripped in the fall of 2006 and combined with Angel Hill North to form the Angel Hill Gold Zone. Diamond drilling of Angel Hill South was performed during the winter of 2007.

1.5 Previous Work

The first documented work on the Crow Lake area was performed in 1883 by A. C. Lawson of the Geological Survey of Canada who conducted initial surveys of the rock units surrounding Lake of the Woods (Lawson, 1887). The first compilation work for the

Kakagi-Rowan Lake greenstone belt was generated by Burwash (1933), though by this time many prospectors had been working small claims throughout the area. Fahrig (1965) of the Geological Survey of Canada undertook K/Ar dating of the Kakagi Sill and determined an age of 1.925 Ga. Goodwin (1965) investigated the volcano-stratigraphy of the Lake of the Woods-Manitou Lake-Wabigoon region. Ridler (1965) investigated the petrology and petrography of the Kakagi Sills, whereas Cuddy (1971) looked at the structure of the volcanic-plutonic sequences. Mapping by Davies and Morin (1972) led to research in the area with Smith et al. (1973) investigating the petrography and geochemistry of the felsic volcanic rocks of the Emm Bay Formation. Detailed mapping of the Kakagi-Rowan Lakes greenstone belt, began with Kaye (1973) with the most detailed compilation completed by Davis and Morin (1976). The Ministry of Northern Development and Mines examined the regional geology of Kakagi-Rowan Lake greenstone belts as part of a metallogeny study throughout the 1980s (Johns, 1986). In the mid-to late 1980s D. R. Melling performed several studies on the Cameron Lake Mine. He characterised both petrographic and isotopic signatures of the alteration and gold mineralization (Melling, 1985, 1986, 1987, 1988, 1989).

1.6 Orogenic Gold Overview

Orogenic lode gold, or mesothermal, deposits are arguably the predominant gold deposit type in metamorphic orogenic belts, and include several giant (>250 t Au) and numerous world-class (>100 t Au) deposits (Groves et al., 2003). Examples within the Superior Province include: Dome and Pamour, Campbell, Red Lake and Kerr Addison Mines (Thorpe and Franklin, 1984). Though predominantly of Archean age, younger

examples include the Mesozoic Carolin and Bralorne deposits in British Columbia and the Motherlode deposit in California (Thorpe and Franklin, 1994). Lode gold systems are traditionally found in Archean greenstone terrains with gold occurring as veins in zones of brittle deformation and zones of alteration within highly schistose zones of ductile deformation (McCuaig and Kerrich, 1998). Associated rocks include volcaniclastic rocks, volcano-sedimentary, felsic, mafic and ultramafic intrusive rocks. Gold occurs in veins and bodies of quartz along fractures and faults as either native gold or as gold telluride phases with associated pyrite, arsenopyrite, muscovite and carbonate (Thorpe and Franklin, 1994; McCuaig and Kerrich, 1998; Groves et al., 2003). Genetic models for gold mineralization suggest gold is scavenged from host rocks by large scale metamorphic fluids and deposited in fractures and faults. Alteration assemblages of the host rock generally reflect alteration from interaction with large volumes of carbon dioxide rich fluids (Thorpe and Franklin, 1994; McCuaig and Kerrich, 1998; Groves et al., 2003).

1.7 Structure of Thesis

The following chapter will discuss sampling and analytical methods. Chapter Three is a summary of the regional geology, and Chapter Four is a discussion of the property-scale mapping and host rock lithologies. Chapter Five is a review and analysis of whole-rock and radiogenic geochemical analyses. Chapter Six is a detailed characterization of the Angel Hill Gold Zone and includes stable isotope geochemistry of fluid and sulphide phases. Chapter Seven is the conclusion of this study. Analytical results and sample data are presented in the Appendices A-D.

Chapter 2:
Methods

2.1 Field Mapping and Sampling

Field mapping at the property scale (1:5000) was undertaken of the West Cedartree Gold Project. Sampling was conducted over the property as well as in detail across the Angel Hill Gold Zone and included samples from diamond drill holes and channel samples. Lithology codes and nomenclature for geologic units were adapted from previous mapping by Davies and Morin (1976). Sample descriptions are provided in Appendix A and simplified core logs in Appendix B.

2.2 Petrography

An Olympus BX-51 transmitted and reflected light microscope with an attached Olympus DP-70 digital camera was used to describe, catalogue and photograph polished thin sections. Simplified thin section descriptions are presented in Appendix C.

2.3 Scanning Electron Microscope

Scanning electron microscopy was performed on 25 thin sections at Lakehead University using an SEM-EDS JEOL 5900 scanning electron microscope equipped with an Oxford energy dispersion system with a resolution of 139eV using a backscatter electron detector (BSE) in order to analyze gold phases and gangue phases associated with mineralization. The analyses were carried out with an accelerating voltage of 20kV and a beam current of 0.475 pA, with a beam width of less than 0.2 micrometres. Elements were standardized using samples available from the Lakehead University

Instruments Laboratory's standard library. Standards include hornblende (Mn-Hor) for FeO, periclase for MgO, orthoclase for K_2O, ilmenite for TiO_2, jadeite for Na_2O, wollastonite for CaO, corundum for Al_2O_3, pyroxene for SiO_2, and gold for Au.

2.4 Geochemistry

Whole-rock geochemistry was undertaken using X-ray fluorescence and inductively coupled plasma mass spectrometry analysis performed at the Geoscience Laboratory (GeoLabs) in Sudbury, Ontario. Samples were cut, crushed and then milled in an agate ring mill in order to reduce the risk of contamination of trace elements (Jenner, 1996). Trace elements were analyzed by X-ray fluorescence using a pressed pellet to allow comparison with data generated by inductively coupled plasma mass spectrometry. Totals for major element oxide data were generally 100%± 2% and have been recalculated to a 100% volatile-free basis. Detection limits for major elements are 0.01 weight % and relative standard deviations of duplicate analyses are within 5%. Trace elements, including the REE and HFSE analyzed at the Geoscience Laboratories were completed on a Perkin-Elmer Elan 9000 ICP–MS following a variation on the protocol described by Burnham and Schweyer (2004) and Tomlinson et al. (1998). Twenty four trace elements were determined using 200 mg aliquots of powder digested by a two stage procedure involving an initial decomposition in a closed beaker by a mixture of HF with lesser HCl and $HClO_4$, followed by a second mixture of dilute HCl and $HClO_4$ as described by Burnham et al. (2002). Detection limits for some critical elements, defined as 3σ of the procedural blank, are as follows: Th (0.032 ppm), Nb (0.044 ppm), Hf (0.085 ppm), Zr (3.2 ppm), La (0.048 ppm) and Ce (0.08 ppm; Burnham and Schweyer 2004).

Ratios of HFSE/HFSE* are calculated following the method of McCuaig et al. (1994). Results are presented in Appendix D.

2.5 Secondary Ion Mass Spectrometry

Sulfur isotope compositions of pyrite, galena, and sphalerite, and oxygen isotope compositions of quartz and carbonate phases were measured in situ using a CAMECA IMS 7f secondary ion mass spectrometer at the Department of Geology at the University of Manitoba. Both sulphur and oxygen isotope ratios ($^{34}S/^{32}S$ and $^{18}O/^{16}O$) were measured using a Cs^+ primary beam. A normal-incidence flood gun was employed to neutralize potential sample charging. The primary ion beam was focused to a 15 × 30 μm spot using a 100 μm aperture. Secondary ions were detected sequentially by switching the magnetic field. The detection system using an electron multiplier was coupled with an ion counting system with an overall dead time of 10.5 ns. A typical analysis lasted between 12 and 15 minutes, which comprises 60-80 analysis cycles. During the isotope measurement instrumental mass fractionation is introduced. Several processes combine to produce this fractionation, including secondary atom extraction (sputtering) and ionization and secondary ion transmission; however, the greatest contributors to instrumental mass fractionation are sputtering and ionization. These factors depend on sample composition and are referred to as compositionally dependent fractionations or matrix effects (Valley et al., 1997). Correction for this mass fractionation was done by comparing measurements of a standard, which is chemically and isotopically similar to the unknown sample. Standards used for sulphur analyses were the Balmat sphalerite (14.0‰ CDT), Balmat pyrite (14.6‰ CDT), and Balmat galena (15.6‰ CDT) from the

Balmat mine, New York (Crowe and Vaughan, 1996). Standards used for oxygen isotopes on quartz were Brazil quartz (20.5‰ SMOW) and Fe-dolomite for carbonate phases (9.97 ‰ SMOW). The precision and accuracy of analyses include errors arising from counting statistics, calibration to a known standard, and uncertainty in dead-time corrections owing to variable count rates. The overall analytical precision for the pyrite is ± 0.6 ‰, for sphalerite ± 0.6 ‰, for galena ± 0.4 ‰, for quartz ± 1.2 and for carbonate phases ± 1.2 ‰. Values are reported in standard notation relative to Cañon Diablo Troilite (CDT) and standard mean ocean water (SMOW). Results are presented in Table 6.1.

2.6 Radiogenic Isotope Geochemistry

Chemical separations and isotopic analyses were performed at Carleton University's Department of Earth Sciences Isotope Geochemistry and Geochronology Research Centre (IGGRC) in Ottawa, Ontario. Between 100 and 200 mg of sample powder were weighed into a screw-cap Teflon vial, to which a mixed ^{148}Nd-^{149}Sm spike was added. The powder-spike mixture was dissolved in HNO_3-HF, and then further attacked with HNO_3 and HCl until no residue was visible. The bulk REE were separated using cation chromatography with 2.5N HCl (Dowex 50-X8). The REE-bearing residue was dissolved in 0.26N HCl and loaded into a 10-ml borosilicate glass chromatographic column containing Teflon powder coated with HDEHP [di(2-ethylhexyl)] orthophosphoric acid (Richard et al., 1976). Nd was eluted using 0.26N HCl, followed by Sm in 0.5N HCl. Total procedural blanks for Nd are < 50 picograms; < 6 picograms for Sm. Concentrations are precise to +/- 1%, with $^{147}Sm/^{144}Nd$ ratios reproducible to 0.5%.

Samples were loaded with 0.3N H_3PO_4 on one side of a Re double filament assembly, and ran at temperatures of 1700-1800 ^{o}C in a 5-cup Finnigan MAT261 multicollector mass spectrometer. Isotope ratios were normalized to $^{146}Nd/^{144}Nd = 0.72190$. Analyses of the USGS standard BCR-1 yield Nd = 29.02 ppm, Sm =6.68 ppm, and $^{143}Nd/^{144}Nd$ = 0.512668 + 20 (n=4). The La Jolla standard averaged $^{143}Nd/^{144}Nd = 0.511847$ +/- 7 (Feb 2005 – June 2007). Internal lab standard = 0.511818 $\pm$ 8, n = 28 (Feb 2005-June 2007) and 0.511819 $\pm$ 10 n = 94 (Feb 2005 – Aug 2009). Results are presented in Table 5.2.

Chapter 3:
Regional Geology

3.1 The Superior Province

The West Cedartree Gold Project (WCGP) is located in the Kakagi-Rowan Lake greenstone belt, which lies on the western edge of the Wabigoon Subprovince of the Superior Province. The Superior Province extends from eastern Quebec to eastern Manitoba and from southern Minnesota to parts of northern Ontario and Manitoba and is the largest Archean craton in the world (Fig. 3.1; Thurston et al., 1991). The Superior Province, which ranges in age from 3.2 to 2.5 billion years old, is bounded to the southeast by the 1.1 billion year old Grenville Province, to the northwest by the Trans Hudson Orogen, and it is overlain on its northern and western borders by Paleozoic sedimentary rocks around Hudson and James Bay and in Manitoba (Fig. 3.1; Card and Ciesielski, 1986; Thurson et al., 1991, Percival et al., 2006). The Superior Province formed as a result of the creation and accretion of new continental lithosphere as well as oceanic terrains in an active tectonic setting (Percival, 2006). The Superior Province has been subdivided into subprovinces based on their tectonic setting and lithologic properties (Fig. 3.1; Card and Ciesielski, 1986). These subprovinces have been subdivided based on lithology, structure and metamorphism into four main types (Stott, 1997). The first of these four types are volcanic-plutonic greenstone belts which are dominated by supracrustal volcanic rocks with associated synvolcanic plutonic rocks (Card and Ciesielski, 1986; Thurston et al. 1991; Stott, 1996; Percival et al, 2006). The second type of subprovince is composed of metasedimentary rocks comprised of long linear belts of altered sedimentary rocks (Card and Ciesielski, 1986; Thurston et al. 1992;

Stott, 1996; Percival et. al, 2006). Thirdly, there are large scale felsic plutonic provinces composed primarily of granite batholiths (Card and Ciesielski, 1986; Thurston et al. 1992; Stott, 1996; Pervical, 2006). And lastly, there are subprovinces of high grade gneissic terranes (Card and Ciesielski, 1986; Thurston et al. 1991; Stott, 2007; Percival et al., 2006). The subprovinces are generally separated by long strike-slip faults and record the different geodynamic environments in which they formed. These geodynamic environments include oceanic floor, plateau, island arc and back-arc settings (Percval et. al, 2006).

3.2 Wabigoon Subprovince

The Wabigoon Subprovince (Fig. 3.2) is a 900 km-long, 150 km-wide granite-greenstone subprovince comprised of metamorphosed volcanic and sedimentary belts ranging from 3 to 2.71 Ga in age, with intrusive complexes ranging in age from 3 to 2.69 Ga generally comprised of granitoid batholiths, gabbroic sills and felsic stocks (Blackburn et al., 1991). The Wabigoon Subprovince is bordered to the northwest by the metaplutonic Winnipeg River Subprovince, to the northeast by the metasedimentary English River Subprovince and to the south by the metasedimentary Quetico Subprovince (Blackburn et al., 1991; Pervical, 2004; Fig. 3.2). The western boundary is formed by the rocks of the 1.8 billion-year-old Trans-Hudson Orogen (Blackburn et al., 1992). The subprovince is cross cut in the central region by the Nipigon Embayment, a series of diabase dikes and sills (Blackburn et al., 1991; Pervical, 2004). The Wabigoon Subprovince is divided into three parts based on geographic distribution of lithologic association; the eastern, central and western (Fig. 3.2).

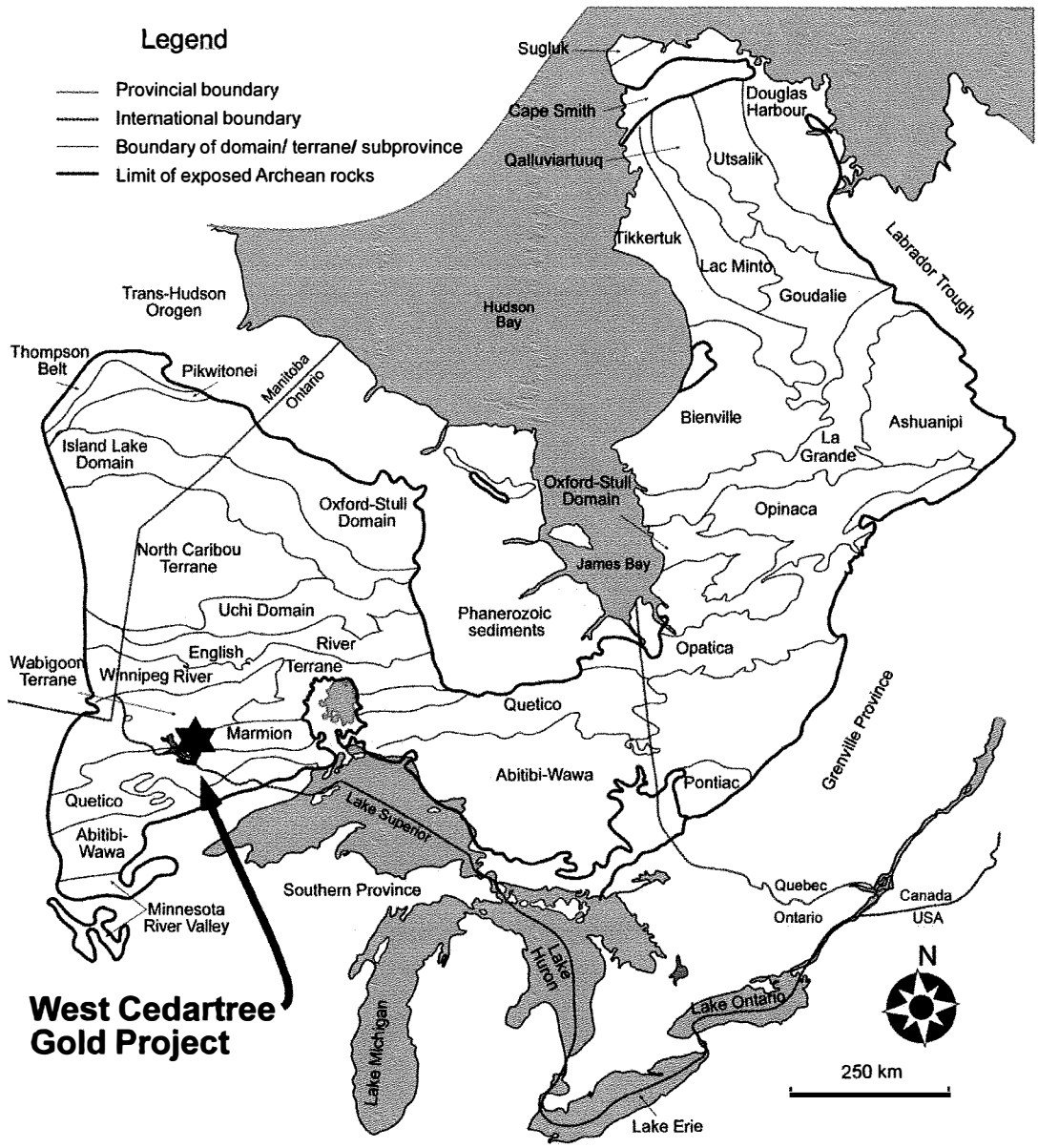

Figure 3.1 Subprovinces of the Superior Province. Modified from Card and Ciesielski (1986).

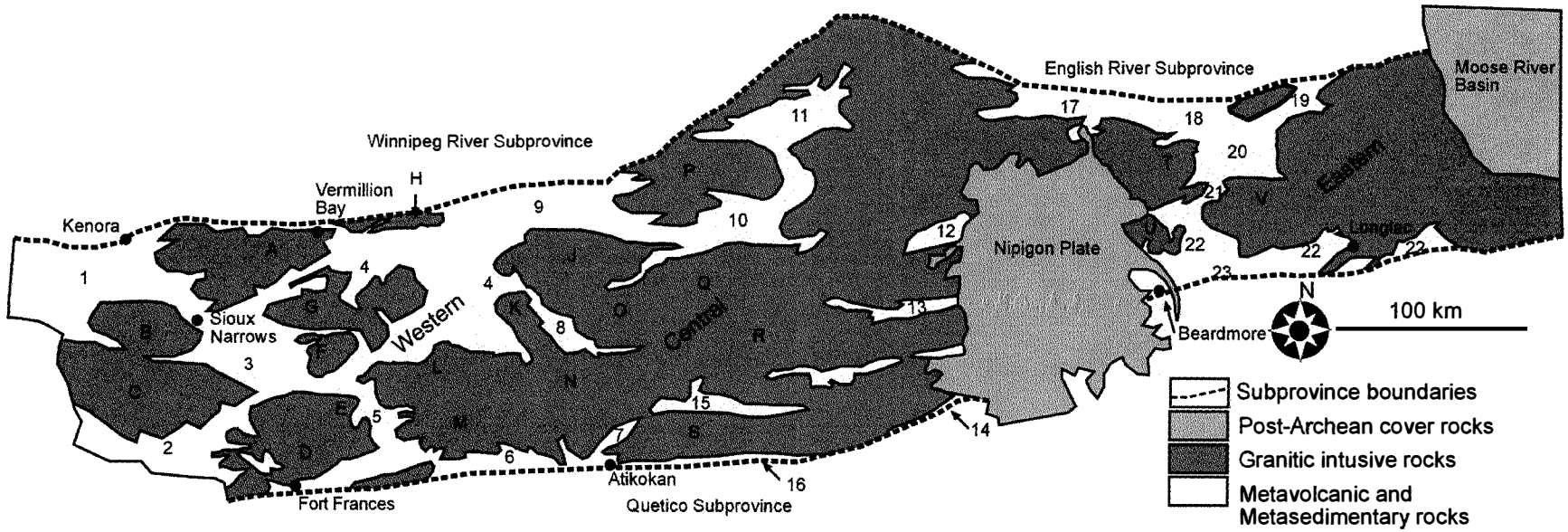

Figure 3.2 Greenstone belts and granite intrusions and regions of the Wabigoon Subprovince. Modified from Blackburn et al. (1992).
*Greenstone Belts:*1- Lake of the Woods; 2- Rainy Lake; 3- Kakagi-Rowan Lakes; 4- Eagle-Wabigoon-Manitou Lakes; 5- Otukomamoan Lake; 6- Calm Lake; 7- Finlayson Lake; 8- Raleigh Lake; 9- Abram-Minnitaki Lakes; 10- Sturgeon Lake; 11- Savant Lake; 12- Obonga Lake; 13- Garden Lake; 14- Bo Lake-Heaven Lake; 15- Lumby Lake; 16- Lac des Milles Lacs; 17- Caribou Lake; 18- Marshal Lake; 19- O'Sullivan Lake; 20- Gzowski-Oboshkeghan; 21- Onamen River; 22- Elmhirst-Castlewood-Klotz; 23- Beardmore-Geraldton.
Granitic Intrusions: A- Dryberry Batholith; B- Aulneau Batholith; C- Sabaskong Batholith; D- Rainy Lake Batholith Complex; E- Jackfish Lake- Weller Lake Pluton; F- Lawrence Lake Batholith; G- Atikwa Batholith; H- Ghost Lake Batholith; J-Basket Lake Batholith; K- Revell Batholith; L- Entwine Lake Batholith; M- Irene-Eltrut Lakes Batholith Complex; N- White Otter Lake Batholith; O- Indian Lake Batholith; P- Lewis-Robinson-Lake of Bays Batholith Complex; Q- Sowden-Wabikimi Lakes Batholith Complex; R- McCausland Pluton; S- Marmion Lake Batholith; T- Obabika Batholith; U- Northwind Lake Batholith; V- Onamam Lake Batholith.

3.2.1 Eastern Wabigoon

The eastern Wabigoon Subprovince consists of greenstone belts surrounded by granitoid units and transected by the Proterozoic Nipigon Embayment to the south west (Blackburn, 1992). Metavolcanic units are predominantly located in concentric volcanic centers as exemplified by Marshall Lake, the Gzowski-Oboshkegan area, and the Elmhirst-Rickaby centre (Fig. 3.2; Percival, 2004). Metasedimentary rocks are predominantly found along the northern and southern boundaries with the English River and Quetico subprovinces, respectively (Blackburn et al., 1992). Age dating of the volcanic units has grouped them into several assemblages. The oldest rocks are the tholeiitic basalts of the Toronto assemblage ranging from 3.0 to 2.92 Ga (Percival, 2004; Tomlinson, 2004). Younger units range in age from 2.778 to 2.777 Ga for the Onaman assemblage, 2.745 to 2.735 Ga Marshal assemblage, 2.725 to 2.715 Ga Metcalfe-Venus assemblage, and the youngest, the metasedimentary conglomerate assemblage, at 2.707 Ga (Percival, 2004; Tomlinson et al., 2004).

3.2.2 Central Wabigoon

The central Wabigoon (Fig. 3.2) Subprovince is composed predominantly of large granitoid intrusions and gneissic rocks (Davies and Morrin, 1976; Blackburn et al., 1992; Percival, 2004). The central Wabigoon Subprovince is a 200 km wide strip of granitoid rocks separating the volcanic-dominated eastern and western Wabigoon subprovinces (Percival, 2004). The central Wabigoon consists of gneissic rocks cross cut and surrounded by younger massive and foliated granitic bodies forming large-scale dome and basin structures (Blackburn et al., 1992). Dating of greenstone belts has yielded ages

of 3.075 to 2.703 billion years and granite intrusions at 3.075 to 2.680 billion years (Percival, 2004; Tomlinson et al., 2004).

3.2.3 Western Wabigoon

The western Wabigoon (Fig. 3.2) is a series of greenstone belts and granitoid batholiths. Volcanic rocks range in composition from tholeiitic to calc-alkaline, representing ocean floor or plateau and arc environments (Pervical, 2004). Metasedimentary sequences are mostly clastic rocks with minor chemical metasedimentary rocks including iron formation (Blackburn et al., 1992). Mafic to ultramafic sills and stocks are marginal to batholiths or intrude the metavolcanic sequences (Blackburn et al., 1992). Volcanic rocks range in age from 2.745 to 2.712 Ga (Percival, 2004; Tomlinson et al., 2004). Plutonic rocks have much broader age ranges, with synvolcanic granodiorites ranging in age from 2.735 to 2.715 Ga (Percival, 2004), younger intrusions of granodiorite batholiths of 2.710 Ga and of monzodiorite and monzogranite of 2.698 to 2.690 Ga (Percival, 2004; Tomlinson et al., 2004)

3.3 Local Geology

The Kakagi-Rowan Lakes greenstone belt has been extensively mapped by Davies and Morin (1976; Fig. 3.3). They have shown that the oldest rocks in the map-area are a series of mafic metavolcanic flows and tuffs overlain by a series of intermediate to felsic metavolcanic rocks which have been intruded by mafic to ultra-mafic sills. These sequences of volcanic and intrusive rocks were then deformed into large scale steeply dipping folds with steeply dipping and vertical, east-northeast-trending

axial planes. These sequences were then intruded by large granite stocks and late stage quartz-feldspar porphyry dikes. Relative timing of the units is presented in Table 3.1.

Table 3.1 Table of lithologies and relative timing for rocks of the Kakagi-Rowan Lakes Greenstone belt. Modified from Davies and Morin (1976).

PHANEROZOIC
- CENOZOIC
  - QUATERNARY
    - RECENT
      - Swamp and stream deposits
    - PLEISTOCENE
      - Sand, gravel, boulders, clay

PRECAMBRIAN
- MIDDLE TO LATE PRECAMBRIAN
  - (PROTEROZOIC) MAFIC INTRUSIVE ROCKS
    - Diabase dikes
  - EARLY PRECAMBRIAN (ARCHEAN)
    - Late Mafic Dikes
      - Gabbro, diorite, lamprophyre
    - FELSIC INTRUSIVE ROCKS
      - Late Felsic Intrusive Rocks
        - Foliated and massive granodiorite, massive diorite, contaminated diorite
      - Early Felsic Intrusive Rocks
        - Granodiorite, feldspar porphyry, quartz porphyry, quartz-feldspar porphyry, fine-grained granodiorite and aplite dikes
    - MAFIC AND ULTRAMAFIC INTRUSIVE ROCKS
      - Gabbro, diorite, quartz gabbro, anorthositic gabbro, pyroxenite, peridotite orthopyroxenite
    - METAVOLCANIC AND METASEDIMENTARY ROCKS
      - Metasedimentary rocks
        - Volcanic sandstone, volcanic conglomerate, argillite, chert
      - Felsic to Intermediate Metavolcanic rocks
        - Dacite, porphyritic dacite, rhyodacite, tuff-breccia, lapilli-tuff, tuff, ignimbrite, spherulitic ash flows

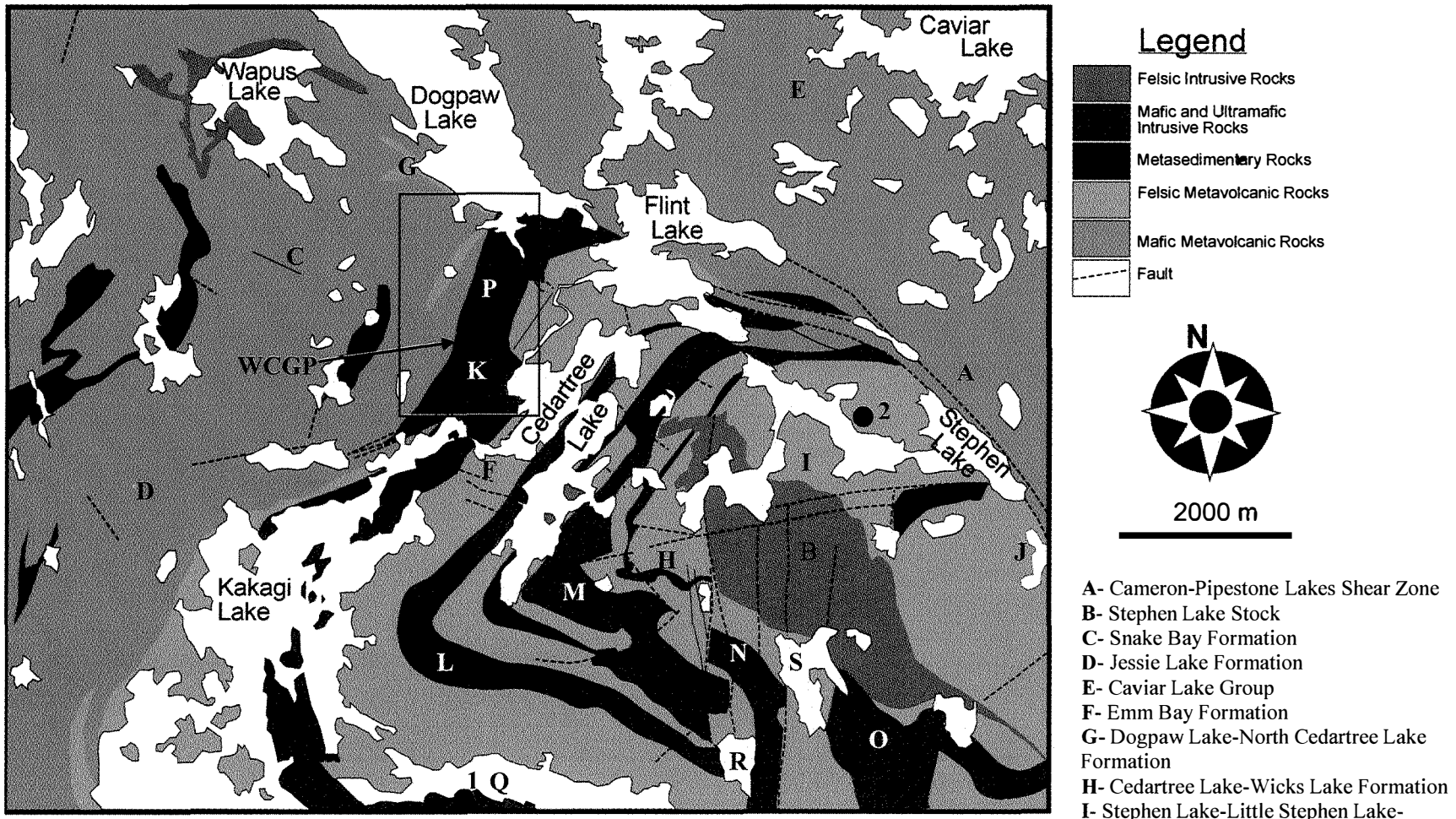

Figure 3.3 Simplified geology map of the Kakagi and Rowan Lakes greenstone belt, modified from Davies and Morin (1976) showing location of samples taken by Davis and Edwards (1982) for geochronology. Boxed outline indicates approximate area of the WCGP. Sample location 1 (sampled from a pegmatitic portion of gabbro from the Kakagi Sill) is dated at 2724.8 +/- 2.5 Ma. Sample location 2 (sampled from a felsic tuff near the top of the Kakagi Lake Group-felsic metalvolcanic rocks) dated at 2711.1 +/- 1.3 Ma (Davis and Edwards, 1982).

A- Cameron-Pipestone Lakes Shear Zone
B- Stephen Lake Stock
C- Snake Bay Formation
D- Jessie Lake Formation
E- Caviar Lake Group
F- Emm Bay Formation
G- Dogpaw Lake-North Cedartree Lake Formation
H- Cedartree Lake-Wicks Lake Formation
I- Stephen Lake-Little Stephen Lake-Weisner Lake Felsic Formation
J- Bog Bay-Mongus Lake Felsic Formation
K- Kakagi Sill #1
L- Kakagi Sill #2
M- Kakagi Sill #3
N- Kakagi Sill #4
O- Kakagi Sill #5
P- Angel Hill Gold Zone
Q- Peninsula Bay
R- Wicks Lake
S- Weisner Lake

3.3.1 Mafic Metavolcanic Rocks

The mafic metavolcanic rocks in the Kakagi-Rowan Lakes greenstone belt comprise the Rowan Lake Group which consists mainly of pillowed basalt flows with minor interbedded pyroclastic tuff units. Mafic to intermediate volcanic rocks dominate the north and western portions of the Kakagi-Rowan Lake greenstone belt and underlie the other units in the area (Davies and Morin, 1976; Johns, 1986). Top determinations from pillows with well preserved selvages and vesicles indicate younging direction to the northeast; this unit also dips steeply to the northeast. The basalts have been metamorphosed to greenschist facies with chlorite defining the foliation, though up to amphibolite facies has been observed (quartz-hornblende-plagioclase). Mafic tuffs, including lapillistone tuffs and tuff-breccias are weakly to strongly foliated and strongly altered to chlorite. The Snake Bay Formation; consisting of interlayered massive, pillowed, and porphyritic mafic flows is intruded by synvolcanic gabbros of the Kakagi Gabbro Sills (Johns, 1986). The Jessie Lake Formation is comprised of mafic tuff and lapilli-tuff roughly 60 m thick and 1200 m long. The Caviar Lake group consists of lapillistone and tuff breccia 210 m thick and 3900 m long (Davies and Morin, 1976; Johns, 1986).

3.3.2 Felsic Metavolcanic Rocks

Felsic to intermediate metavolcanic rocks occur in the central and southern parts of the Kakagi-Rowan Lakes greenstone belt forming the Kakagi Lake group (Fig. 3.3; Johns, 1985). These occur as dacitic to rhyolitic tuffs, breccias and debris flows that

overlie the mafic rocks in the area. The rocks of the Rowan Lake group can be subdivided into five formations: the Cedartree Lake-Emm Bay-Peninsula Bay Formation (referred to here as the Emm Bay Formation) composed of dacitic tuff breccias and tuffs, the Dogpaw Lake-North Cedartree Lake Formation composed of dacitic tuffs with minor breccias, Cedartree Lake-Wicks Lake Formation composed of fine grained dacitic tuffs, Stephen Lake-Little Stephen Lake-Weisner Lake Felsic Formation composed of dacitic tuffs and tuff-derived sedimentary rocks, and the Bog Bay-Mongus Lake Felsic Formation composed of tuff breccias of dacitic to rhyolitic composition (Davies and Morin, 1976; Johns, 1985). Interbedded within the felsic volcanic sequence, and likely derived from these rocks, are small volumes of metasiltstone, metawacke, and graphitic rocks (Fig. 3.3; Johns, 1986).

3.3.3 Kakagi Gabbro Sills

Mafic and ultramafic intrusive rocks occur throughout the Kakagi-Rowan Lake greenstone belt in two forms; as irregular podlike intrusions into the basaltic pile and as differentiated ultramafic and gabbro sills within the intermediate to felsic metavolcanic sequence (Davies and Morin, 1976). The sills have been broken into five distinct mafic to ultramafic sills.

Sill # 1 (Fig. 3.3) is located south of Dogpaw Lake, through Emm Bay and south of Peninsula Bay (the one in the study area). It intrudes between the mafic volcanic rocks of the Snake Bay Formation and the felsic volcanic rocks of the Emm Bay Formation. It varies in thickness from 760 m at the west end of Peninsula Bay to 1,370 m in the

vicinity of the Cedartree Lake-Emm Bay Portage of Kakagi Lake (Burwash, 1933; Davies and Morin, 1976). The sill contains ultramafic rocks that form a basal unit as well as conformable lenses within the gabbro (Fig. 3.3; Davies and Morin, 1976). Sill # 2 is located in the middle of Cedartree Lake, north of Peninsula Bay and west of Wicks Lake and ranges in thickness from 305 in the north to 760 m in the south and contains a basal pyroxenite layer that is up to 135 m thick (Fig. 3.3; Davies and Morin, 1976). Sill # 3 is located on the eastern side of Cedartree Lake and northwest of Wicks Lake and has been extensively faulted and ranges from 490 m in thickness in the south of Flint Lake to 1,005 m northwest of Wicks Lake (Fig. 3.3; Burwash, 1933; Davies and Morin, 1976). Like Sill # 2, Sill # 3 consists of a basal layer of peridotite ranging up to 490 m thick and overlain by medium- to coarse-grained gabbro (Fig. 3.3; Davies and Morin, 1976). Sill # 4 is located west and south of Little Stephen Lake and south of Weisner Lake and ranges from 60 m to 150 m in thickness and does not contain a basal pyroxenite layer (Fig. 3.3; Burwash, 1933; Davies and Morin, 1976). Lastly, Sill # 5 (Fig. 3.3) is located south of the eastern part of Stephen Lake and is 490 m thick and consists of a basal layer of pyroxenite, 60 m thick, an upper basal layer of peridotite 60 m thick with an upper gabbro unit up to 360 m thick (Fig. 3.3; Davies and Morin, 1976). The sill has been truncated to the south west, where it has been involved in large scale folding (Davies and Morin, 1976).

3.3.4 Felsic Intrusive rocks

The Stephen Lake Pluton is a granite-granodiorite stock 3,600 m long and 2,400 m wide trending north-northwest. The pluton is in contact with felsic and intermediate

metavolcanic rocks and the # 4 and # 5 ultramafic-mafic Kakagi sills (Davies and Morin, 1976). Quartz-feldspar porphyry and feldspar porphyry dikes up to 10 meters wide cross-cut all units and visible structures, they have been observed from several meters to hundreds of meters in length to thousands of meters in length (Burwash, 1933). A northwest-trending 30 m wide diabase dike cross-cuts the northern part of the greenstone belt (Davies and Morin, 1976).

3.3.5 Structure

The geology of the Kakagi-Rowan Lakes greenstone belt is divided by the southeast-striking, northeast-dipping Pipestone-Cameron Fault (Fig. 3.3; Davies and Morin, 1976; Melling et al., 1986). The Pipestone-Cameron shear zone divides the Dog Paw-Rowan Lakes area to the northwest and the Cameron-Kakagi Lakes to the southwest and is a regional scale strike slip fault with dextral sense of motion (Fig. 3.3). Though no magnitude of displacement has been determined, a lack correlation of units across the fault suggests major offset.

Two major anticlines are present within the study area flanked by a total of three major synclines (Fig. 3.3). The isoclinal folds, which trend east-northeast, have steep plunges in conjunction with steeply dipping limbs (Davies and Morin, 1976; Melling et al., 1986). Axial planes are vertical and a strongly developed schistosity is prominent in hinge areas of the folds. Many minor folds are present in the felsic volcanic rocks. Davies and Morin (1976) have suggested the large scale folds are the result of compressive strain from the boundaries of the more competent sills during regional scale deformation.

3.3.6 Geochronology

Davis and Edwards (1982) dated a pegmatitic portion of a gabbro from the Kakagi Sill (sample location 1 from Fig. 3.3) using U-Pb on zircons, determining an age of 2724.8 +/- 2.5 Ma. U-Pb dating of a zircon from the felsic tuff of the Kakagi Lake Group (sample location 2 from Fig. 3.3) yielded an age of 2711.1 +/- 1.3 Ma (Davis and Edwards, 1982). Since the age of the Kakagi Sill is from the lowermost section and the sill intrudes the base of the Kakagi Lake Group, and the date from the Kakagi Lake Group is from the top of the sequence, these dates have been interpreted to suggest the sill intruded a continuously growing volcanic pile resulting in a span of deposition of 13.7 +/- 3.7 m.y. (Davis and Edwards, 1982). Alternatively the zircon dated from the sill could be an inherited zircon from felsic volcanic rocks which were assimilated during emplacement.

Chapter 4:

Property Geology

4.1 Introduction

A map of the geology within the study area is presented in condensed form in Figure 4.1, a larger printout is attached at the end of this thesis. The map area consists of a block approximately four kilometers north-south and three and half kilometers east-west (Fig. 4.1). The geology of the study area can be divided into five main units based on lithology and time of emplacement. The oldest rocks occupy the eastern part of the study area and are mafic metavolcanic flows and tuffs of the Snake Bay Formation. Overlying these, to the east, are the felsic-intermediate metavolcanic tuffs and breccia tuffs of the Emm Bay Formation. Intruding these units is the #1 sill of the Kakagi Gabbro Sills which contains a basal and interformational peridotite-pyroxenite unit (Fig. 4.1). Lastly these units have been cross cut by late stage felsic and lamprophyre dikes. This chapter will use petrologic and petrographic classification to describe and characterize the rock units of the WCGP; further classification of rock types and tectonic setting is presented in Chapter Five using major, trace element and radiogenic isotope geochemical data.

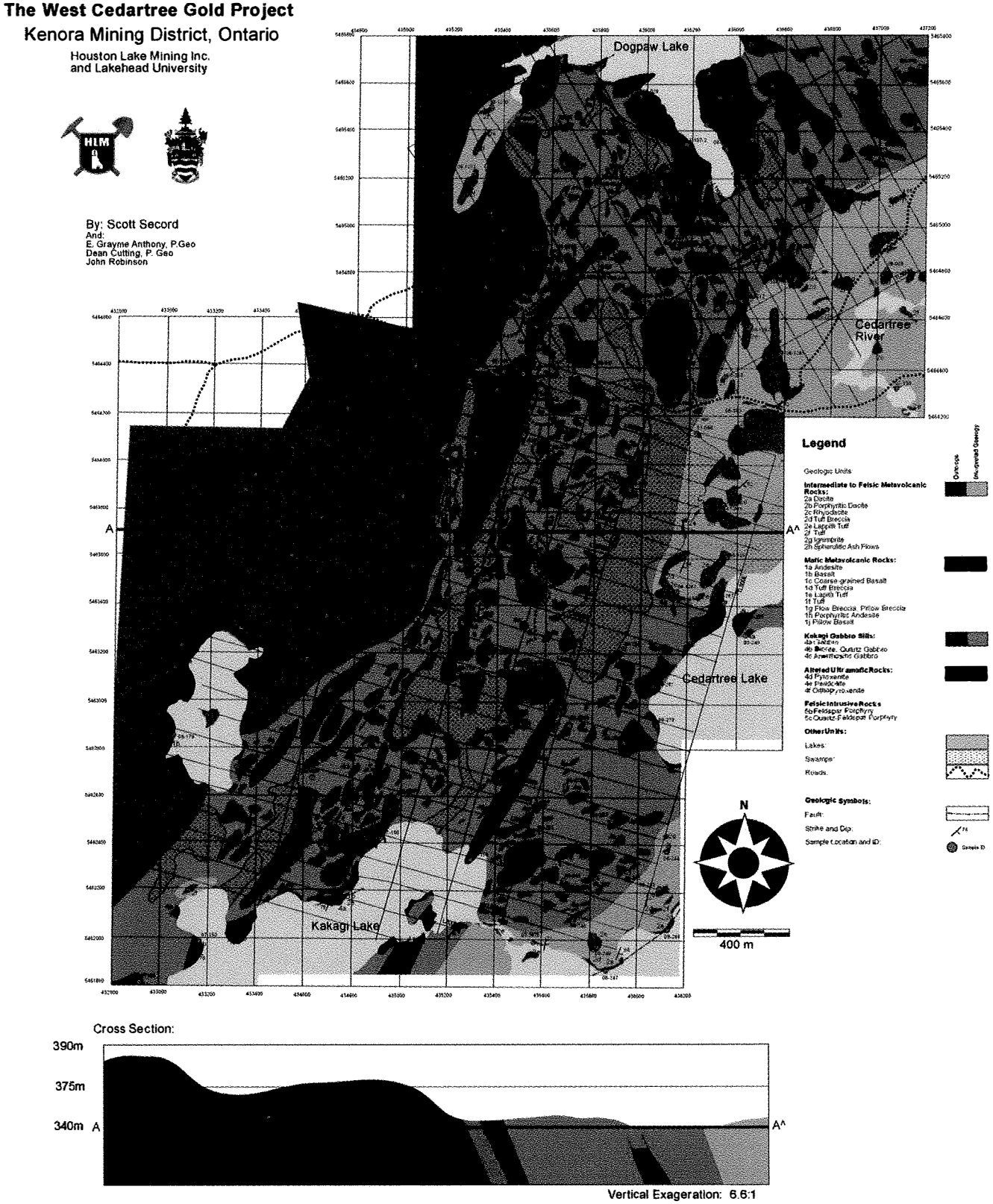

Figure 4.1 Geological map of the study area.

4.2. Snake Bay Formation

Rocks of the Snake Bay formation are mafic to intermediate volcanic rocks and out crop in the western portion of the study area north of Kakagi Lake and south of Dogpaw Lake (Fig. 4.1). These rocks account for roughly one third of all exposed rocks in the study area. The basaltic rocks are grey-green on the weathered surface and dark green on the fresh surface. The unit comprises mafic metavolcanic rocks that occur as basaltic flows, pillowed basalts and minor interbedded massive fine grained tuffs and lapilli tuffs. Units are generally conformable along strike though internal contacts are often discontinuous or poorly defined (Fig. 4.1).

Basaltic rocks account for almost 75% of all mafic metavolcanic rocks that out crop within the study area. They are generally fine grained to aphanitic and strongly altered to chlorite. They are often strongly foliated. Basalts are comprised of massive flows; though locally out crop as pillows. Pillow basalts are only observed in the northwestern parts of the exposed Snake Bay Formation and account for less than 20% of all exposed basaltic rocks (Fig. 4.1). They generally form well rounded pillows and are only locally distorted (Fig. 4.2 A, B). They often display well preserved triple points (Fig. 4.2 A), selveges and vesicles (Fig 4.2 B) which indicated way up directions and younging to the northeast, consistent with the regional stratigraphy as defined by Davies and Morin, (1976).

Ophitic to poikilitic textures are present in lapilli tuffs and basalt flows though fine grained tuffs are generally massive to weakly foliated (Fig. 4.2 C). The basalt has pervasive slaty cleavage throughout, with only local distortion of foliation planes. Figure 4.2 B is an example of the small scale fracturing which is prevalent throughout the unit. These fractures are carbonate altered brittle fractures that are very weakly mineralized with up to trace amounts of pyrite and

pyrrhotite. Locally, there are also locally thin irregular stringers of epidote-quartz-carbonate infilling these late fractures (Fig. 4.2 C).

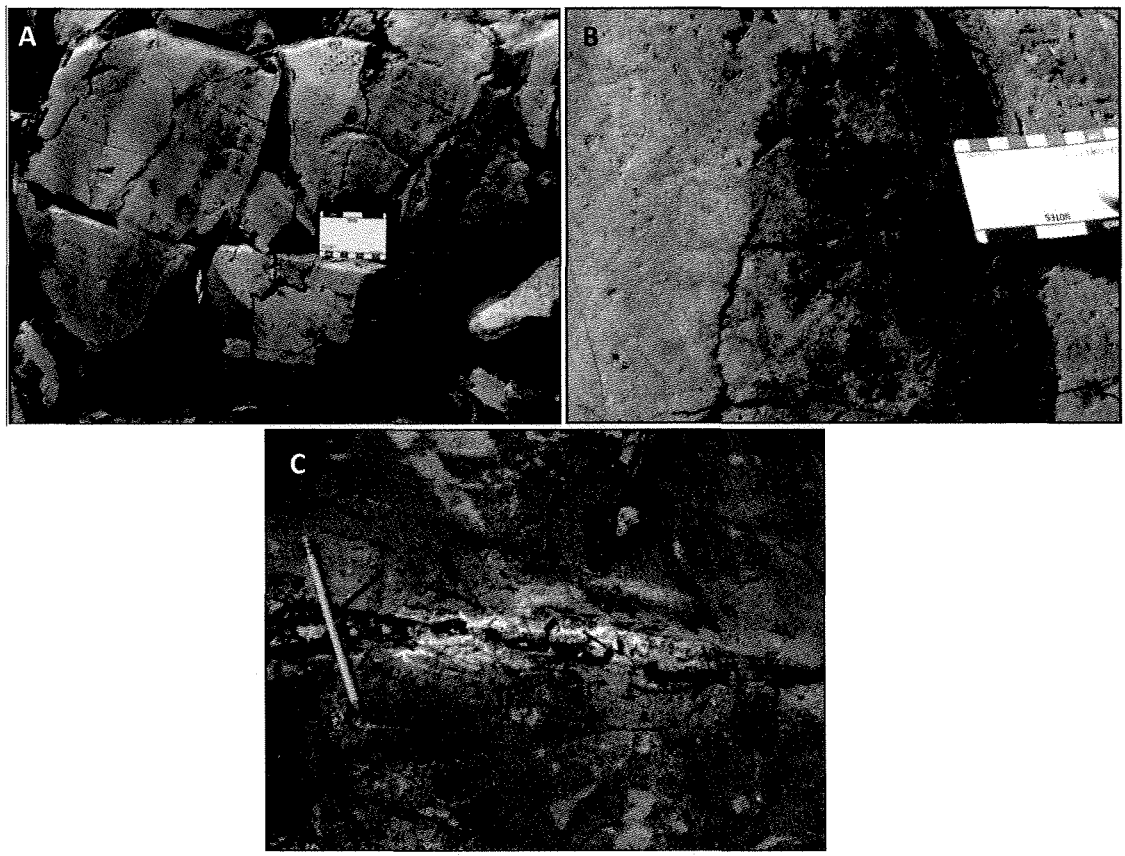

Figure 4.2. Representative photographs of mafic metavolcanic rocks from the Snake Bay Formation. A- pillowed basalt. B- pillow selveges. C- epidote and chlorite altered carbonate veinlet in filling a late fracture in a mafic tuff.

4.3 Emm Bay Formation

The felsic to intermediate metavolcanic rocks that occupy the area north of Kakagi Lake and on the southwest edge of Cedartree Lake are of the Emm Bay Formation of the Kakagi Lake Group suite (Fig. 4.1). These metavolcanic rocks consist mainly of dacitic tuff-breccias to lapilli tuffs. The tuff-breccia is composed of large, angular to sub-angular pale green to whitish coloured felsic clasts within a matrix of fine grained felsic to intermediate medium to fine

grained green to light grey green coloured tuff (Fig. 4.3 A). These clasts are up to 15 cm in diameter, often with well preserved vesicles and show a poor preferential alignment roughly east-north-east. Within these tuff breccias are lenses and discomformable layers up to 15 meters wide of coarse- to medium grained lapilli tuffs; these, however, are not continuous and do not show any particular trends in direction or concentration. The variance in clast size and stratigraphy suggests that these pyroclastic rocks were deposited suddenly either subaerialy or in a shallow water environment. Localized shearing is observed in the southern parts of the study area particularly at the waterfall between Kakagi Lake and Cedartree Lake and along the northern and eastern shores of Cedartree Lake. This is the unit which hosts the Dubenski occurrence that lies to the east outside the study area. The felsic metavolcanic rocks northeast and south of Cedartree Lake and northwest of Wicks Lake are primarily well-layered, fine-grained dacitic tuff (Fig. 4.1). The tuff is usually light grayish to green-brown in colour on the weathered surface and pale gray-green on the fresh surface. The highly foliated layers range in thickness from a few millimeters up to five centimeters. The unit remains competent except where there is evidence of strong shearing which is observed just south of Dogpaw Lake and along the Dalby Bay Shear (Fig. 4.3 B).

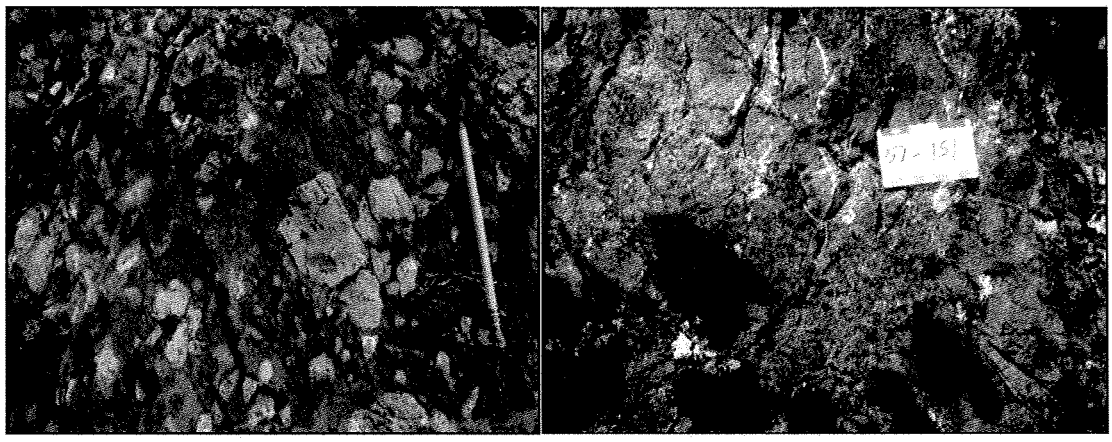

Figure 4.3. Representative photographs volcanoclastic rocks of the Emm Bay Formation. A- felsic tuff breccias. B- strongly foliated lapilli tuff.

4.4 Kakagi Sill

Intruding between the Emm Bay and Snake Bay Formations is the Kakagi Sill. The Kakagi Sill, as described in Chapter 3, is a mafic-ultramafic gabbroic body with a basal unit of peridiote and pyroxenite (Fig. 4.1). The Kakagi Sill accounts for nearly half of all rocks exposed in the study area.

The gabbros are dark brown to greenish grey on the weathered surface and medium green-grey on the fresh surface (Fig. 4.4 A). These rocks are medium to coarse grained and weakly to non-foliated, contain roughly equal amounts of plagioclase and amphibole and are extensively altered to chlorite. The gabbros are relatively homogeneous and show little differentiation along or across strike. However, there are small pods up to five meters in width that are coarse-grained to pegmatitic sporadically throughout the sill. The lower contact with the Snake Bay Formation is relatively sharp and no metamorphic contact aureole is observed. The upper contact with the Emm Bay Formation, however, is slightly more ambiguous. Lack of well defined chill margins and numerous xenoliths suggests that the sill intruded a still warm volcanic

pile. The gabbro unit reaches a maxium thickness of 1200 metres (Fig. 4.1). The gabbros form large continuous outcrops with excellent exposure, large cliffs and ridges are common throughout the entirety of the sill (Fig. 4.4 C).

The ultramafic rocks form a basal unit and are an intraformational unit up to 100 m in thickness (Fig. 4.1). These rocks are composed of cumulate textured peridotites and coarse grained orthopyroxenites. Both are rusty brown red on the weathered surface and dark black on the fresh surface (Fig. 4.4 B). They are strongly altered to serpentine and chlorite and are weakly magnetic. Locally they are altered to carbonate. There is no spatial separation or grading of the units and peridotite accounts for roughy 65% of all ultramafic rocks.

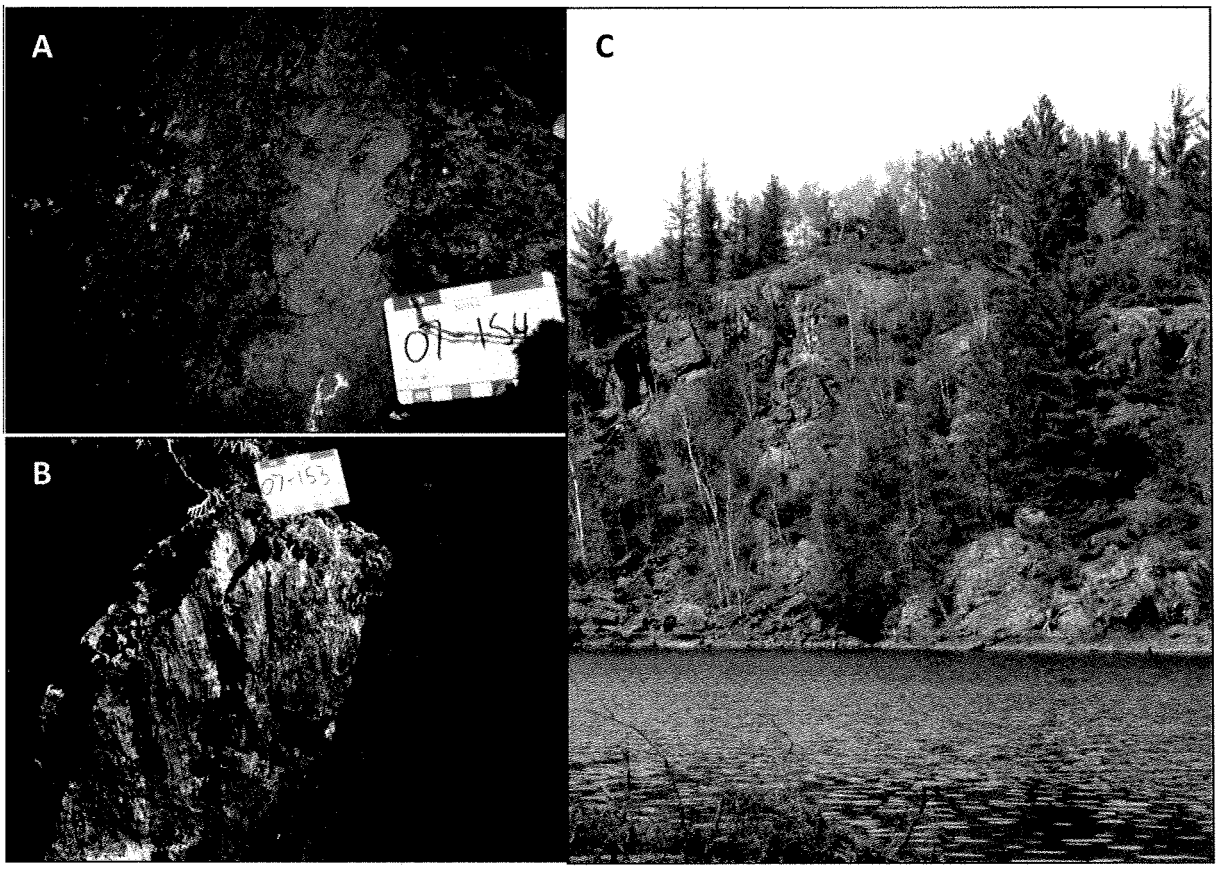

Figure 4.4 Photographs of rocks from the Kakagi Sill. A- weathered surface of typical medium grained gabbro. B- dark black fresh surface of serpentinised ultramafic rocks. C- typical exposure of gabbro throughout the WCGP.

4.5 Felsic dikes

Several quartz porphyry, feldspar porphyry and quartz-feldspar porphyry dikes were observed within the study area. These vertical dikes are up to ten meters wide but on average are between one and three meters wide. All dikes cross-cut all observed structure, and vary in length from a few tens of meters to kilometers. These dikes weather to a white-beige colour and are pinkish-brown on the fresh surface (Fig. 4.6). Lamprophyre dikes occured in two localities within the exploration trenches of the Dogpaw Gold Zone. They are medium- to coarse grained,

brownish black in colour and strongly foliated. They are composed of subhedral amphibole and mica in a fine grained groundmass of similar mineralogy.

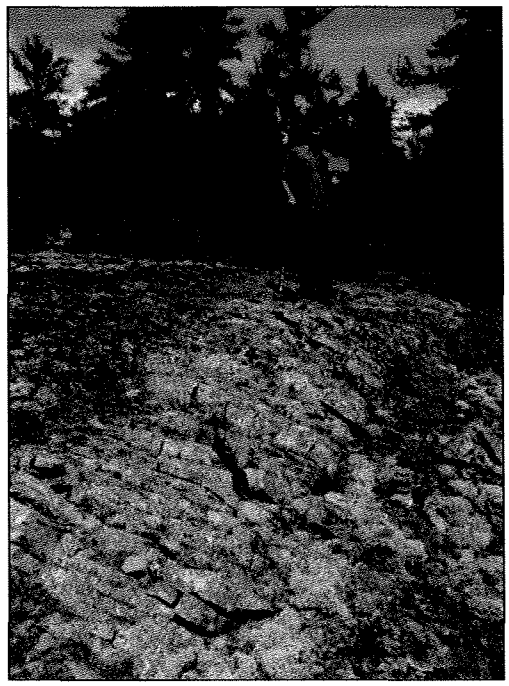

Figure 4.6 Photograph of a quartz feldspar porphyry dike cross cutting basalt of the mafic metavolcanic rocks of the Snake Bay Formation.

4.7 Structure

The structure of the WCGP is relatively simple and best illustrated in the cross section of Figure 4.1. The Emm Bay Formation overlies the Snake Bay Formation and both these units have been intruded by the Kakagi Sills with all three units dipping steeply to the east (Fig. 4.1). Throughout the sill and both volcanic units, are local indiscriminate shears and small faults on the meter- to centimeter-scale which display minor and local offset. Along the internal contact of the ultramafic and gabbroic rocks is brittle faulting, which likely formed from competency differences during regional scale deformation as reflected by the Cameron-Pipestone Lakes shear

zones. A major shear structure, the Dalby Bay Shear, cross cuts known stratigraphy and has produced mylonitised gabbro which is host to the Dogpaw Gold Zone (Fig. 4.1).

4.8 Petrography

4.8.1 Snake Bay Formation

The mafic volcanic rocks of the Snake Bay Formation are composed of fine- to medium grained chlorite with plagioclase feldspar, hornblende and/or actinolite-tremolite with interstitial quartz (alteration product) and lesser amounts of clinopyroxene (Fig. 4.7). Plagioclase phenocrysts are locally altered to mica (muscovite) and carbonate (calcite and Fe-dolomite locally) along grain boundaries and cleavage planes (Fig. 4.7 B). Mafic phases (phenocrysts and groundmass of hornblende and pyroxene) are locally moderately altered to carbonate, primarily ankerite as well as actinolite-tremolite (Fig. 4.7 A and C). Sulphide minerals include disseminated pyrite, pyrrhotite and chalcopyrite. Oxide minerals include trace amounts of magnetite and ilmenite. Porphyritic basalts contain up to 30% locally of medium to coarse grained plagioclase phenocrysts within a fine grained chlorite altered groundmass (Fig. 4.7 B). These phenocrysts are generally subhedral and strongly altered to muscovite. Figures 4.7 A and C show the distinct differences between tuffaceous and basaltic rocks, respectively. The tuffaceous rocks are generally aphanitic and moderately foliated whereas basaltic rocks are generally more crystalline, with subhedral to anhedral plagioglase, and are weakly foliated.

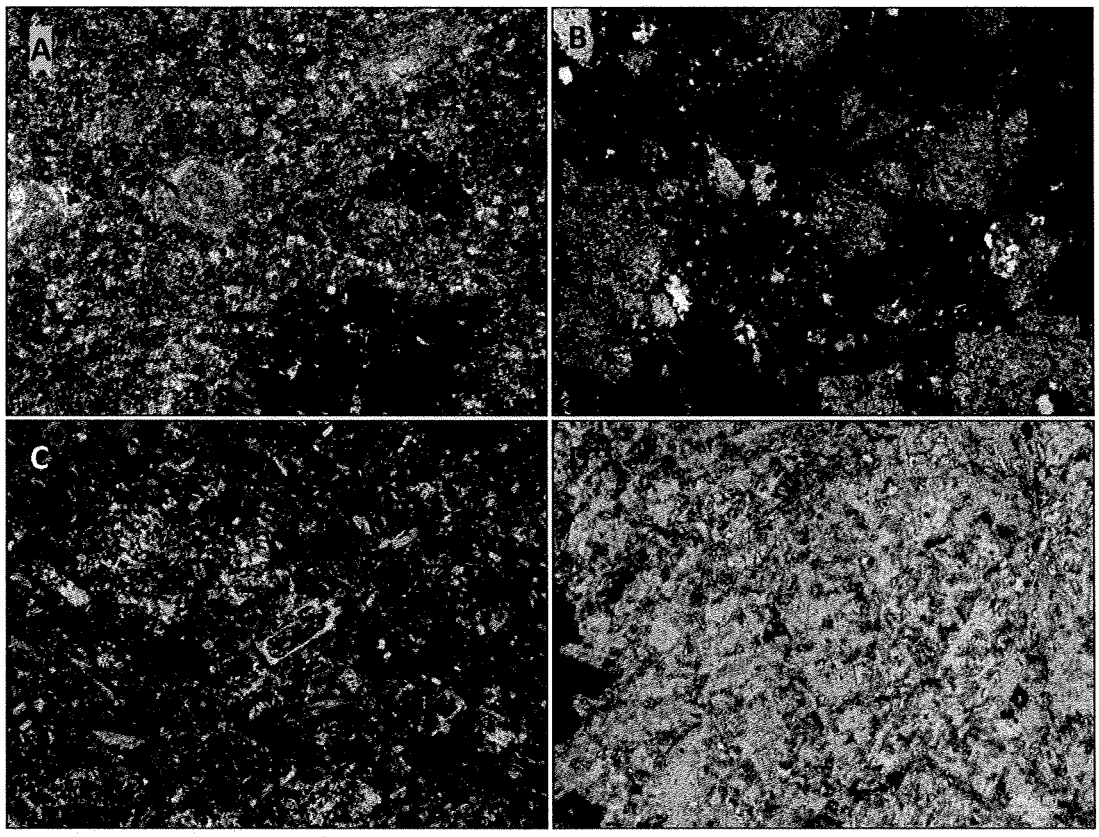

Figure 4.7 Photomicrographs of typical basalt of the Snake Bay Formation. A- fine grained chlorite altered tuff, sample 07-135 plane polarized light. B- porphyritic basalt, sample 07-138 plane polarized light. C- typical chlorite and plagioclase groundmass, sample 07-139 plane polarized light. D- extensive chlorite altered basalt, sample 07-97 transmitted light.

4.8.2 Emm Bay Formation

Mineralogically these rocks are comprised nearly entirely of chlorite, plagioclase, muscovite and quartz in varying amounts (Fig. 4.5). The groundmass of the tuffaceous rocks and tuff breccias is strongly foliated and composed of elongate needles and mats of chlorite and associated, plagioclase (Fig. 4.5 A and D). Breccia fragments are composed of medium- to coarse grained quartz and plagioclase with chlorite; vesicles have been infilled with carbonate (Fig. 4.5 B). The lapilli tuff is mostly composed of subhedral grains of plagioclase within a fine-

grained chlorite altered groundmass nearly identical to the rest of the tuff from throughout the rest of the Emm Bay Formation (Fig. 4.5 C).

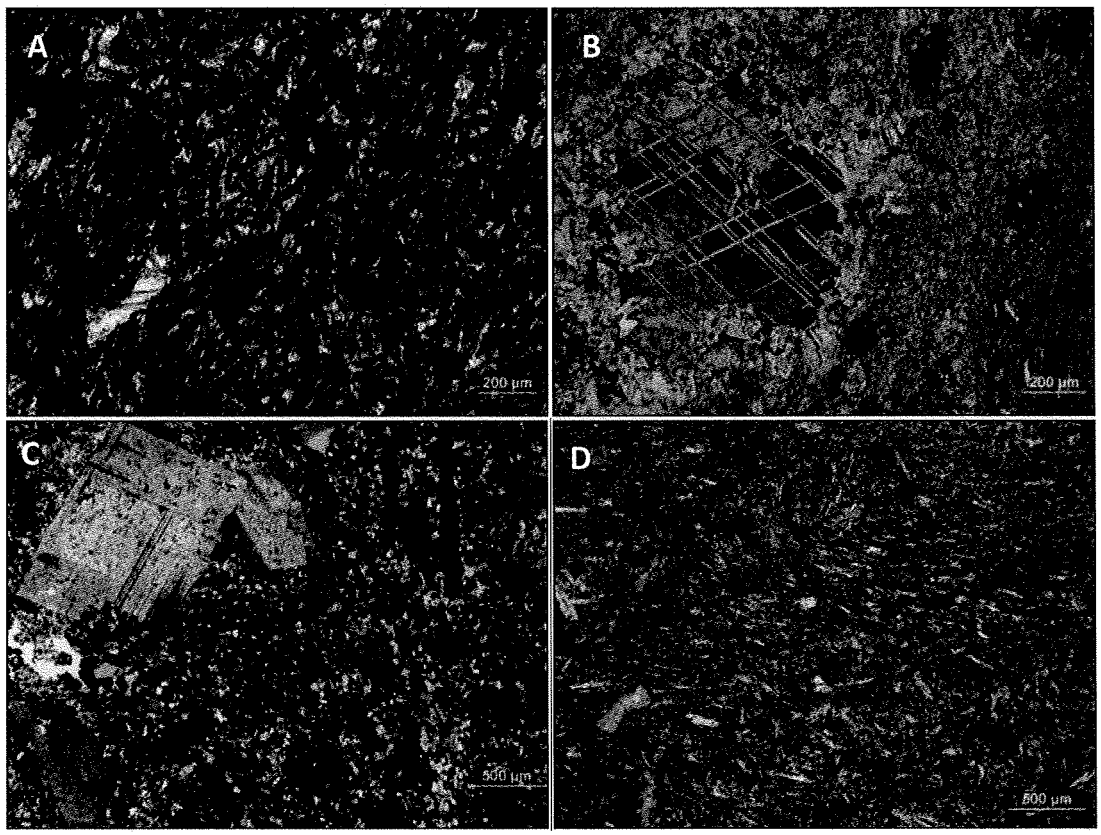

Figure 4.5. Photomicrographs of samples from the Emm Bay Formation. A- chlorite altered tuff, sample 07-139 plane polarized light. B- carbonate filled vesicle from a sample of tuff breccias, sample 197104 plane polarized light. C- coarse plagioclase from lapilli tuff, sample 07-93 plane polarized light. D- fine grained chlorite altered tuff groundmass from a sample of tuff breccias, sample 07-96 transmitted light.

4.8.3 Gabbro

The gabbros are composed of equal amounts of coarse grained plagioclase feldspar and actinolinite-tremolite (Fig. 4.6). These rocks contain lesser amounts of alteration minerals including chlorite and quartz along with muscovite and carbonate. Plagioclase occurs as large coarse grained euhedral crystals as well as small subhedral grains as part of the groundmass (Fig.

4.6 A and B, respectively). Plagioclase is often extensively altered to muscovite as well as locally to carbonates (Fig. 4.6 C). Actinolite-tremolite forms small brown green crystals which are subhedral to anhedral and moderately pleochroic (Fig. 4.6). Chlorite alteration is extensive throughout all samples of gabbro (Fig. 4.6 C and D).

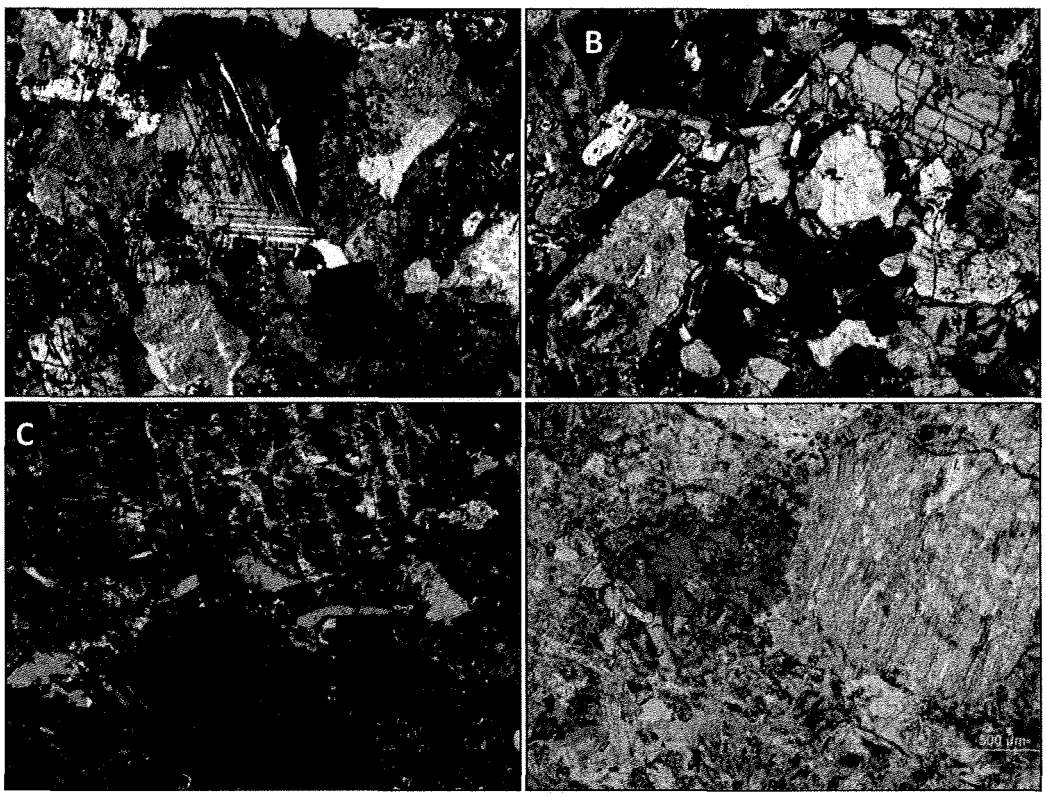

Figure 4.6. Photomicrographs of samples from the Kakagi Gabbro sill. A- coarse grained plagioclase with amphibole, sample 07-65 plane polarized light. B- medium grained gabbro with interstitial augite and carbonate alteration, sample 07-58 plane polarized light. C- abundant chlorite alteration, sample 07-70 plane polarized light. D- strongly chlorite altered gabbro, sample 07-79 transmitted light.

4.8.4 Ultramafic Rocks

Peridotites contain coarse grained cumulate textured olivines which have been extensively altered to serpentine (Fig. 4.7 A). Olivine can form cumulates with up to 65% interstitial orthopyroxene and clinopyroxene and lesser amounts of plagioclase. In the

pyroxenites hypersthene forms the coarsest grained and most abundant phase at roughly 65%. Orthopyroxene generally forms subhedral grains which are generally strongly altered to serpentine and chlorite (Fig. 4.7 B and D). Locally, small inclusions of olivine are observed within orthopyroxene grains, however, olivine never accounts for more than 2% of total volume, and these olivines are almost always strongly altered to serpentine (Fig. 4.7 C). Subhedral grains of plagioclase and clinopyroxene (augite) form interstitially to coarser hypersthene grains (Fig. 4.7 D). Alteration of the primary minerals is virtually identical in both the peridotites and pyroxenites. Quartz, hornblende and magnetite are present in lesser amounts in most samples (Fig. 4.7 D). The quartz occurs adjacent to the plagioclase and has slightly replaced the plagioclase in most rocks. Interstitial plagioclase is altered to muscovite and amphibole rims olivine (Fig. 4.7).

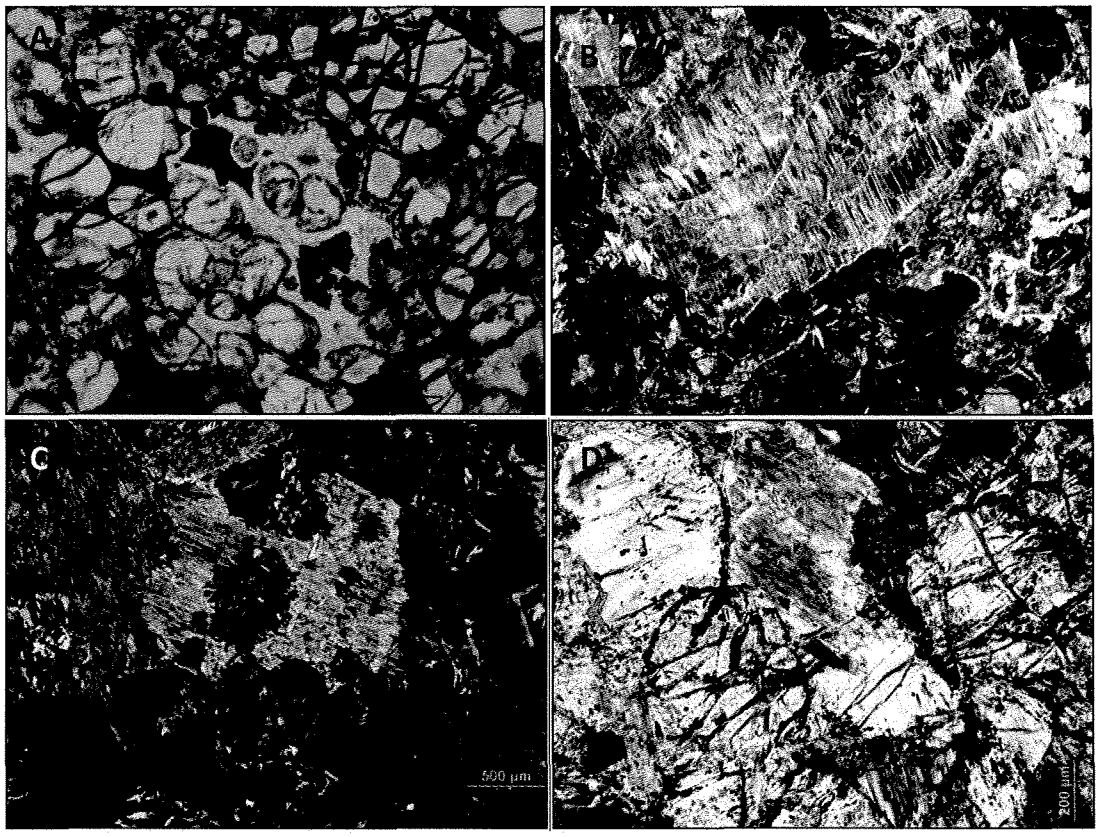

Figure 4.7. Photomicrographs of samples from the ultramafic rocks of the Kakagi Sill. A- cumulate textured olivine in peridotite, sample 07-149 plane polarized light. B- altered orthopyroxene, sample 07-64 plane polarized light. C- orthopyroxene with inclusions of olivine, sample 07-80 plane polarized light. D- altered pyroxenite, sample 07-131 plane polarized light.

Chapter 5:

Whole Rock and Radiogenic Isotope Geochemistry

5.1 Introduction

Major and trace element geochemical analyses of rocks from the WCGP were undertaken to investigate the tectonic setting of the belt, to provide correlations with other assemblages within the Kakagi-Rowan Lakes greenstone belts and to add to the small data set which exists for the Snake Bay Formation, Emm Bay Formation and Kakagi Gabbro Sills. Fifty samples were analyzed from the four main suites (eleven from the Snake Bay Formation, nine from the Emm Bay Formation, twenty from the Kakagi Gabbro Sill, seven from the ultramafic basal unit of the Kakagi Sill) and three from quartz-feldspar porphyry dikes. Sample locations are shown on Figure 4.1. The full data set can be found in Appendix D with representative geochemical data provided in Table 5.1.

Table 5.1 Representative major and trace element data for rocks of the WCGP.

	Snake Bay Formation		Emm Bay Formation		Kakagi Sills		Kakagi Sills	
	Mafic Metavolcanic Rocks		*Felsic Metavolcanic Rocks*		*Gabbro*		*Ultramafic Rocks*	
Sample ID	07-51	07-142	197104	197106	07-112	07-124	07-128	07-147
Al_2O_3	14.38	12.94	13.05	14.11	16.54	16.02	9.16	8.84
CaO	6.92	4.69	5.72	4.72	11.89	9.11	6.53	10.59
Fe_2O_3	16	17.05	5.46	5.21	10.19	11.48	12.11	10.85
K_2O	0.07	0.09	0.64	0.93	0.28	0.28	0.15	0.08
LOI	3.44	4.7	5.69	5.76	2.66	3.46	5	1.64
MgO	6.1	4.49	2.36	2.61	6.71	5.91	19.97	16.89
MnO	0 22	0.19	0.09	0.11	0.18	0.22	0.22	0.21
Na_2●	2.89	3.98	4.6	4.74	2.2	2.39	0.84	0.58
P_2O_5	0.16	0.22	0.12	0.19	0.03	0.04	0.04	0.01
SiO_2	48.73	49.68	60.9	60.72	50.25	50.94	45.31	51.03
TiO_2	1.68	2 09	0.7	0.57	0.56	0.53	0.39	0.25
Total	100.6	100.11	99.31	99.67	101.49	100.38	99.72	100.97
Ba	29.4	34.5	116.6	299.7	47.5	85.3	41.8	9
Be	0.72	0.77	0.61	0.95	0.18	0.25	0.17	0.07
Bi	0.012	0.024		0.067	0.012	0.021	0.033	0.057
Cd	0.08	0.05	0.05	0.08	0.03	0.03	0.07	0.04
Ce	17.4	22.4	21.8	46.3	4.8	5.9	4.5	1.8
Co	40.6	35.1	20.5	20.6	81.8	312.6	88.1	66.1
Cr	154	91	111	110			>600	>600
Cs	0.912	0.614	0.611	1.051	0.459	0.398	1.273	0.746
Cu	60	45	38	20	46	119	63	26
Dy	5.5	6.7	2.3	2.2	1.8	1.7	1.5	0.9
Er	3.29	4.04	1.31	1.15	1.15	1.08	1.03	0.6
Eu	1.284	1.417	0.879	1.159	0.404	0.481	0.402	0.189
Ga	19.83	20.81	12.8	15.98	14.15	14.57	8.2	6.87
Gd	4.56	5.8	2.53	3.01	1.32	1.36	1.19	0.67
Hf	2.79	3.56	2.16	2.73	0.78	0.87	0.73	0.34
Ho	1.198	1.436	0.454	0.403	0.402	0.378	0.356	0.211
La	6.86	8.58	9.56	22.33	2.08	2.66	1.95	0.81
Li	16.5	20.5	9.2	11.9	5.2	11.9	25.5	4.2
Lu	0.547	0.642	0.19	0.161	0.186	0.182	0.173	0.101
Mo	0.42	0.65	0.57	0.37	0.16	0.34	0.16	0.15
Nb	4.88	6.78	2.89	3.51	1.09	1.32	0.91	0.33
Nd	12.75	16.34	11.8	21.98	3.43	3.77	2.92	1.43
Ni	65	38	30	30	58	50	667	236
Pb	3.2	2.3	1.1	2.4	0.5	0.8	1.9	0.5
Pr	2.53	3.28	2.85	5.7	0.72	0.81	0.62	0.28
Rb	2	1.9	17.7	26.9	6.1	5.3	3.1	2.5
Sb	0.35	0.72	0.16	0.22		0.16	0.1	0.07
Sc	35.1	38.3	15.3	14.8	44.1	44.4	34.1	48.1
Sm	3.89	4.83	2.63	4.02	1.05	1.08	0.88	0.49
Sn	1.96	0.76	0.68	0.76	0.25	0.48	0.31	0.12
Sr	178	165	267	262	141	162	24	42
Ta	0.4	0.4	0.2	0.2	0.2	1		
Tb	0.813	1.026	0.38	0.404	0.249	0.244	0.219	0.129
Th	0.65	0.85	1.34	3.66	0.34	0.34	0.33	0.11
Ti	7785	9665	4281	3685	2715	2827	2026	1262
Tl	0.024	0.012	0.058	0.089	0.024	0.023	0.02	0.021
Tm	0.538	0.648	0.189	0.16	0.181	0.172	0.165	0.093
U	0.16	0.23	0.31	0.79	0.09	0.09	0.09	0.03
V	289	331	122	118	221	234	169	161
W		0.5	14.9	11	>120	>120	4.8	6.3
Y	34.42	41.2	12.57	11.13	11.3	10.96	10.03	5.85
Yb	3.403	4.268	1.247	1.053	1.178	1.12	1.042	0.607
Zn	127	115	44	53	48	58	109	57
Zr	104	136	83	107	27	33	26	11
$(La/Yb)_{cn}$	1.44	1.11	5.49	15.20	1.26	1.70	1.34	0.95
$(La/Sm)_{cn}$	1.13	0.96	2.34	3.58	1.27	1.59	1.43	1.06
$(La/Y)_{cn}$	1.42	1.16	5.03	13.28	1.21	1.60	1.28	0.91
Nb/Nb*	0.67	0.93	0.25	0.12	0.45	0.41	0.40	0.33
Zr/Zr*	1.02	1.06	1.03	0.78	0.98	1.13	1.12	0.90
Ti/Ti*	1.12	1.14	0.68	0.41	1.23	1.17	1.03	1.15

5.2 Element Mobility

Traditional geochemical classification using major and trace elements for igneous rocks, generally does not work well for Archean rocks because most elements used in these classifications rely on mobile elements and most Archean rocks show strong evidence for mobility of these elements (Pearce, 1996). For example elements such as Si, Ca, Na, K and Mg are highly mobile during greenschist facies metamorphic reactions (Pearce, 1996). Since the rocks of the WCGP have undergone metamorphism from mid to upper greenschist facies to even as high as lower amphibolite facies (Chapter 3), traditional plots like the total alkali ($Na_2O + K_2O$) versus silica (SiO_2) diagram of Le Bas et al. (1986) must be used with caution. Instead it is imperative to investigate element mobility through comparison with immobile elements. Elements which are traditionally immobile under these conditions consist of the high field strength elements (HFSE) which include Th, Nb, Ta, Zr, and Hf and the rare earth elements (except Eu and Ce) as well as Y, Sc, and V which are least prone to mobility during metamorphism (Pearce, 1996). Before discrimination plots using immobile elements can be used to classify igneous suites, the immobility of key elements for the rocks at the WCGP must be determined. Plots of Na_2O, K_2O, Al_2O_3, CaO, MgO, and SiO_2 versus TiO_2 are shown in Figure 5.1 and Th, La, Y, Yb and Zr versus Nb in Figure 5.2.

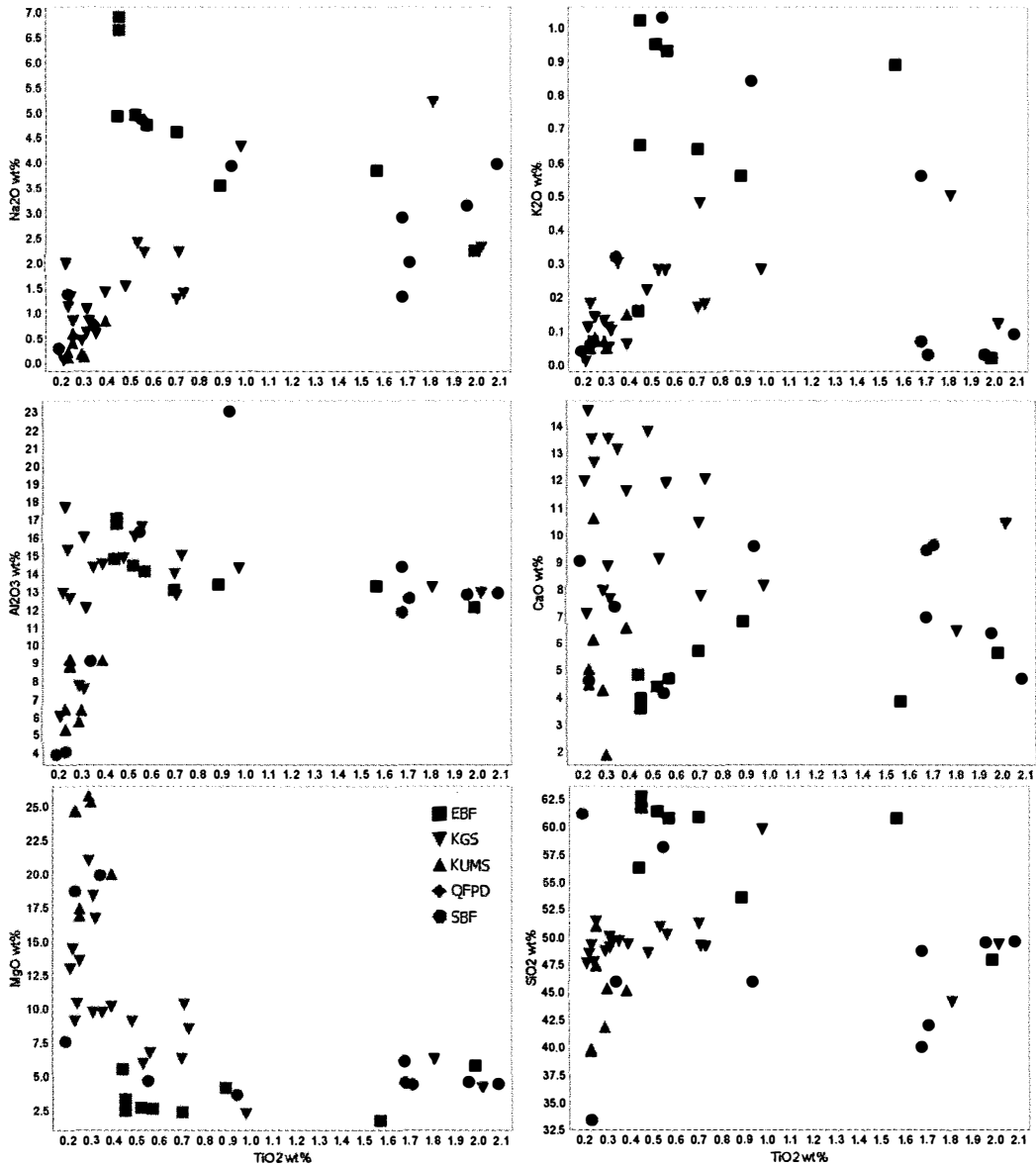

Figure 5.1 Variation diagram showing mobile elements and immobile elements versus TiO_2, values are in weight percent oxides. Legend description: SBF are samples from the Snake Bay Formation, EBF are samples from the Emm Bay Formation, KGS are samples from the Kakagi Gabbro Sill, KUMS are samples from the ultramafic rocks of the Kakagi Sill and QFPD are samples of quartz feldspar porphyry dikes.

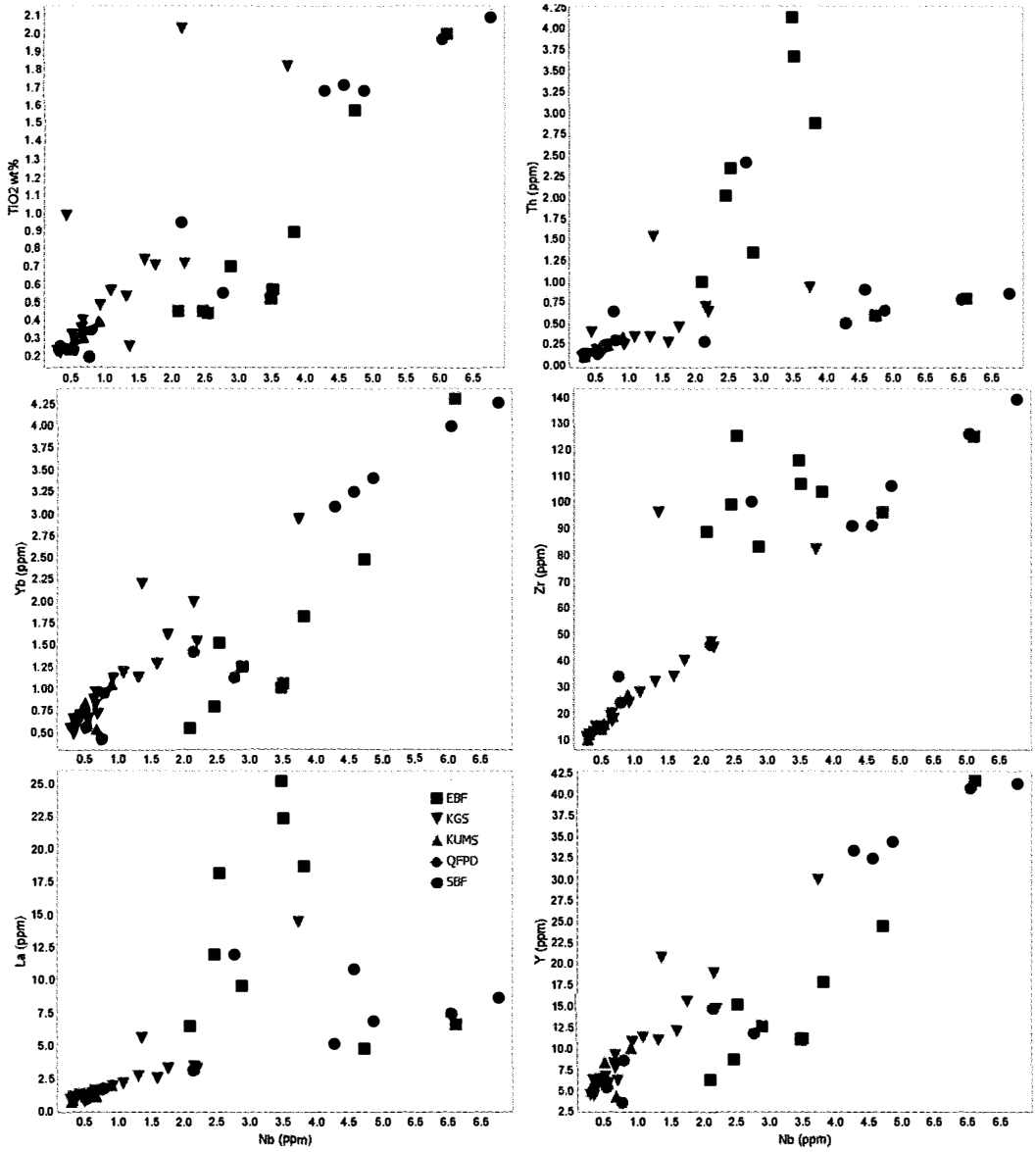

Figure 5.2 Variation diagram for mobile and immobile elements plotted against Nb. Elements are in parts per million and oxides are in weight percent. Legend description is the same as for Figure 5.1.

Plots which show a roughly linear distribution that passes through the origin are interpreted to be relatively immobile whereas scattered plots indicate predominantly more mobile elements (MacLean, 1990). The relatively scattered data of SiO_2, Na_2O, K_2O, CaO from Figure 5.1 suggests that these elements were highly mobile during metamorphism. The relatively tight cluster of TiO_2, Nb, Th, La, Y, Yb and Zr in Figure

5.2 suggests that these elements were relatively immobile and thus were not significantly reset during regional metamorphism and therefore can be used for chemostratigraphy, petrological inferences, and rock classification.

5.3 Geochemical Classification

The rocks of the Snake Bay Formation generally lie within the basalt field of a total alkali versus silica diagram (TAS) with a few samples plotting in the picro basalt and foidite field (Rollinson, 1993; Fig. 5.3). Rocks of the Kakagi sill (both ultramafic and gabbro) plot within the basalt field where the rocks from the Emm Bay formation plot within the basalt through the trachyandesitic fields (Fig. 5.3). However, as discussed above, the mobility of alkali phases means that the TAS diagram may not accurately represent true affinity of the rocks.

A modified Winchester and Floyd (1977) plot can be used to determine rock type using immobile elements. This plot uses Zr/TiO_2 as a fractionation monitor instead of SiO_2 and uses the ratio Nb/Y as a proxy for alkalinity, all of which are elements that are interpreted to be relatively immobile for the rocks of the WCGP. The rocks of the Snake Bay Formation plot predominantly in the basalt-andesite field and rocks of the Emm Bay Formation plot within the andesite to rhyodacite field, which is consistent with field and petrographic observations (Fig. 5.4). Intrusive rocks of the Kakagi Sill plot in the basalt field, comparable to the mafic volcanic rocks of the Snake Bay Formation (Fig. 5.4).

The basaltic to andesitic rocks of the Snake Bay Formation have been further assessed based on MgO content. Only two samples (07-150 and 07-57; both samples of basaltic flows) of the eleven samples contain greater than 18 wt. % MgO characteristic of

komatiitic rocks (Hill et al., 1990); however, these rocks show no sign of a quenched or spinifex texture in hand sample or thin section, and these elevated MgO contents are likely related to an increase in dolomitic carbonate and serpentine alteration or original cumulate olivine now altered to these phases. This is supported by the high loss on ignition in these samples (Appendix D).

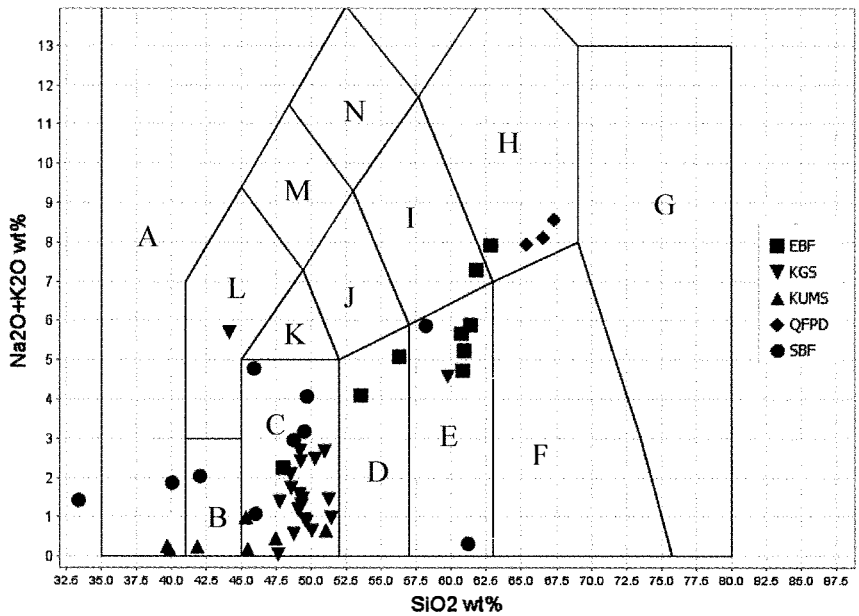

Figure 5.3. Total alkalis versus silica diagram for the rocks of the WCGP modified from Rollison (1993). Fields: A- foidite, B- picro basalt, C- basalt D- basaltic andesite, E- andesite, F- dacite, G- rhyolite, H- trachydacite, I- trachyandesite, J- basaltic trachyandesite, K- trachybasalt, L- tephrite, M- phonotephrite, N- tephriphonolite. Legend description: SBF is the Snake Bay Formation, EBF is the Emm Bay Formation, KGS is the Kakagi Gabbro Sill, KUMS is the ultramafic rocks of the Kakagi Sill and QFPD are samples from the quartz feldspar porphyry dikes.

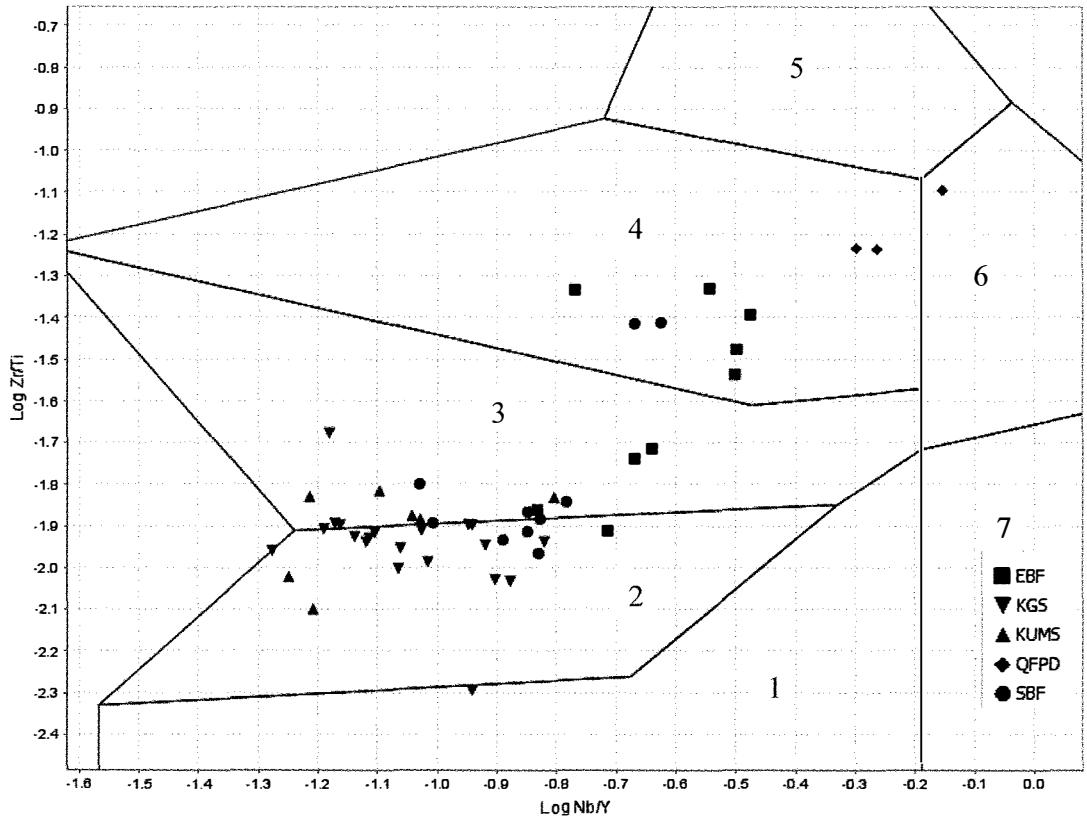

Figure 5.4 Winchester and Floyd (1977) rock type discrimination diagram for rocks of the WCGP. Fields are defined as follows: 1- subalkaline basalt, 2- andesite-basalt, 3- andesite, 4- rhyodacite-dacite, 5- rhyolite, 6- Trachyandesite, 7- alkaline basalt. Legend description: SBF is the Snake Bay Formation, EBF is the Emm Bay Formation, KGS is the Kakagi Gabbro Sill, KUMS is the ultramafic rocks of the Kakagi Sill and QFPD are samples of quartz feldspar porphyry dikes.

5.4 Primitive mantle normalised multi-element plots

5.4.1 Introduction

Trace element plots normalised to values of primitive mantle from Sun and McDonough (1989) have been used to discriminate each lithology and evaluate the tectonic setting in which they were formed. Since the rocks of the WCGP have been shown to have undergone extensive greenschist facies to lower amphibolite facies metamorphism (Chapter 4), the high field strength elements (HFSE; Th, Nb, Zr and Hf)

as well as the rare earth elements (REE), which remain relatively immobile are used for these diagrams.

5.4.2 Trace element plots of the Snake Bay Formation

Rocks of the Snake Bay Formation have been plotted on a primitive mantle normalised plot in Figure 5.5. Two suites (suite I- black solid circles and II- black dashes) have been identified based on the differences in REE slopes and HFSE concentrations. Suite I is characterised by a large negative Nb anomaly (Nb/Nb* = 0.54-0.17; Fig. 5.6) and relatively shallow light REE slope with La/Sm_{cn} values between 1.17 and 1.59 and minor heavy REE fractionation with Gd/Yb_{cn} values between 0.95 and 2.39. Silica contents for suite I range from 40 to 64 wt% (as samples with high silica wt% show abundant silicification this is not thought to be a primary feature; Fig. 5.7). Suite II (black dashes Figs. 5.5 and 5.6) is characterised by much smaller negative Nb anomalies (Nb/Nb* = 0.67-0.80; Fig. 5.6). The REE slope of suite II is almost flat with La/Sm_{cn} values between 1.09 to 1.15 and with Gd/Yb_{cn} values between 1.12 and 1.16. Silica values for the suite II mafic volcanic rocks range between approximately 40 wt% and 50 wt% (Fig. 5.7).

The negative Nb anomaly may be a primary feature of a supra subduction zone melt or it may suggest crustal contamination of the source melts for the volcanic rocks of the SBF, with the differences between suite I and II being the result of varying degrees of contamination. Figure 5.6 can be used to assess crustal. Rocks of the Emm Bay Formation show the strongest correlation between decreasing Nb/Nb* values and in increasing in SiO_2 indicative of crustal contamination.

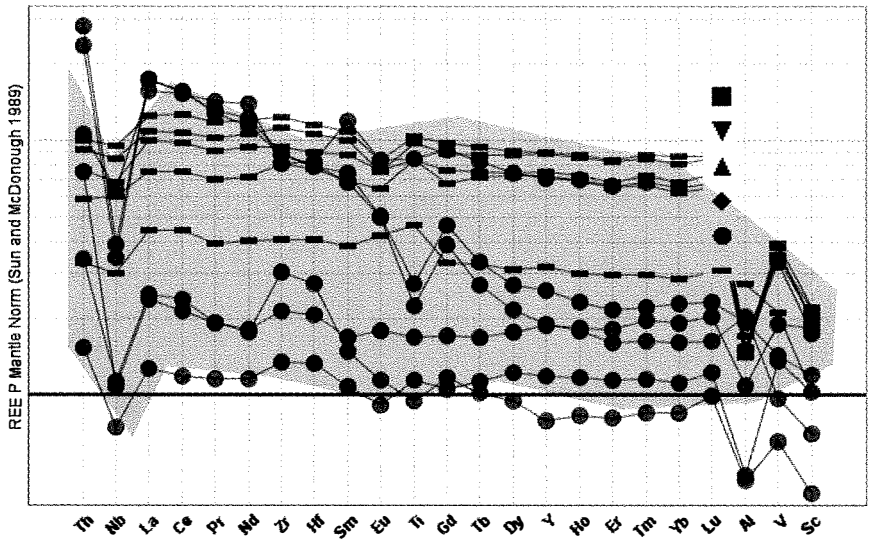

Figure 5.5. Primitive mantle normalised plots of samples from the Snake Bay Formation. Samples from suite I plot as circles and suite II as dashes. Normalising values are from Sun and McDonough (1989). Grey fields indicate range for contaminated Archean basalts from Hollings and Kerrich (1999).

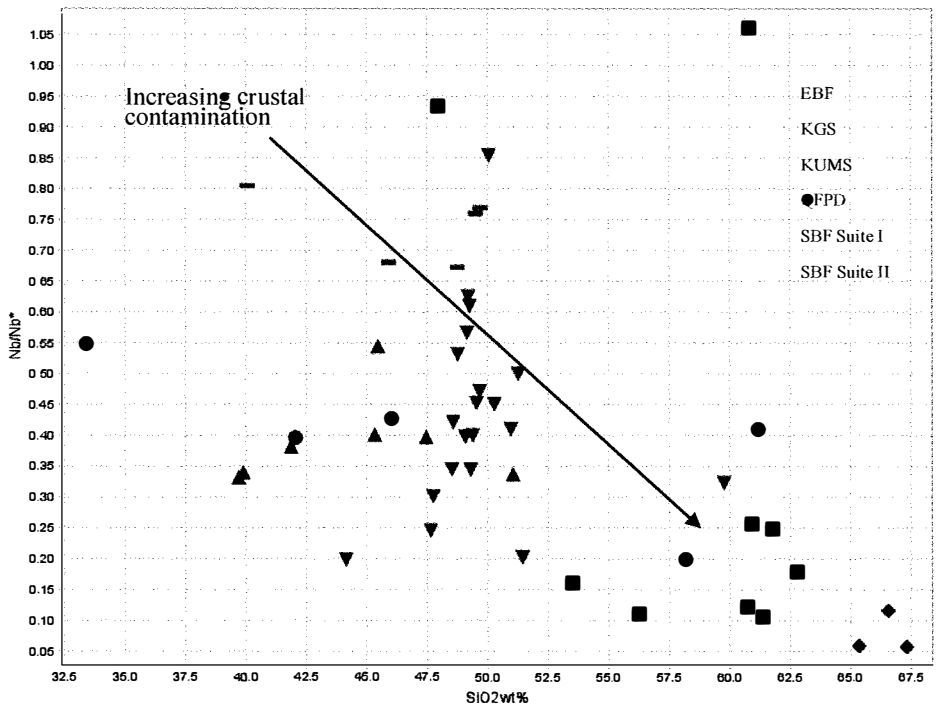

Figure 5.6. Nb/Nb* versus SiO_2 diagram for rocks of the WCGP. Legend is the same as Figure 5.1. Samples from suite I of the SBF plot as circles and suite II as dashes.

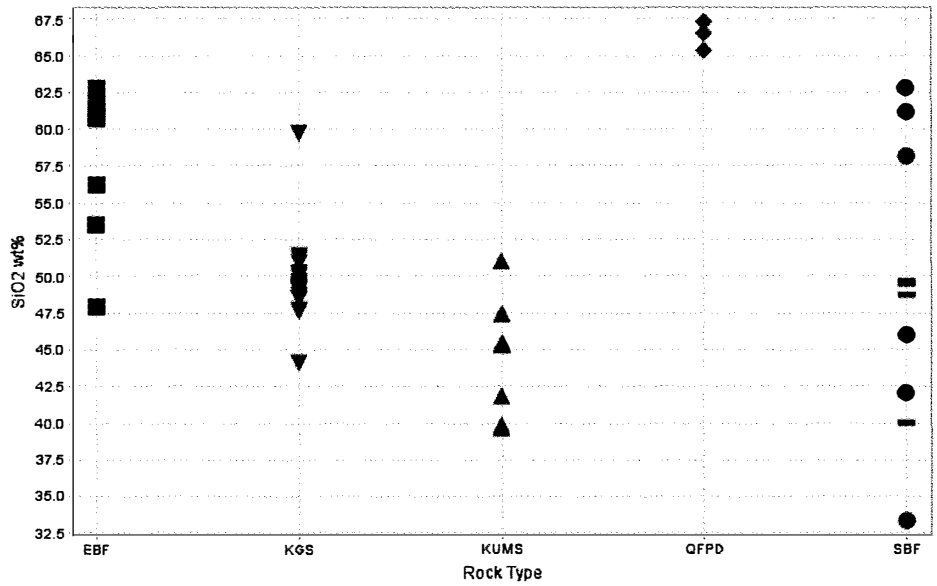

Figure 5.7. Silica content versus lithology for rocks of the WCGP. Legend is the same as Figure 5.1. Samples from suite I of the SBF plot as circles and suite II as dashes.

5.4.3 Trace element plots of the Emm Bay Formation

Rocks of the Emm Bay Formation have been plotted on a primitive mantle normalised plot on Figure 5.8. These samples are characterised by a strong negative Nb anomaly ($Nb/Nb^* = 0.15$-0.25; Fig. 5.6), La/Sm_{cn} values between 2.34 and 3.81 and Gd/Yb_{cn} values between 1.67 and 2.61. Silica contents for the EBF range from 53 to 63 wt% (Fig. 5.7).

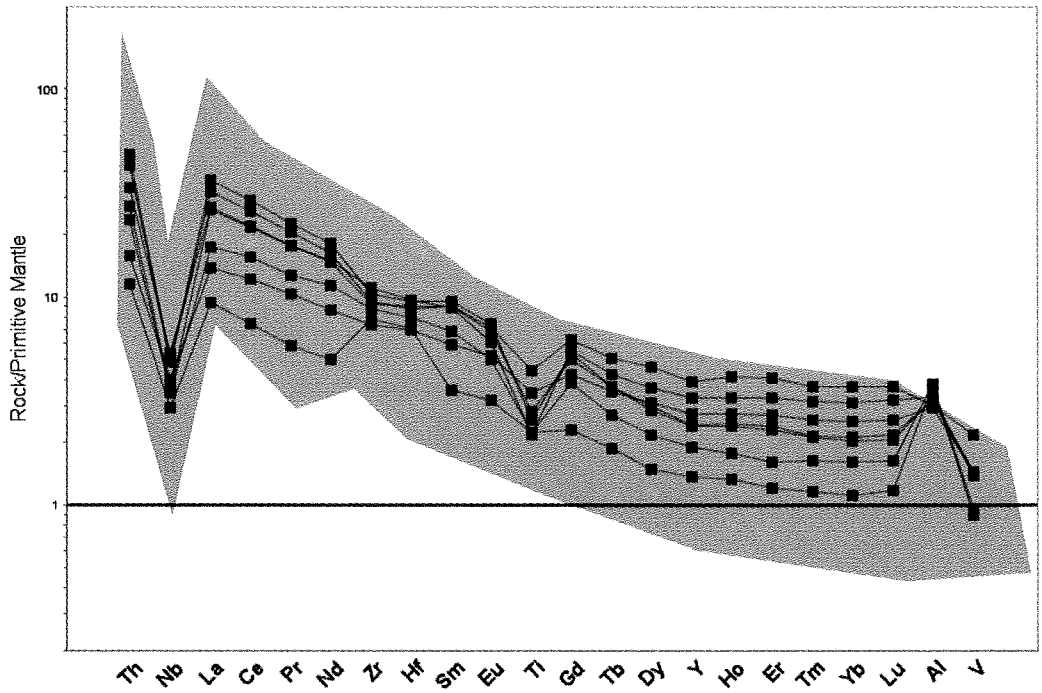

Figure 5.8. Primitive mantle normalised plots of samples from the Emm Bay Formation. Normalising values are from Sun and McDonough (1989). Grey fields for typical Archean island arc tholeiites from Hollings and Wyman (1999).

5.4.4 Trace element plots of the gabbro of the Kakagi Sill

Gabbroic rocks of the Kakagi Sill have been plotted on a primitive mantle normalised plot in Figure 5.9. These samples are characterised by a moderate to strong negative Nb anomaly (Nb/Nb* = 0.19- 0.85; Fig. 5.9), moderate light REE enrichment with La/Sm_{cn} values between 0.85 and 2.37 and moderate heavy REE fractionation with Gd/Yb_{cn} with values between 0.71 and 1.26. Silica contents range from 44 to 60 weight percent (Fig. 5.7). Samples with elevated silica content (greater than 45% SiO_2) show only weak silicification and their silica content as reported likely reflects a transition from gabbro to mela-gabbro proximal to the sill's contact with rocks of the Emm Bay Formation, either suggestive of internal differentiation of the sill or assimilation of more felsic material into the melt. A negative or positive Ti anomaly (Fig. 5.9) on the

primitive mantle normalised plots in some samples are likely related to the absence or presence, respectively, of rutile within individual samples.

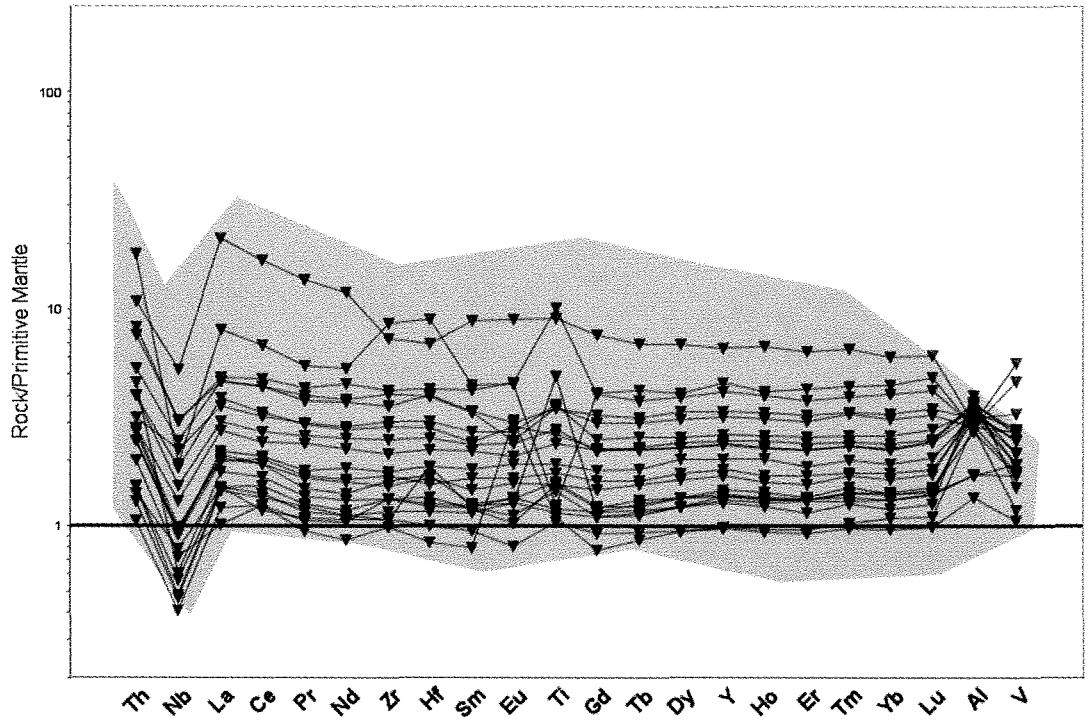

Figure 5.9. Primitive mantle normalised plots of samples for the gabbro of the Kakagi Sill. Normalising values are from Sun and McDonough (1989). Grey fields indicate range for contaminated Archean basalts from Hollings and Kerrich (1999).

5.4.5 Trace element plots of the ultramafic basal unit of the Kakagi Sill

Ultramafic rocks (cumulate peridotites and pyroxenites) of the Kakagi Sill have been plotted on a primitive mantle normalised plot in Figure 5.10. These samples are characterised by a strong negative Nb anomaly (Nb/Nb* = 0.33- 0.54; Fig. 5.6) and relatively flat light REE slope with La/Sm_{cn} values between 1.06 and 1.34 and weak heavy REE fractionation with Gd/Yb_{cn} values between 0.75 and 0.96. Silica contents range from 39 to 51 wt% (Fig. 5.7); however, samples with elevated silica content show more pronounced silicification and likely do not represent primary compositions.

Europium anomalies, either positive or negative, are a reflection of the percentage of interstitial plagioclase. The pyroxenites, which have interstitial plagioclase feldspar, plot with elevated Eu values whereas cumulate peridotites, which are predominantly devoid of interstitial plagioclase, plot with negative Eu values as plagioclase sequesters Eu (Phinney, 1990).

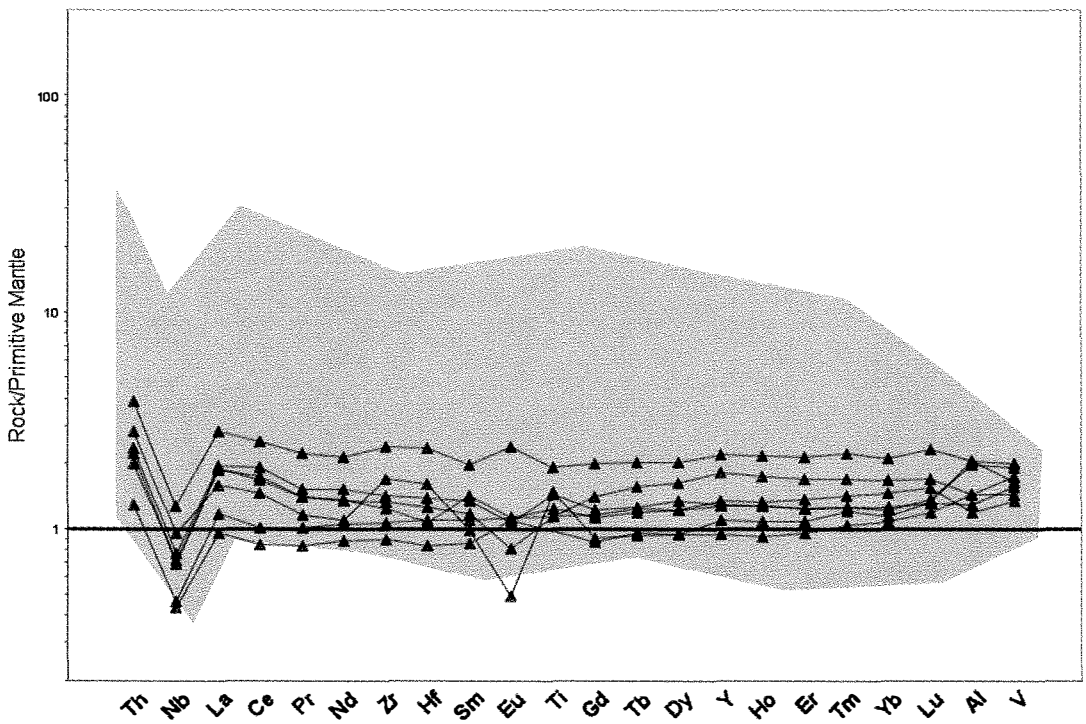

Figure 5.10. Primitive mantle normalised plots of samples for the ultramafic basal unit of the Kakagi Sill. Normalising values are from Sun and McDonough (1989). Grey fields indicate range for contaminated Archean basalts from Hollings and Kerrich (1999).

5.5 Tectonic Setting

Distinguishing between calc-alkaline and tholeiite volcanic rocks can be undertaken using an AFM (alkali-iron oxide- magnesium oxide) ternary plot; however, the mobility of these phases as shown in Figures 5.1 and 5.2 precludes using this plot. It is possible, however, to distinguish between tholeiitic and calc alkaline volcanism by

analysing the slope of the REE on a primitive mantle normalised plots (Hollings, 1998). A tholeiitic trend for the volcanic rocks of the Snake Bay Formation (suite I and II) is suggested by the low La/Yb_{cn} values (1.13 to 1.44; Hollings, 1998). In contrast the volcanic rocks of the Emm Bay Formation are characterised by elevated La/Yb_{cn} values (5.49 to 15.20), suggesting a calc-alkaline affinity. Gabbroic rocks of the Kakagi Sill show a tholeiitic trend evidenced by low La/Yb_{cn} ratios between 0.72 and 1.80, which is comparable to the ultramafic rocks of the Kakagi Sill with La/Yb_{cn} values between 0.83 and 1.54.

Determining the tectonic setting of the Archean volcanic and intrusive rocks of the WCGP can be accomplished by comparing them with analogs from modern settings or other well documented Archean suites (Figs. 5.5, 5.9 and 5.10). A diagram plotting Nb/Nb* values versus La/Yb_{cn} has been used to discriminate suites based on their tectonic environment of emplacement (Fig. 5.11). Samples from the tholeiitic Snake Bay Formation and the gabbroic and ultramafic suites of the Kakagi Sill lie within the field of magmatism associated with either plume derived ocean plateau settings or oceanic island arc tholeiite basalts (Fig. 5.11). The calc-alkaline suite of the Emm Bay Formation can be compared with rocks of modern back arc systems (Fig. 5.11). The strongly negative Nb anomaly, combined with a steep REE slope, indicate subduction-related volcanism (Fig. 5.8; Pearce, 2007). This is a result of dehydration of down going slab, which yields a fluid enriched in LILE with respect to HFSE and from fluid mixing with partially melted mantle wedge material (Pearce and Peate, 1995; Pearce, 2007).

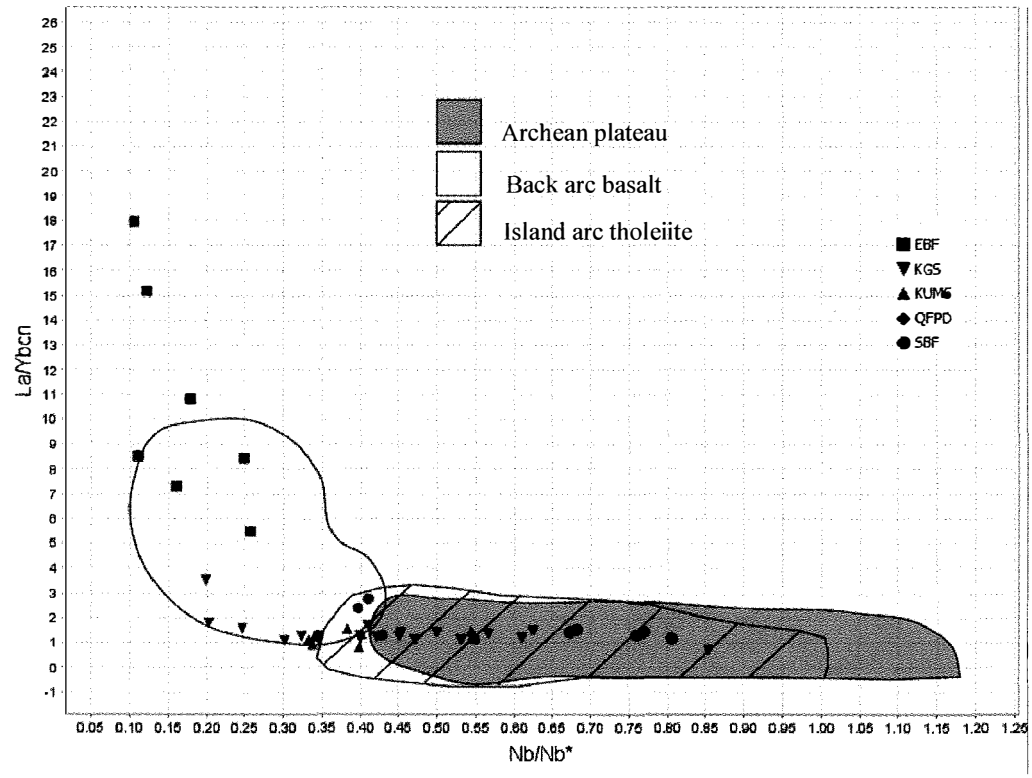

Figure 5.11. Plot of Nb/Nb* versus La/Yb_{cn} for samples of the WCGP. Defined fields are from Kerrich et al. (1999) for Archean plateau, Shinjo (1998) for back-arc basalts from the Okinawa back-arc basin and Hollings et al. (1999) for island arc tholeiites from the North Caribou Greenstone Belt. Legend description: SBF is the Snake Bay Formation, EBF is the Emm Bay Formation, KGS is the Kakagi Gabbro Sill, KUMS is the ultramafic rocks of the Kakagi Sill and QFPD are samples of quartz feldspar porphyry dikes.

Discrimination of depth of melting may help to further restrict the tectonic setting of the source rock for each of the units in the WCGP. Ocean plateau basalts are generally accepted to form from large scale partial melting from high temperature mantle plumes which have been interacting with the upper mantle. In contrast, mid-ocean ridge basalt (MORB) volcanism and tholeiitic to calc-alkaline oceanic arc sequences are interpreted to reflect partial melts from a shallower depleted source (Sun and McDonough, 1989; Pearce, 2007). However, it is important to determine if these samples represent primary melts or have undergone contamination during emplacement and to do this LILE/HFSE and LILE/REE ratios are examined in Figure 5.12. Th/Nb ratios may be used as a proxy

for LILE/HFSE ratios since Th and Nb are relatively immobile elements and have been shown to be immobile elements for rocks of the WCGP (Figs. 5.1 and 5.2). The upper continental crust is highly enriched in Th when compared with rocks of MORB affinity. Consequently, contamination of a melt by continental crust will produce elevated Th/Nb ratios (Pearce, 2007). Therefore Th/Yb ratios and Nb/Yb ratios can be used to distinguish between MORB, OIB, and volcanic arc settings (Fig 5.12).

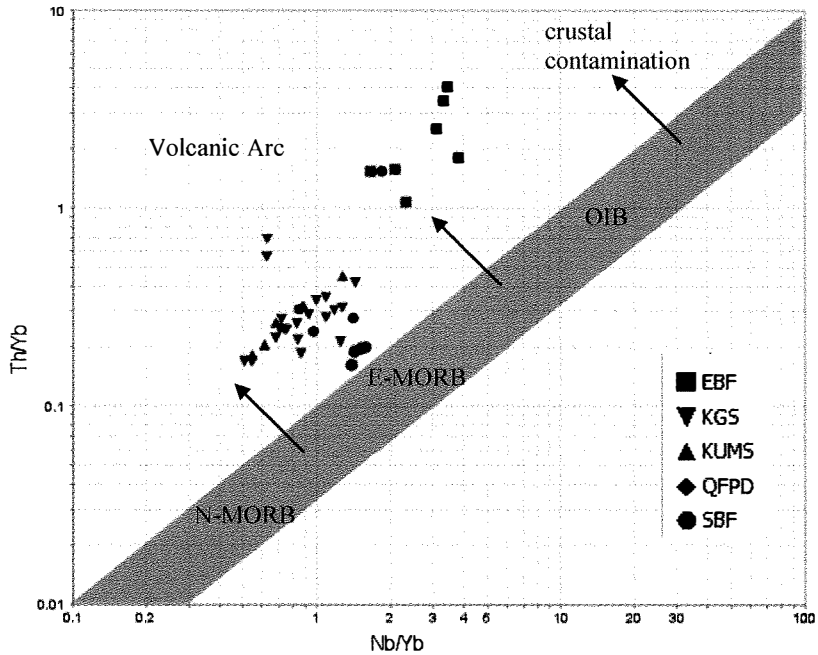

Figure 5.12. MORB-OIB array diagram from Pearce (2007). Legend description: SBF is the Snake Bay Formation, EBF is the Emm Bay Formation, KGS is the Kakagi Gabbro Sill, KUMS is the ultramafic rocks of the Kakagi Sill and QFPD is samples of quartz feldspar porphyry dikes.

Th/Yb ratios increase independently of Nb/Yb as enrichment of Th occurs with interaction with fluids from a down going slab (Fig. 5.12; Pearce, 2007). Modern uncontaminated MOR basalts have Th/Yb ratios less than 0.07. Rocks of the Snake Bay Formation, and the ultramafic and gabbroic suites of the Kakagi sill have Th/Yb ratios

between 0.16 and 2.1 indicating enriched values and possible contamination by continental crust. Rocks of the Emm Bay Formation have Th/Yb ratios between 0.18 and 2.53 again indicative of crustal contamination. Therefore samples which plot above the field on the MORB-OIB diagram are interpreted to be the result of enirichment via slab metasomatism or crustal contamination from basement rocks (Sun and McDonough, 1989; Pearce, 2007). Samples from the Emm Bay Formation plot well outside the MORB-OIB field which coupled with the pronounced negative Nb anomaly and with the LREE-enrichment, is typical of subduction related volcanism and this occurs when dehydration of a down going slab creates fluids becoming increasingly enriched in LILE with respect to HFSE (Pearce, 2007). This results in a metasomatised mantle that has a lower solidus due to fluid addition. Samples from the Snake Bay Formation, as well as the gabbro and ultramafic suites of the Kakagi Sill, plot above the E-MORB field of the MORB-OIB array which suggests that these rocks formed from deeper sources, however, have been effected by some degree of either crustal contamination or slab metasomatism (Figs. 5.5 and 5.12; Pearce, 2007).

5.6 Radiogenic Isotopes

Fourteen samples were analysed for samarium (^{147}Sm) and neodymium (^{144}Nd and ^{143}Nd) isotopes from the four main lithologies present within the study area (WCGP); four from the mafic metavolcanic rocks of the Snake Bay Formation, two felsic-to-intermediate metavolcanic rocks of the Emm Bay Formation, four from the gabbroic and four from the ultramafic units of the Kakagi Sill (Fig. 5.13). These analyses were undertaken to investigate whether the pronounced negative Nb anomalies and elevated

Th/Yb ratios were a product of crustal contamination from basement rocks upon emplacement or are the result of metasomatic alteration.

This isotope study was also undertaken to test the idea put forth by Davis and Edwards (1982) who dated a pegmatitic portion of gabbro from the Kakagi Sill and tuffaceous material of the Emm Bay Formation and determined that the sill was actually older than the rocks which it intruded (sample location A and B, respectively; Fig. 5.14). Davis and Edwards (1982) determined an age of 2724.8 +/- 2.5 Ma for the gabbros of the Kakagi Sill and an age of 2711.1 +/- 1.3 Ma for a felsic tuff from the Kakagi Lake Group (sample location B from Figure 5.14). They suggested that since the age of formation of the Kakagi Sill is from the lowermost section and the sill intrudes the base of the Kakagi Lake Group, and the age from the Kakagi Lake Group is from the top of the sequence these age dates could suggest the sill intruded a continuously growing volcanic pile resulting in a span of deposition of 13.7 +/- 3.7 Ma (Davis and Edwards, 1982). Alternatively, it could indicate a renewed period of volcanism. If the sill were to intrude a growing volcanic pile the degree of crustal contamination would increase with proximity to the upper contact and reflect values closer to that of the rocks from the Emm Bay Formation. If, however, the age of formation for the Emm Bay Formation represents renewed volcanism, the degree of crustal contamination would remain relatively unchanged across the sill. A second possibility, however, is that Davis and Edwards (1982) analyzed an inherited zircon entrained within the Kakagi Sill upon emplacement.

Table 5.2. Sm-Nd results for samples analyzed.

SBF = Snake Bay Formation, EBF = Emm Bay Formation, KGS = Kakagi Gabbro Sill, KUMS = ultramafic rocks of the Kakagi Sill.

Sample ID	**197155**	**07-89**	**07-132**	**07-142**	**07-057**
Unit	EBF	EBF	SBF	SBF	SBF
Nd (ppm)	25.26	21.11	16.32	19.06	2.68
$^{143}Nd/^{144}Nd$ (current)	0.51126	0.51148	0.5125	0.5125	0.5124
Sm (ppm)	4.91	4.61	5.09	5.92	0.81
$^{147}Sm/^{144}Nd$	0.1176	0.1321	0.1887	0.1878	0.1837
$^{143}Nd/^{144}Nd$ initial	0.509173	0.50913	0.50920	0.509178	0.509168
$\varepsilon Nd_{(T=2700)}$	0.781275	-0.0593	1.433633	0.864358	0.665373

Sample ID	**07-085**	**07-039**	**07-070**	**07-112**	**07-140**
Unit	SBF	KGS	KGS	KGS	KGS
Nd (ppm)	2.39	1.99	2.23	3.53	6.09
$^{143}Nd/^{144}Nd$ (current)	0.5120	0.5125	0.5126	0.5125	0.5124
Sm (ppm)	0.64	0.62	0.73	1.10	1.88
$^{147}Sm/^{144}Nd$	0.1635	0.1894	0.1976	0.1888	0.1863
$^{143}Nd/^{144}Nd$ initial	0.509174	0.509180	0.509152	0.509183	0.509175
$\varepsilon Nd_{(T=2700)}$	0.788438	0.915509	0.360213	0.960081	0.805467

Sample ID	**07-128**	**07-147**	**07-154**	**07-155**
Unit	KUMS	KUMS	KUMS	KUMS
Nd (ppm)	2.96	1.40	1.49	1.90
$^{143}Nd/^{144}Nd$ (current)	0.5134	0.5129	0.5125	0.5123
Sm (ppm)	0.90	0.49	0.47	0.57
$^{147}Sm/^{144}Nd$	0.1839	0.2118	0.1894	0.1802
$^{143}Nd/^{144}Nd$ initial	0.510169	0.509163	0.509171	0.509161
$\varepsilon Nd_{(T=2700)}$	0.662207	0.577340	0.723111	0.537055

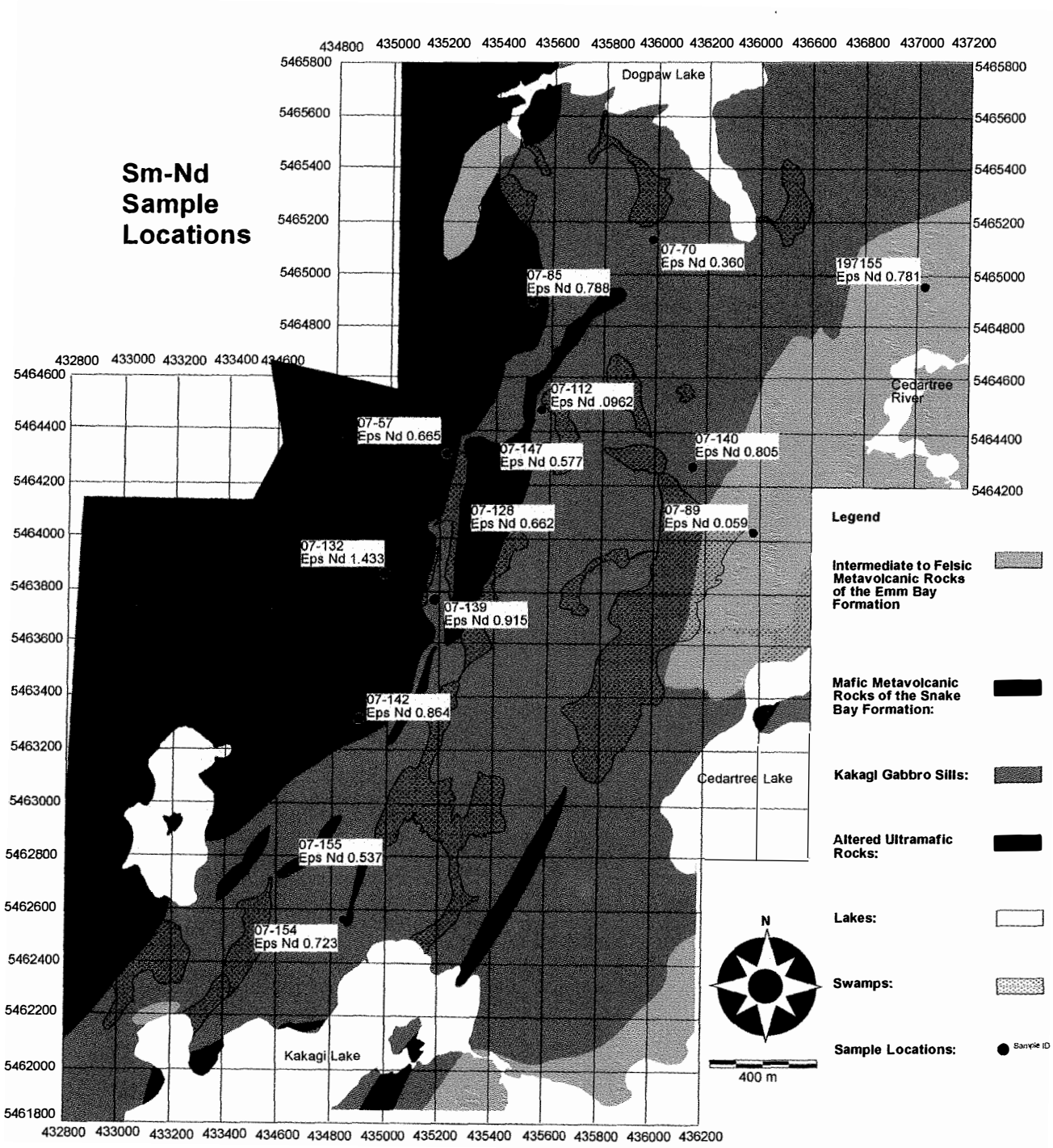

Figure 5.13. Simplified geology map of WCGP, showing sample locations for analyzed Sm-Nd isotopes. ε_{Nd} values are calculated for an age of 2700 m.y.

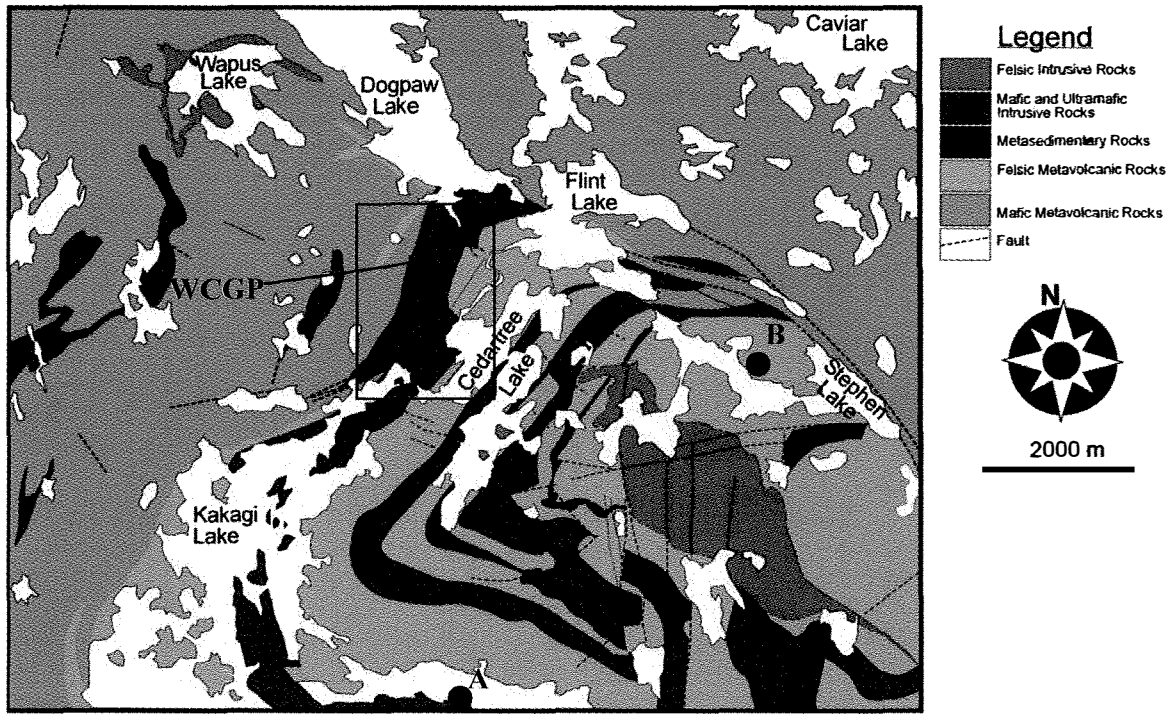

Figure 5.14. Simplified geology map of the Kakagi and Rowan lakes greenstone belts showing location of samples taken by Davis and Edwards (1982) for age dates. Boxed outline indicates approximate area of the WCGP. Sample location A (sampled from a pegmatitic portion of gabbro from the Kakagi Sill) is dated at 2724.8 +/- 2.5 Ma. Sample location B (sampled from a felsic tuff near the top of the Kakagi Lake Group felsic metalvolcanic rocks) dated at 2711.1 +/- 1.3 Ma (Davis and Edwards, 1982).

5.6.1 ε_{Nd}

Contamination of mantle melts by significantly older crust will result in ε_{Nd} values lower than mantle values. This occurs because older crustal material will have lower Sm-Nd ratios which, when assimilated, lowers the ε_{Nd} of younger melts. To calculate ε_{Nd} for the rocks of the WCGP an assumed age of formation of 2700 Ma was used based on age dates determined for units with Kakagi-Rowan lakes greenstone belts (Fig. 5.14; Davis and Edwards, 1982). These values were compared with DePaolo (1981) who has calculated ε_{Nd} for depleted mantle at 2700 Ma to be +3. The $\varepsilon_{Nd(T=2700)}$ values for

the gabbro unit range from +0.36 to +0.96 and for ultramafic rocks from + 0.53 to +0.73. The $\varepsilon_{Nd(T=2700)}$ for the mafic volcanic rocks of the Snake Bay Formation range in values from +0.66 to +1.43 and -0.05 to +0.78 for the felsic volcanic rocks of the Emm Bay Formation (Figs. 5.13 and 5.15).

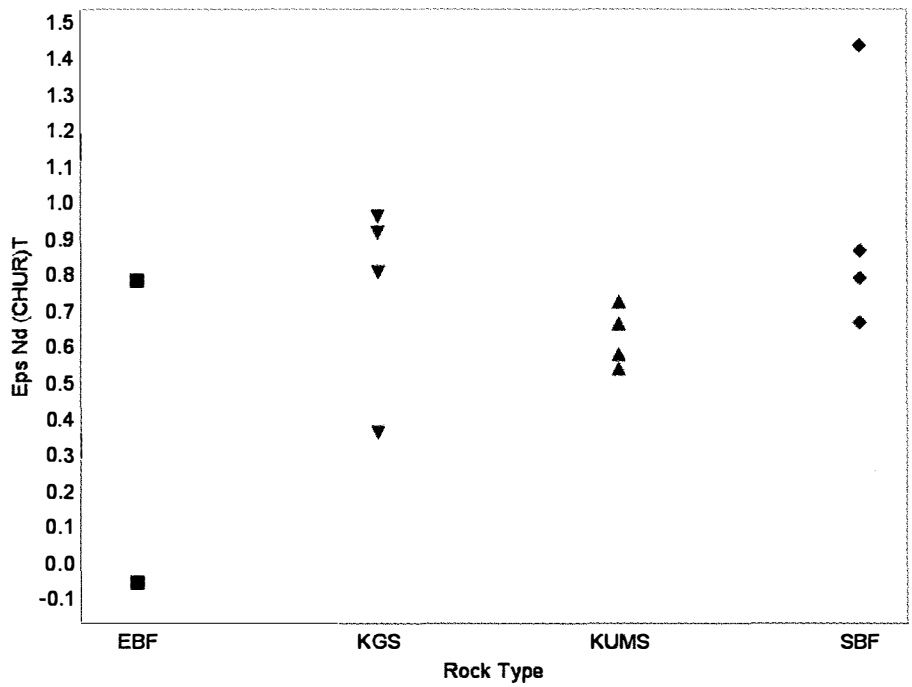

Figure 5.15. $\varepsilon_{Nd(T=2700)}$ values for sampled lithologies. SBF is the Snake Bay Formation, EBF is the Emm Bay Formation, KGS is the Kakagi Gabbro Sill, KUMS is the ultramafic rocks of the Kakagi Sill

ε_{Nd} versus Nb/Nb* for rocks sampled within the WCGP have all been plotted in Figure 5.16 in order to illustrate evolution of $\varepsilon_{Nd(T=2700)}$ with respect to increasing contamination.

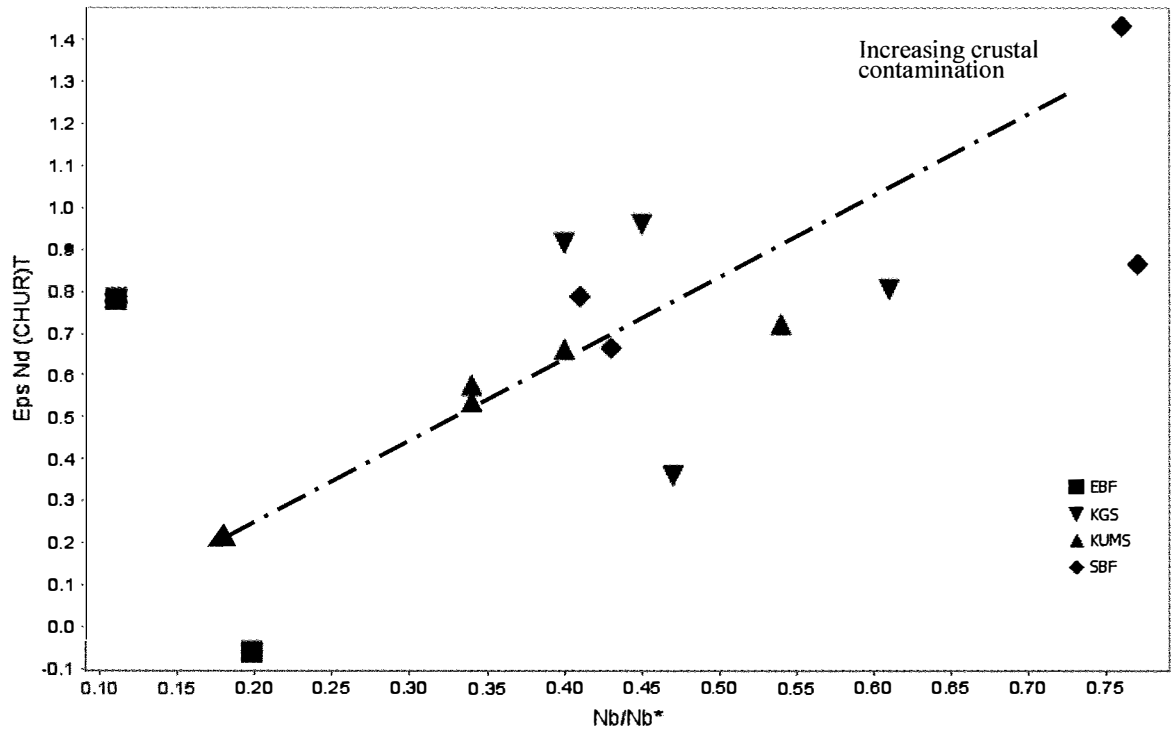

Figure 5.16. Plot of $\varepsilon_{Nd(T=2700)}$ versus Nb/Nb*. Legend description: SBF are samples from the Snake Bay Formation, EBF are samples from the Emm Bay Formation, KGS are from the Kakagi Gabbro Sill, KUMS are from the ultramafic rocks of the Kakagi Sill.

The lower $\varepsilon_{Nd(T=2700)}$ values (as compared with the value of depleted mantle of +3 as determined by DePaolo, 1981) for the Emm Bay Formation suggests these rocks have undergone minor contamination. Comparing the samples from the Emm Bay Formation with those of the Snake Bay Formation or either unit of the Kakagi Sill indicate that even though their $\varepsilon_{Nd(T=2700)}$ values are not as low, still show some degree of contamination (Figs. 5.15 and 5.16). They do, however, show an increase from east to west in contamination (Fig. 5.13). This is possibly related to assimilation felsic metavolcanic rocks during emplacement of the sill. Assimilation of rocks from the Snake Bay Formation would likely have had little effect on the isotopic signature of the intrusive rocks given their similar ages.

Tomlinson et al. (2004) have compiled extensive ε_{Nd} data for both extrusive and intrusive rocks from the Western Wabigoon subprovince. Volcanic rocks of the Savant Lake-Sturgeon Lake greenstone belt (Fig. 3.2) which have erupted onto Central Wabigoon crust, show a range of ε_{Nd} values from +0.6 to +1.7 at 2.85 Ga which is lower than the ε_{Nd} of +2.3 for depleted mantle at 2.85 Ga (DePaolo, 1981) and was interpreted to indicate that the volcanic rocks were contaminated by the older crust through which it was emplaced (Tomlinson et al., 2004). Volcanic rocks from further west of the contact with the Central Wabigoon subprovince, while being younger at 2.775-2.718 Ga also have ε_{Nd} values of +1 to +2.6 which were interpreted to reflect a derivation from a depleted mantle (depleted mantle at 2.7 Ga is +3; DePaolo, 1981; Tomlinson et al., 2004). 2.74-2.72 Ga volcanic rocks in the Lake of the Woods area (Fig. 3.2) have ε_{Nd} values between +1.1 to +2.3 where as younger rocks (2.70 Ga) have ε_{Nd} values ranging from -0.4 to +0.4 (Tomlinson et al., 2004). The lower ε_{Nd} values of these younger rocks suggest that these volcanic rocks were derived from either heterogeneously mixed depleted and enriched mantle sources, or by contamination with older crust (Tomlinson et al., 2004). These ε_{Nd} values are similar to ε_{Nd} values determined for rocks of the WCGP and given broadly similar geochemistry and likely reflect similar environments of emplacement. The lower ε_{Nd} values for all rocks in the WCGP sample suite indicate that they have undergone some degree of contamination resulting in isotopically enriched sources with the primitive mantle normalized plots showing varying degrees of LREE enrichment (Fig. 5.17).

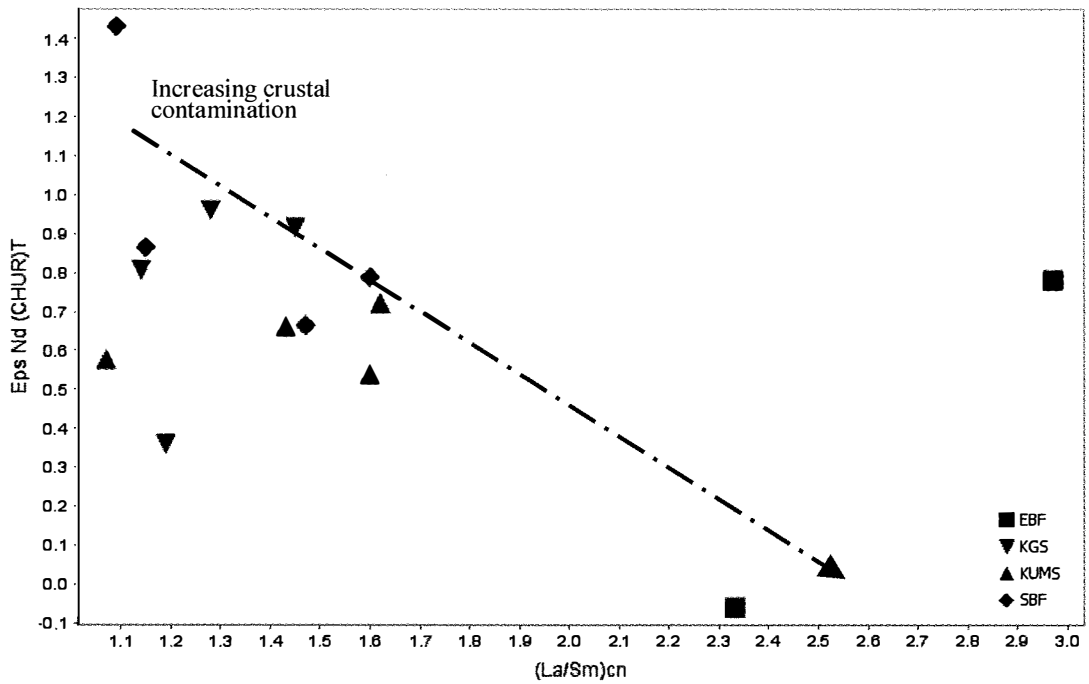

Figure 5.17. Crustal contamination diagram: $\varepsilon_{Nd(T=2700)}$ versus La/Sm. Legend description: SBF are samples from the Snake Bay Formation, EBF are samples from the Emm Bay Formation, KGS are samples from the Kakagi Gabbro Sill, KUMS are samples from the ultramafic rocks of the Kakagi Sill.

This likely resulted from partial melting of an isotopically enriched mantle source forming an LREE enriched and isotopically enriched residue which formed the final magma (Tomlinson et al., 1998). The gabbroic and ultramafic rocks of the Kakagi Sill which have ε_{Nd} values ranging between +0.4 to +1 and negative Nb anomalies suggests these rocks formed from a depleted mantle source which was had undergone metasomatic alteration and not contamination by older basement rocks (Fig. 5.18; Tomlinson, 2000). Both volcanic suites, the mafic metavolcanic Snake Bay Formation and felsic metavolcanic Emm Bay Formation have strong and very strong negative Nb anomalies respectively along with ε_{Nd} values ranging between -0.1 to +1.3 indicating that these rocks also formed from depleted mantle which has been weakly contaminated. However, the lack of preserved 3 Ga basement rocks in conjunction with simple mixing models

suggests that these ε_{Nd} values observed in the WCGP reflect interaction of depleted mantle isotopically and LREE-enriched melts formed from mixing with metasomatised arc lithosphere in an arc setting to produce these ε_{Nd} values and pronounced negative Nb anomalies (Figs. 5.12 and 5.18; Stern et al., 1995).

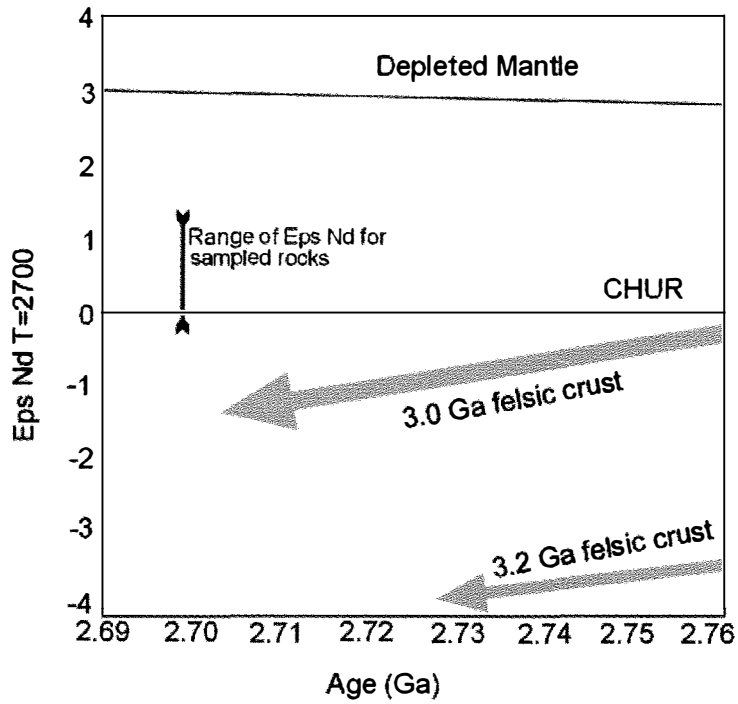

Figure 5.18. ε_{Nd} values plotted against time for samples from the WCGP. Fields modified from Tomlinson (2000).

5.7 Discussion and Summary

The apparent lack of heterogeneity within the gabbro sill suggests that it was emplaced as a crystal mush as opposed to a more fluid melt which would likely be more differentiated. Riddler (1966) suggests that though the individual sills are relatively undifferentiated, the stratigraphic height of the Kakagi Sills (Sills 1 through 5) is related to their degree of differentiation within the package as a whole. According to this model

the lowermost sill (Sill 1) which contains the highest volume of much denser ultramafic rocks forms the basal segment and each successive sill is subsequently less dense with less volume of ultramafic rocks (see Chapter 3). This suggests that the magma source for the sills has been removed successively from an evolving, magma chamber. This coupled with the lack of sharp contacts and the absence of a pronounced contact aureole suggests the Kakagi Sill was emplaced into a relatively hot volcanic pile (Riddler, 1966; Davis and Edwards, 1982). The Kakagi Lake Group has been interpreted to have been emplaced broadly simultaneously with the sill, and likely all five Kakagi sills were also emplaced simultaneously, thus all three units (Rowan Lake Group, Kakagi Sills, and Kakagi Lake Group) may be from a single or at least similar source melt (Davis and Edwards, 1982). Figures 5.13 and 5.16 suggest a progressive increase in contamination from the Snake Bay Formation through the Kakagi Sill and finally to the Emm Bay Formation (west to east). The similarity of the primitive mantle normalised plots (Figs. 5.5, 5.8, 5.9, 5.10) suggests that that they have likely evolved from the same tholeiitic basalt source that first supplied the Snake Bay Formation (Davis and Edwards, 1982). If the date determined by Davis and Edwards (1982) indicates an inherited age then it would therefore represent the span of a minimum deposition window of 13.7 +/- 3.7 Ma for the deposition time of the Kakagi Lake group. However, if the zircon is not inherited and is in fact a true age then it likely suggests that the Kakagi Sills (1 through 5) intruded contemporaneously and throughout a continuously growing felsic volcanic pile. However, this study has failed to resolve this issue.

Both the mafic metavolcanic rocks of the Snake Bay Formation and the intrusive rocks of the Kakagi Sill consist of slab metasomatised ocean plateau-like basaltic rocks.

Felsic to intermediate metavolacnic rocks of the Emm Bay Formation have been shown to represent a subduction related arc. The isotopic signatures and Nb/Nb* ratios of the study rocks indicate the source rocks have undergone contamination by crustal material. The lack of a well defined mixing model and evidence for existing basement rocks suggests that these rocks have not formed from crustal contamination but, coupled with LREE fractionation patterns, also formed from interaction with melts with enriched isotopic signatures likely from interaction from metasomatised arc lithospheric crust in an subduction zone setting (Stern et al., 1995). The tectonic setting for these rocks is that of slab metasomatised island tholeitte basalts of the Snake Bay Formation overlain by the subduction related felsic volcanic rocks of the Emm Bay Formation which have been intruded by the mafic to ultramafic Kakagi Sills. Such an arrangement of tectonic assemblages likely formed in an accreted island arc environment (Stern et al., 1995).

Chapter 6:

The Angel Hill Gold Zone

6.1 Introduction

Drilling of the Angel Hill Gold Zone (AHGZ) has outlined an inferred resource of 106,400 tonnes grading 2.97 g/t Au (Cutting and Anthony, 2005). The mineralised zone straddles the contact between the gabbro hangingwall and ultramafic footwall along their internal contact within the Kakagi Sill. These units are separated by a zone of brittle deformation about five centimetres wide and infilled with quartz and carbonate veins and irregular pods, with a zone of alteration which extends roughly twenty metres into both the hangingwall and footwall. This zone of deformation is infilled with quartz veining and carries the highest gold values. Gold values within the main deformation zone can be as high as 192 g/t Au, whereas proximal hangingwall and footwall rocks generally grade between 1.5 g/t to 0.05 g/t Au and distal rocks contains anomalously low values less than 0.005 g/t Au (Cutting and Anthony, 2005). The Angel Hill Gold Zone has been exposed through two exploration trenches each roughly 150 metres long (Angel Hill North, Fig. 6.1 A and Angel Hill South, Fig. 6.1 B). The two trenches are only separated by the Cameron Lake road (km 8) and essentially form a continuously exposed mineralised zone of 300 m along strike. The distinct features of this occurrence are its prominent lime-green colour caused by the occurrence of abundant fuchsite and subsequent supergene alteration of Fe-bearing carbonate minerals which has resulted in a reddish brown, gossanous appearance (Figs. 6.1 A and B).

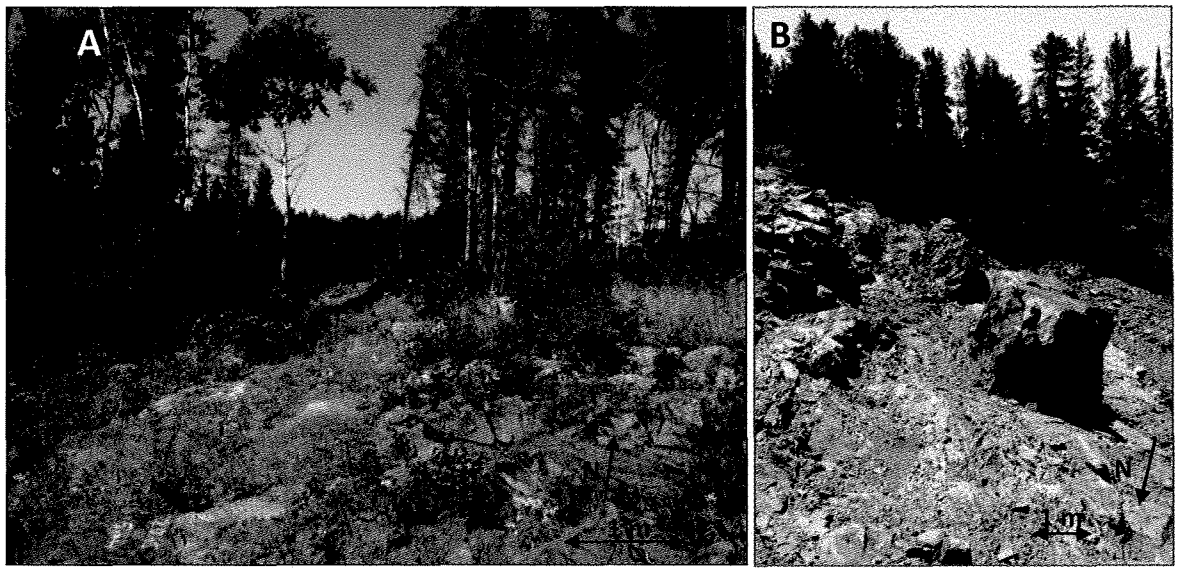

Figure 6.1 Photographs of Angel Hill Gold Zone exploration trenches. A: Angel Hill North strip zone (photo taken facing roughly north), B: Angel Hill South strip zone (photo taken facing roughly south).

6.2 Geology of the AHGZ

The rocks of the AHGZ are comprised of five main zones; distal and proximal hangingwall gabbro, distal and proximal footwall ultramafic intrusive rocks, and the main gold zone itself which is comprised of the "master fault", a zone of brittle faulting up to about five centimetres in width with deformation up to one metre either side, infilled with quartz veins and irregular pods. In addition to these five main zones there is also a lesser unit of variably continuous fine grained feldspar porphyry dike intruding subparallel to parallel to the master fault. The AHGZ transects a number of units from west to east including: least altered ultramafic peridotite through carbonate, fuchsite, and quartz altered peridotite to carbonate and quartz altered gabbro and finally least altered gabbro. Geologic trench maps are presented in Figure 6.2 for the Angel Hill North zone and Figure 6.3 for the Angel Hill South zone.

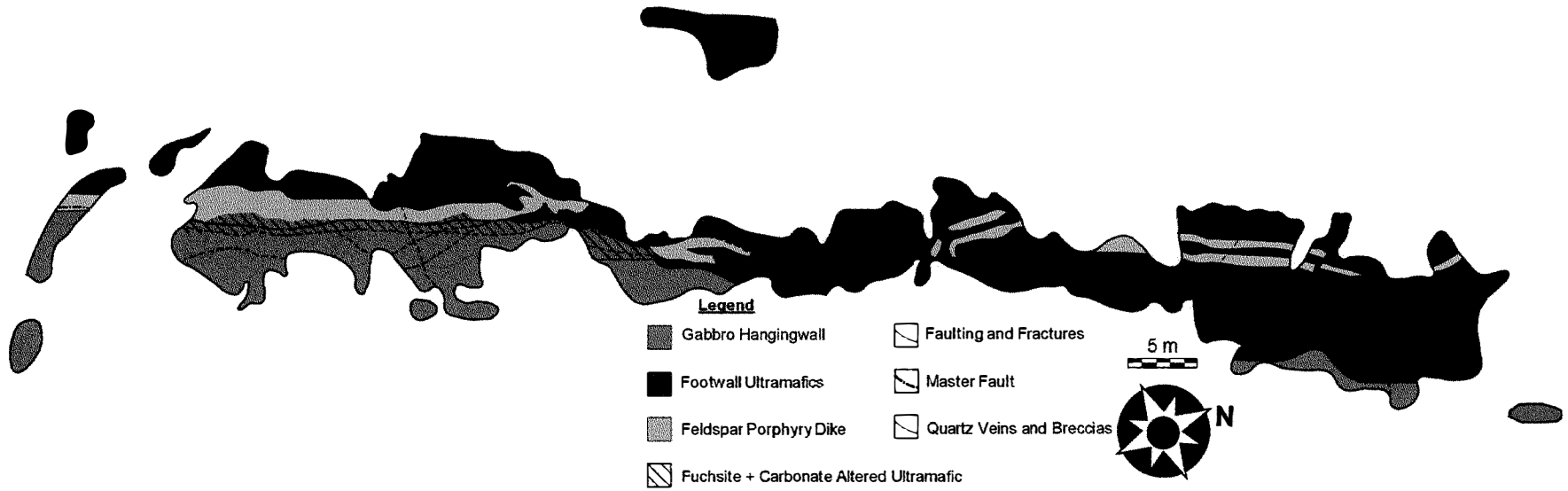

Figure 6.2 Trench map of the Angel Hill North strip zone. Modified from Cutting and Anthony (2005).

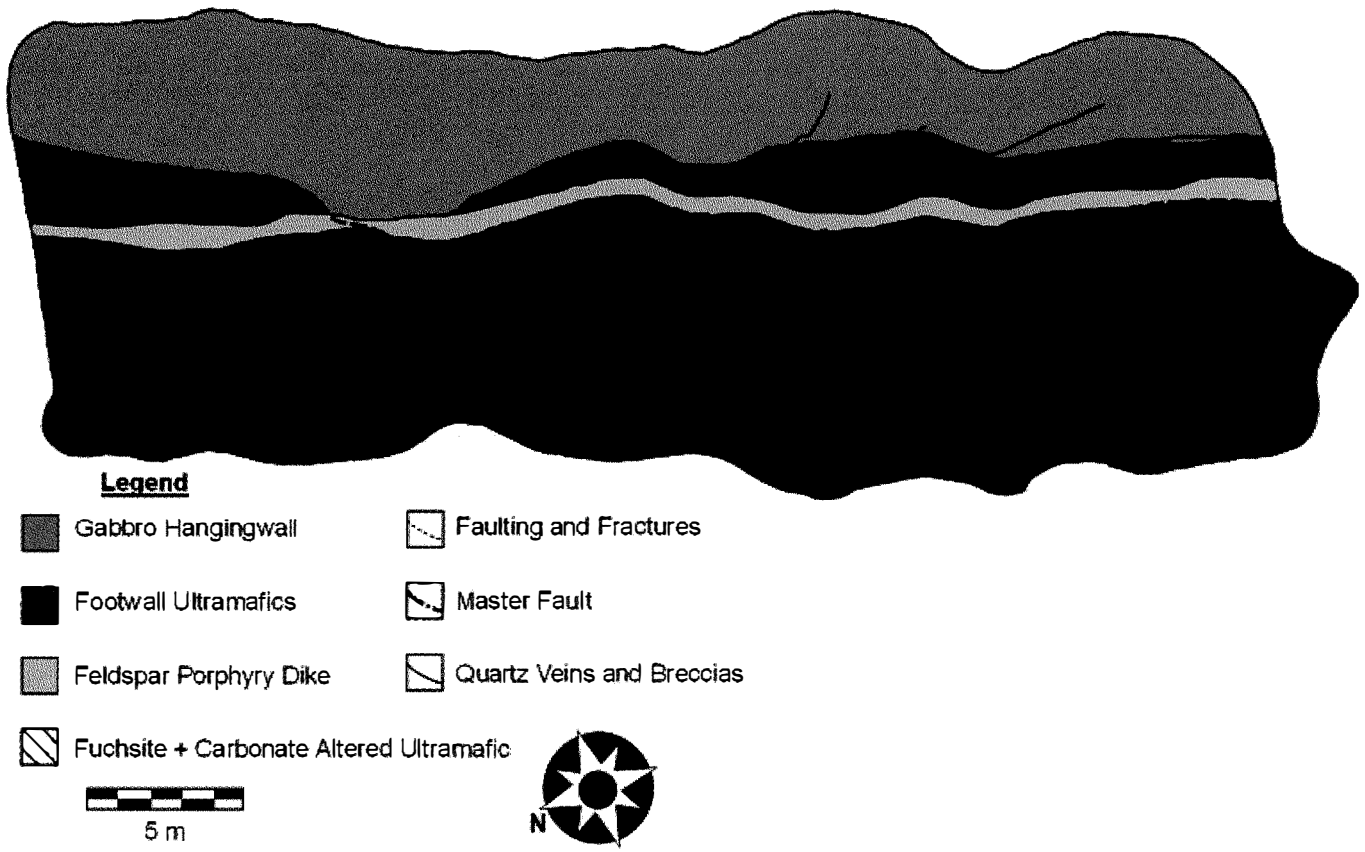

Figure 6.3 Trench map of the Angel Hill South strip zone.

The rocks of the distal footwall display comparable mineralogy to least altered ultramafic rocks from throughout the Kakagi Sill (Figs. 6.2 and 6.3). In hand sample (Fig. 6.4 A), fresh rocks are black and medium-to-coarse grained, weathered rocks are slightly rusty. They are composed of serpentine altered olivine (antigorite) and orthopyroxene (hypersthene, enstatite, weakly to moderately altered to orthoantigorite) as well as interstitial augite, talc, and locally fine grained albite plagioclase feldspar (Fig. 6.4 B). These rocks have been weakly silicified up to about 5% and locally carbonate altered up to about 8%. Carbonate alteration is predominantly ankerite and Fe-dolomite along grain boundaries and cleavage planes of pyroxene, as well as locally altered pseudomorphs of magnesite after serpentine (Fig. 6.4 B).

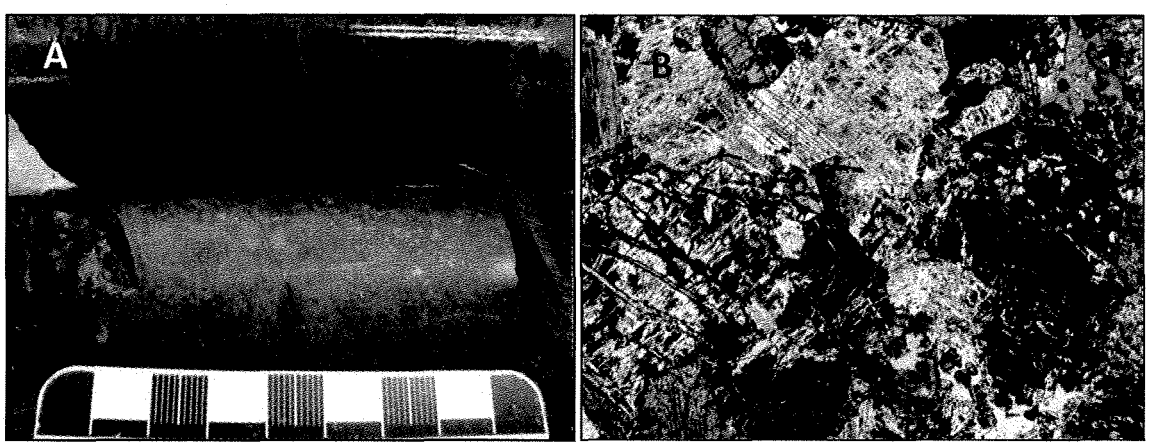

Figure 6.4 A- sample 76305 drill core sample of least altered peridotite. 6.4 B- sample 76308 thin section photomicrograph of least altered peridotite- note serpentinized olivine and carbonate altered interstitial pyroxene.

The proximal footwall is composed of peridotite, has been intensely altered to carbonate and fuchsite (Cr bearing muscovite; Fig. 6.5 A). Augite has been predominantly altered to carbonate and chlorite, hypersthene altered to chlorite and minor carbonate (Fig. 6.5 B). No relict olivine remains and almost all serpentine has been extensively altered to magnesite. This forms what looks in the field to be "carbonate eggs" which are the results of pseudomorphs of carbonate after serpentine after olivine (Fig. 6.5 B). Almost the entire unit is cross cut by

numerous small fractures infilled with quartz-carbonate flooding and veining (Fig. 6.5 A and C). These fractures are brittle in nature and display textures which suggest multiple episodes of deformation including quartz sutured veinlets, network textured cross-cutting quartz-carbonate veins (Fig. 6.5 A and C). Sulphide phases present in the proximal footwall include disseminated pyrite (trace to 3%), generally associated with quartz and carbonate veining, and locally disseminated pyrrhotite (trace to 1%). The degree and intensity of alteration and fracturing decreases away from the faulted zone for up to about twenty meters. Alteration in the proximal footwall ranges in width along strike from 15 to 20 metres from the master fault.

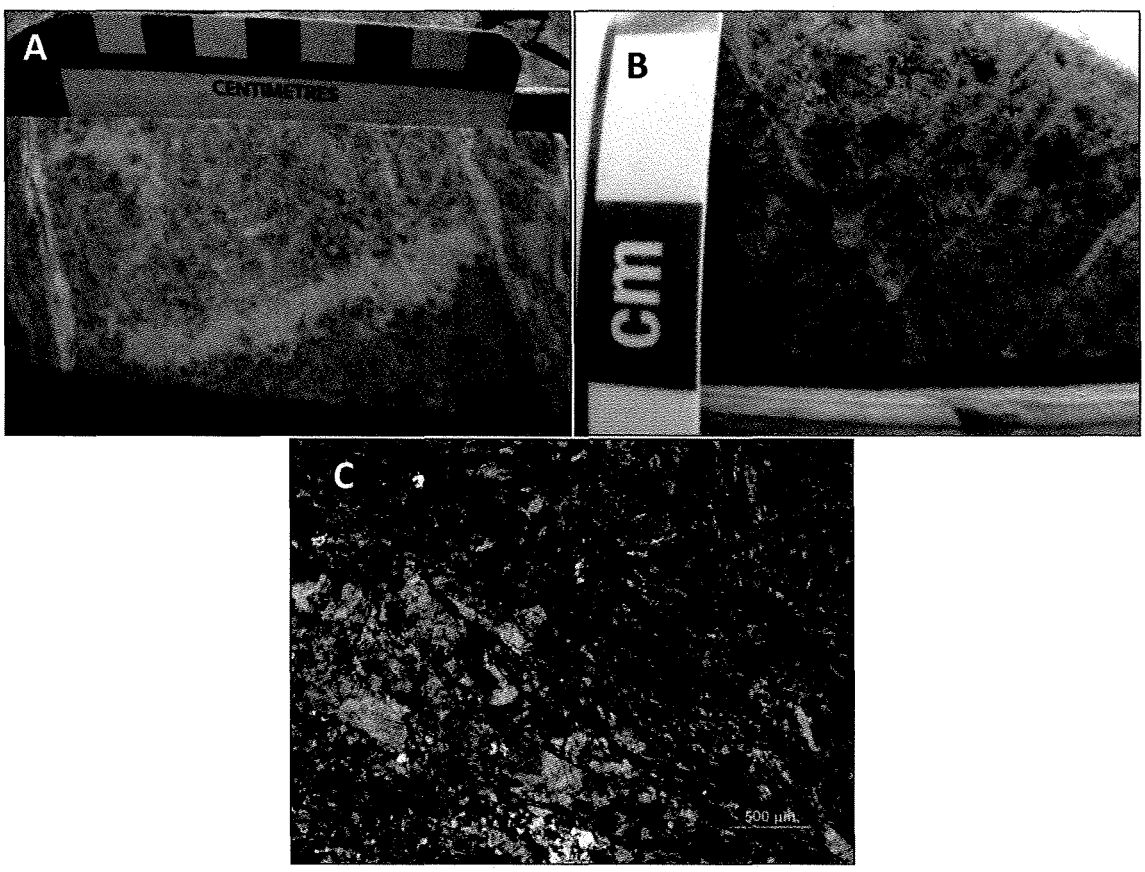

Figure 6.5. A- drill core sample of strongly altered footwall peridotite note extensive green colour caused by abundant fuchsite alteration, sample 76304. B- drill core sample showing pseudomorphs of magnesite after serpentinised olivine, sample 76302. C- thin section photomicrograph of extensively carbonate and fuchsite altered proximal ultramafic footwall showing brittle textured quartz-carbonate veining, sample AHGZ-3.

Similar to the distal footwall, the distal hangingwall shares comparable mineralogy and alteration to the least altered gabbro found throughout the Kakagi Sill (Fig. 6.6 A). Amphibole and pyroxene are only weakly altered to carbonate and plagioclase feldspar is moderately altered to muscovite. The entire unit displays pervasive strong chlorite alteration. Alteration intensity increases with proximity to the main gold zone, with increases in carbonate alteration and silicification (Fig. 6.6 B). Plagioclase is strongly altered to muscovite and mafic phases (pyroxene and amphibole) to Fe-dolomite and ankerite (Fig. 6.6 B). Brittle fractures infilled with carbonate and quartz are abundant.

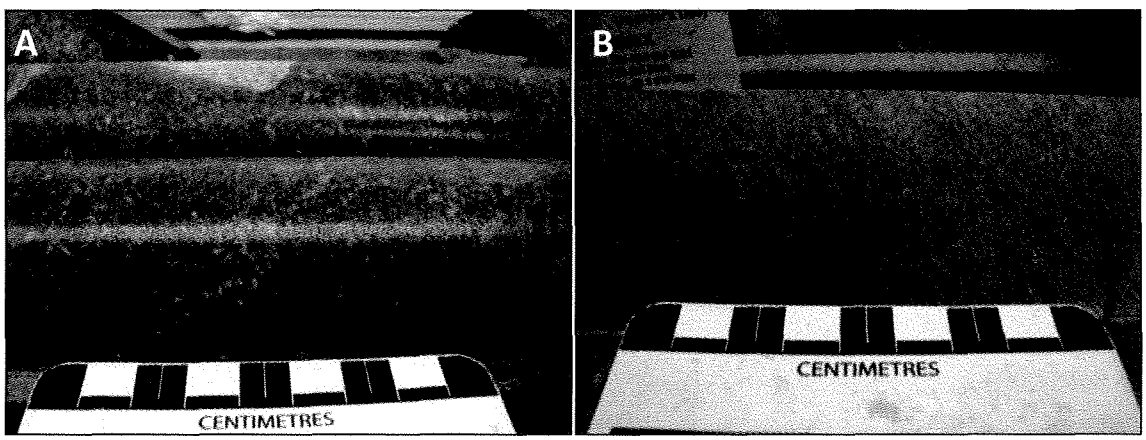

Figure 6.6 A- sample 76307 drill core sample of least altered gabbro from distal hanging wall. B- sample 76302 drill core sample of increasingly altered gabbro closer to the main zone.

The gabbroic rocks of the proximal hangingwall have been extensively altered to a yellowish-brown and brown colour and consist mainly of silica with trace sulphide minerals chiefly pyrite, the presence of fuchsite is limited in this zone and is really only prevalent proximal to the main zone (Fig. 6.7 A). The main carbonate phase in the rock is Fe-dolomite and ankerite and is pervasively carbonatized along fractures, cleavage planes and open pores (Fig. 6.7 A, B and C). Silica is a secondary phase observed as pore space filling and quartz veins and

veinlets (Fig. 6.7 B). Carbonate and quartz veins form a stockwork-like brittle vein texture (Fig. 6.7A and B). Where alteration intensity is highest, no relict igneous textures are preserved (Fig. 6.7 A, B and C). The nature of fracturing and veining suggest episodic events. There are re-fractured and overprinted quartz and carbonate veins, as well cataclastic fracturing with numerous quartz sutures. The proximal hangingwall ranges between 5-15 metres wide along strike and diminishes in intensity away from the main zone.

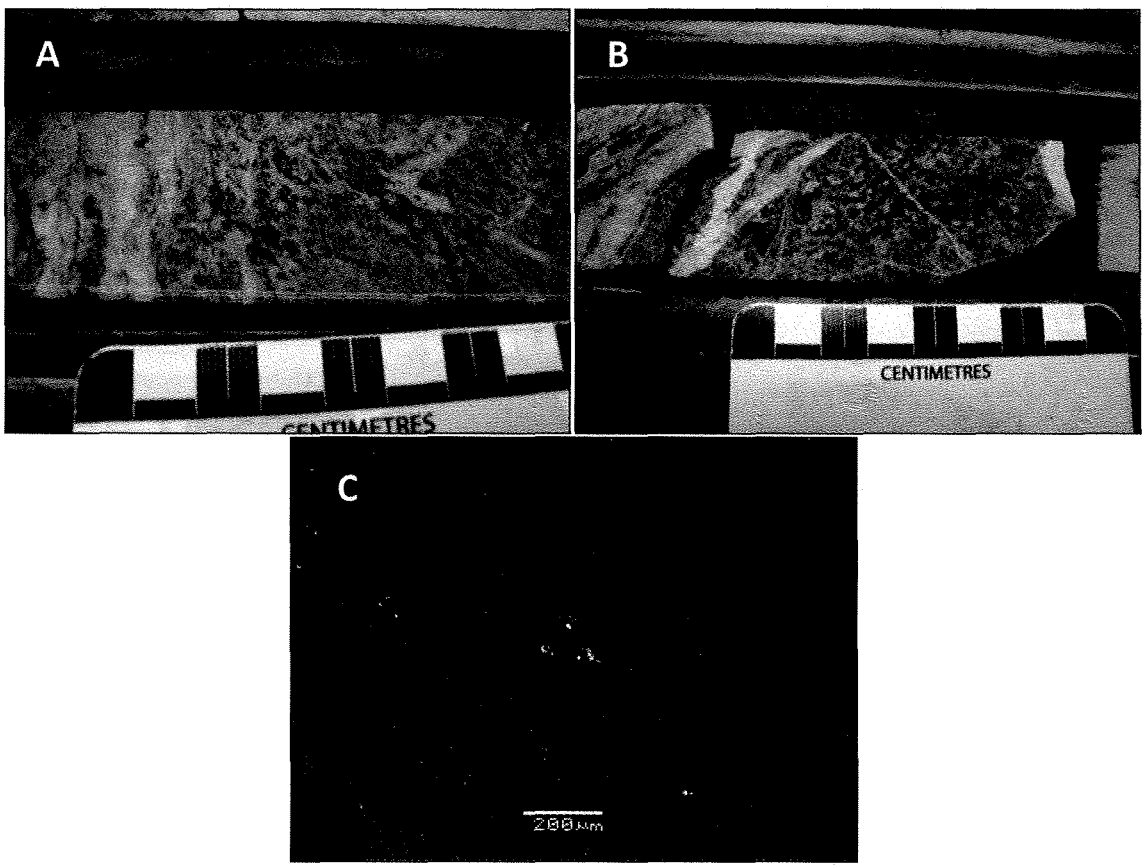

Figure 6.7 A- drill core sample of strongly altered proximal hanging wall with quartz carbonate veining, sample 76301. B- drill core sample of proximal hanging wall displaying replacement of mafic phases with muscovite and carbonate, sample 76310. C- SEM backscatter image of network textured quartz and carbonate overprinting from the proximal gabbro hangingwall, sample 76310.

The main gold zone occurs within deformed ultramafic rocks in a fault known as the "master fault". The zone has been faulted and altered almost completely with very few relict

igneous textures or minerals preserved. The main gold zone is most easily identified by its rusty weathered surface, due to oxidized iron carbonate and the abundant bright green fuchsite (Fig. 6.8). In the AHGZ, fuchsite forms large massive mats throughout the footwall forming intense lime green zones of alteration up to roughly ten meters (Fig. 6.8 A). In thin section fuchsite displays perfect basal cleavage, weak green pleochroism, first to second order interference colours and a monoclinic crystal system (Fig. 6.9). The zone of brittle deformation at the surface is moderately fissile and infilled with quartz and carbonate veining and small irregular pods one to five metres in length boudinaged along strike. Albite is observed forming anhedral grains which are only observed when not overprinted by quartz and carbonate. Mineralization is limited to up to 15% fine grained pyrite, with lesser amounts of galena and sphalerite. Visible gold is only locally observed and generally associated with pyrite.

Figure 6.8. Abundant green fuchsite mats within bulk of AHGZ. Note extensive rusty weathering, typical of the AHGZ.

Figure 6.9. Photomicrograph of fuchsite with quartz-carbonate veinlet, sample AHGZ 1. Cross polarised light.

6.2.6 Feldspar Porphyry Dike

Throughout both the North and South Angel Hill stripped zones there is a single half metre wide, locally discontinuous and weakly boudinaged quartz feldspar porphyry dike (Fig. 6.10). The dike is medium to light grey buff in colour and very fine grained. It appears to have intruded along a structure parallel or sub-parallel to the "master fault", however, it has been strongly deformed by the "master fault" suggesting it predates at least that phase of deformation (Fig. 6.10). The location of the feldspar porphyry dike could represent early stages of deformation between the gabbro hangingwall and ultramafic footwall.

Figure 6.10. Photograph of boudinaged feldspar porphyry dike within the AHGZ.

The "master fault" is continuous over the entire exposed strike length of the AHGZ and is interpreted to be the main fluid pathway for mineralizing fluids (Figs. 6.2 and 6.3). The fault runs along the contact between the gabbro hangingwall and peridotite footwall, though deformation exists up to roughly a metre n either unit. This fault has been interpreted to have formed as the result of competency or rheologic differences between the two host units during regional scale deformation (likely the same event as the related Cameron Lake shear zone). Deformation is interpreted to be episodic, as there is evidence of re-faulted and healed quartz veins and wall rock (Fig. 6.11). The master fault is roughly vertical to sub-vertical and dips steeply to the east; this is consistent with the property wide stratigraphy described in Chapter 4.

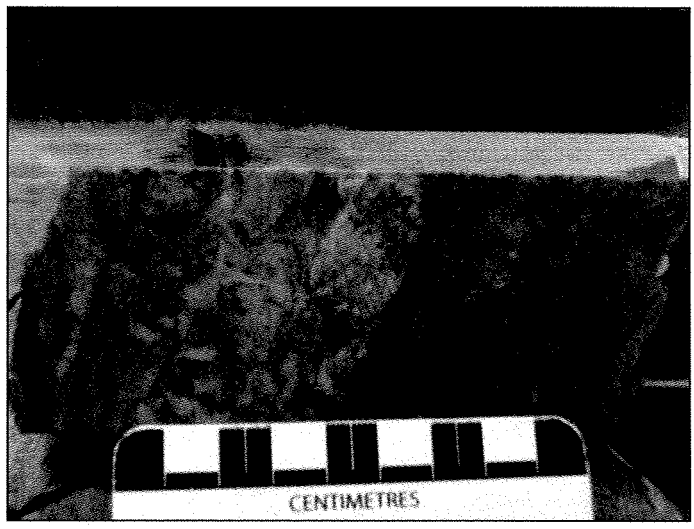

Figure 6.11. The "master" fault in diamond drill core, sample 76306. Note cataclastic fault textures, over printed quartz carbonate veining and abundant fuchsite and carbonate.

6.3 Mineralization

Gold mineralization is almost exclusively contained within the fault zone itself. Sulphide mineralization is the most visible mineralization and is comprised chiefly of fine grained to small blebs up to 30% of subhedral pyrite with lesser amounts of galena and sphalerite. Gold is associated with pyrite, as inclusions and rimming pyrite grains or proximal to pyrite as small grains along fractures within quartz (Fig. 6.12). Observational quantitative estimates suggest that 85% of gold is associated with pyrite, both rimming pyrite grains and as inclusions, and 15% is associated with quartz, forming small grains along fractures and between quartz grains (Fig. 6.12). However, not all pyrite contains gold inclusions, suggesting multiple generations of pyrite. Gold occurs in two phases, native or free gold (Fig. 6.12 A, C and D) and as part of the mineral sylvanite (Fig. 6.12 B, E and F). When gold occurs as sylvanite at Angel Hill it forms nearly equal ratios of Au/Ag. Use of the SEM has indicated that gold is also locked within pyrite grains, which accounts for the lack of observable gold that should be reflected in some high grade

samples (Fig. 6.12 D and F). The high volume of gold associated with pyrite causes erratic overall distribution of gold.

Pyrite mainly occurs as disseminated grains and only forms aggregates in some veinlets (Fig. 6.12 A, C, D and F). In some localities, hematite alteration occurs along fractures and around the margin of pyrite grains (Fig. 6.12 F). This is likely due to supergene weathering, as pyrite samples from drill core which have intersected the zone at depth do not show this feature. Brecciation of pyrite grains and influx of carbonate suggests that pyrite mineralization occurred relatively early in the paragenesis of the gold zone and that deformation and fluid influx continued after their formation, suggesting multiple phases of deformation and fluid influx.

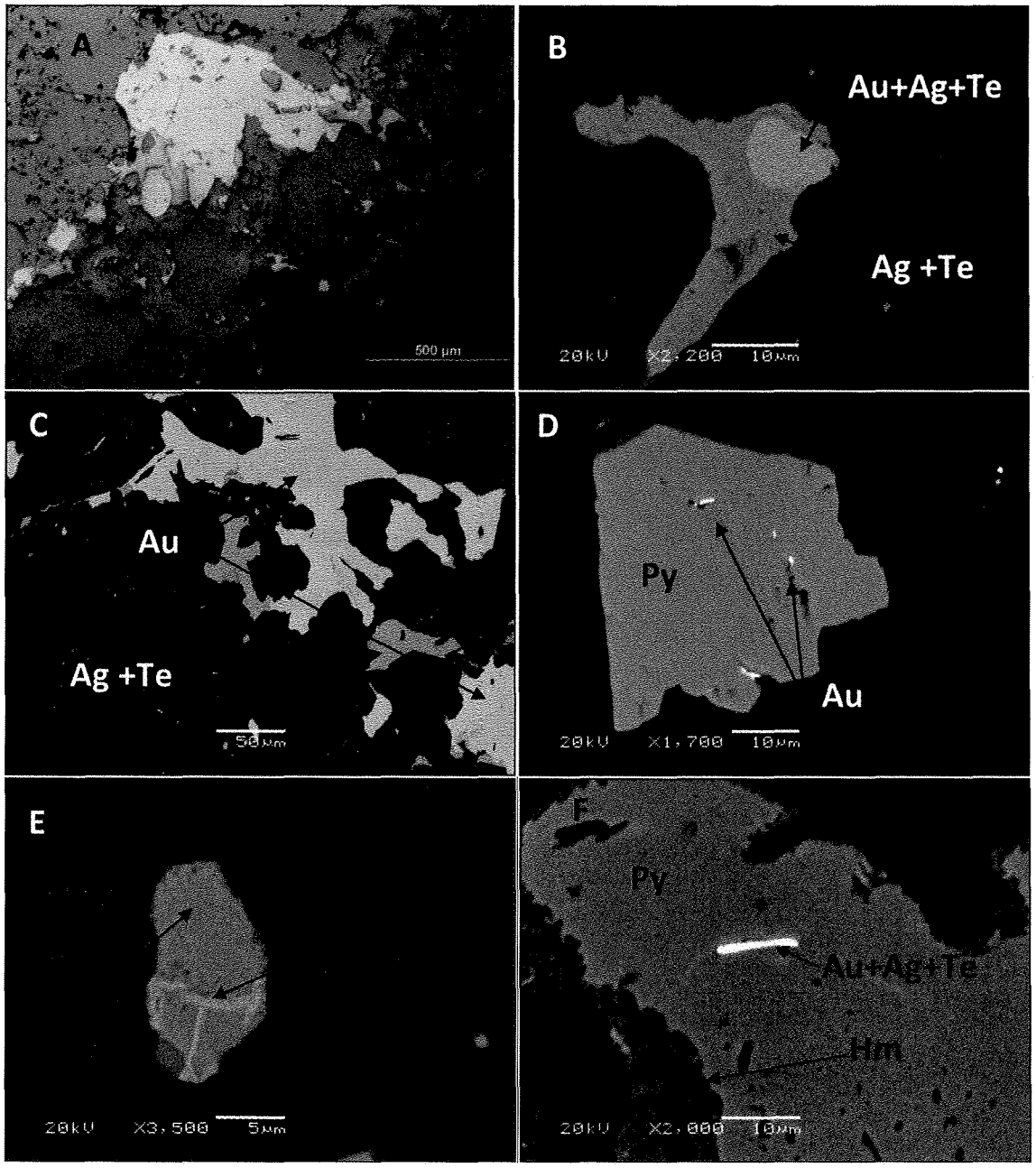

Figure 6.12 A- Photomicrograph of pyrite grain with abundant gold mineralisation, sample 76306. B- SEM backscatter image of sylvanite formed interstitially along fractures between quartz grains. C- SEM backscatter image of Au and Ag with pyrite. D- SEM backscatter image of pyrite with inclusions of gold. E- SEM backscatter image of Ag with Au associated with quartz grains. F- SEM backscatter image of pyrite with inclusion of gold, note hematite alteration of pyrite. Py is pyrite, Au is gold, Hm is hematite, Ag is silver and Te is tellurium.

Sphalerite is found with galena overgrowths in association with some pyrite grains (Fig. 6.13). Sphalerite and galena are only found together, forming subhedral to anhedral blebs with varying degree of galena overgrowths. Sphalerite is always observed as the core mineral (Fig. 6.13). Distribution of sphalerite and galena is very sporadic and does not seem to have an effect on the distribution of gold. Both sphalerite and galena are only observed within the main gold zone, and nowhere else within the hangingwall or footwall, or even in rocks from elsewhere in the property.

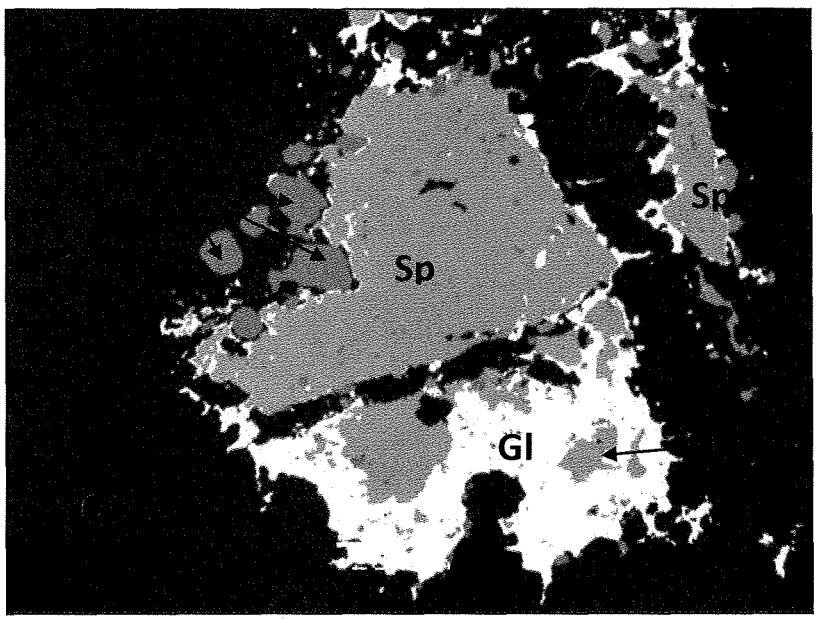

Figure 6.13 SEM backscatter image of sphalerite with galena overgrowths, sample 76306. Py is pyrite, Sp is sphalerite, Gl is galena, Qtz is quartz and Ca is carbonate. Field of view is approximately 1000 microns.

6.3.1 Mineralizing fluids

Figure 6.14 illustrates the nature of carbonate and quartz overprinting. There are several phases of both quartz and carbonate phases, often overprinting each other, suggesting multiple generations. Late stage carbonate veinlets cross cut all structures and mineral phases (Fig. 6.14 B and C). At least two generations of quartz are found. Quartz 1 is interpreted to be primary quartz or vein quartz and forms large coarse grained crystals infilling the faulted zone (Fig. 6.14 B and C). This quartz is often re-faulted and re-emplaced and there appears to be a second generation of quartz, quartz 2, which forms as secondary overgrowths of pre-existing quartz phases and small fine grained recrystallised subordinate grains. This could be suggestive of a change in fluid or a different mineralising fluid altogether.

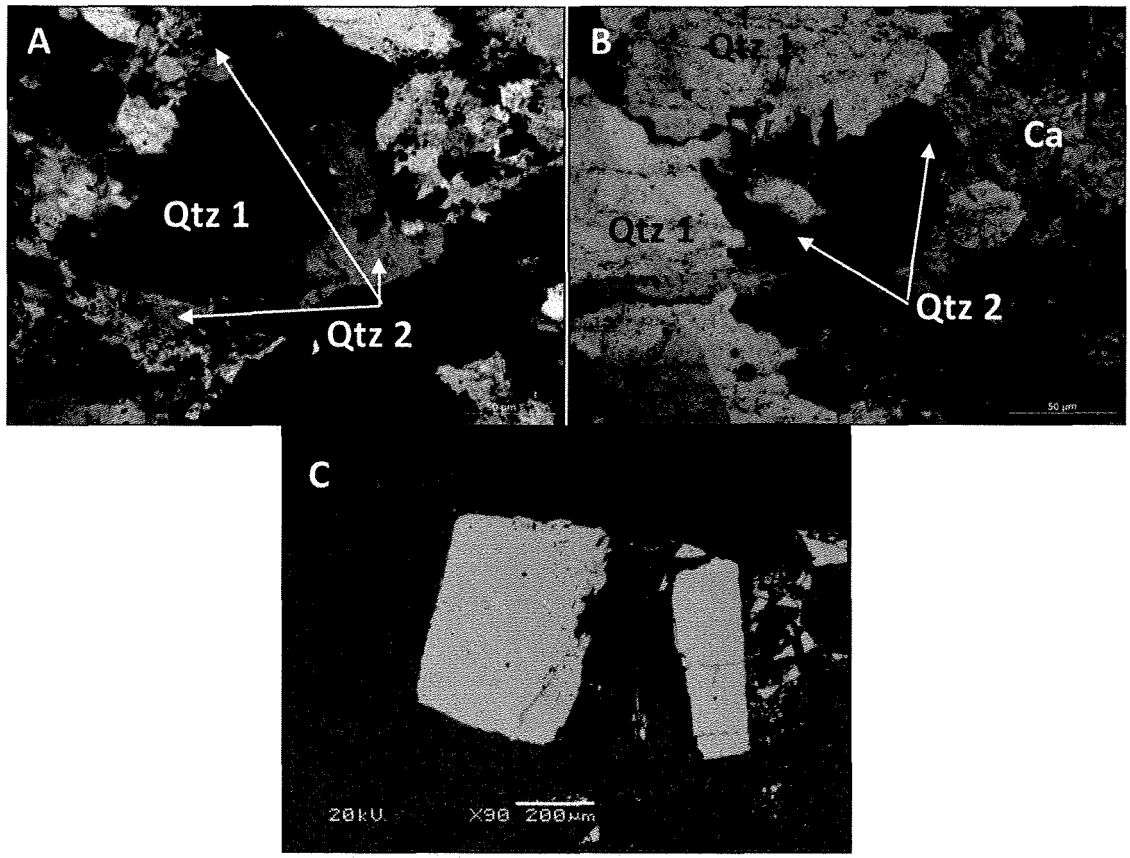

Figure 6.14. A, B- Photomicrographs in cross polarized light of quartz 1 vein quartz with quartz 2 overgrowths and recrystalised quartz fragments with cross cutting carbonate veinlets, opaque mineral is pyrite, samples 76306 and 76301 respectively. C- SEM backscatter image of brecciated pyrite grain with carbonate infilling, sample AHGZ 2.

6.4 Stable Isotope Geochemistry

In situ stable isotope geochemical analyses were undertaken using a secondary ion mass spectrometer (SIMS) on high grade Au- bearing samples of quartz vein material from within the main gold zone, to investigate if the texturally distinct sulphide minerals and fluid phases represented separate isotopically distinct generations and to gain insight into the relationships between mineralising fluids and ore forming minerals. SIMS was used in order to isolate

individual phases of the same mineral. The small spot size of the SIMS provided the ability to analyze the isotopic composition of individual phases of the same mineral which would otherwise be homogenised using bulk analyses, or even mineral separates, given the complex nature of intergrowth of the individual phases.

Oxygen isotope compositions of hydrothermal minerals associated with mineral deposits can provide information on the temperature of mineralization and the source of the ore-forming fluids, whereas sulphur isotope compositions can yield constraints on the source rocks from which these fluids were derived (McCuaig and Kerrich, 1998). $\delta^{18}O$ was analyzed on both quartz 1 (primary vein quartz) and quartz 2 (secondary quartz overgrowth and recrystalised quartz) as well as Fe-dolomite-ankerite phases, in order to investigate whether or not there was a common fluid source or mineralising event. $\delta^{34}S$ was analysed for pyrite, sphalerite and galena phases present in the main gold zone. Pyrite grains were analysed to investigate genetic relationships between gold bearing and barren phases. $\delta^{34}S$ analyses on galena and sphalerite were undertaken to examine a genetic phase relationship between sulphide phases. Results of these analyses are presented in Table 6.1. Results are presented as individual analysis locations, some single grains were analyzed with multiple points.

Table 6.1 Stable isotope geochemistry results.

Pyrite

Spot analyzed	$^{34}S/^{32}S_{meas}$	σ (‰)	$\delta^{34}S$	2 σ
Gold bearing pyrite 1	4.408	0.3	0.7	0.6
Gold bearing pyrite 2	4.406	0.3	0.4	0.6
Gold bearing pyrite 3	4.402	0.3	-0.5	0.6
Gold bearing pyrite 4	4.406	0.3	0.4	0.6
Gold bearing pyrite 5	4.409	0.3	1.0	0.6
Pyrite with galena and sphalerite 1	4.401	0.3	-0.8	0.6
Pyrite with galena and sphalerite 2	4.406	0.3	0.4	0.6
Pyrite with galena and sphalerite 3	4.400	0.3	-1.0	0.6
Gold barren pyrite 1	4.406	0.3	0.4	0.6
Gold barren pyrite 2	4.407	0.3	0.5	0.6
Gold barren pyrite 3	4.406	0.3	0.2	0.6
Gold barren pyrite 4	4.404	0.3	-0.2	0.6
Gold barren pyrite 5	4.405	0.3	0.2	0.6
Gold barren pyrite 6	4.399	0.3	-1.2	0.6

Sphalerite

Sample and spot	$^{34}S/^{32}S_{meas}$	σ (‰)	$\delta^{34}S$	2 σ
Sphalerite 1	4.453	0.3	5.4	0.6
Sphalerite 2	4.445	0.3	3.6	0.6
Sphalerite 3	4.443	0.3	3.0	0.6
Sphalerite 4	4.447	0.3	4.1	0.6
Sphalerite 5	4.444	0.3	3.3	0.6
Sphalerite 6	4.437	0.3	1.8	0.6

Galena

Sample and spot	$^{34}S/^{32}S_{meas}$	σ (‰)	$\delta^{34}S$	2 σ
Galena 1	4.394	0.4	5.9	0.4
Galena 2	4.394	0.3	5.8	0.4
Galena 3	4.400	0.3	7.3	0.4

All δ and σ values are ‰.

Table 6.1 Continued

Quartz

Sample and spot	$^{18}O/^{16}O_{meas}$	σ (‰)	$\delta^{18}O$	2 σ
Q1 Quartz 1	1.894	1.2	8.8	0.8
Q2 Quartz 2	1.902	1.2	13.1	0.8
Q1 Quartz 3	1.897	1.2	10.0	0.8
Q2 Quartz 4	1.900	1.2	11.9	0.8
Q2 Quartz 5	1.900	1.2	11.5	0.8
Q1 Quartz 6	1.896	1.2	9.7	0.8
Q1 Quartz 7	1.896	1.2	9.9	0.8
Q1 Quartz 8	1.894	1.2	8.6	0.8
Q2 Quartz 9	1.897	1.2	10.4	0.8
Ql Quartz 10	1.896	1.2	9.7	0.8
Q2 Quartz 11	1.898	1.2	10.5	0.8
Q1 Quartz 12	1.895	1.2	9.1	0.8
Ql Quartz 13	1.894	1.2	8.9	0.8
Q2 Quartz 14	1.900	1.2	11.7	0.8
Q2 Quartz 15	1.898	1.2	10.8	0.8

Carbonate

Sample and spot	$^{18}O/^{16}O_{meas}$	σ (‰)	$\delta^{18}O$	2 σ
Fe-dolomite 1	1.876	1.2	13.6	0.48
Fe-dolomite 2	1.879	1.2	15.1	0.48
Fe-dolomite 3	1.880	1.2	15.5	0.48
Fe-dolomite 4	1.884	1.2	17.7	0.48
Fe-dolomite 5	1.879	1.2	15.2	0.48
Fe-dolomite 6	1.882	1.2	16.6	0.48
Fe-dolomite 7	1.884	1.2	17.9	0.48
Fe-dolomite 8	1.877	1.2	13.8	0.48
Fe-dolomite 9	1.879	1.2	14.8	0.48
Fe-dolomite 10	1.880	1.2	15.8	0.48

All δ and σ values are ‰.

$\delta^{34}S$ values for pyrite ranged between -1.0 and +1.0 ‰, for sphalerite between +1.8 and +5.4 ‰ and for galena between +5.9 and +7.3‰. All samples of pyrite regardless of whether or not they host gold or were associated with sphalerite or galena were all within the 2σ of the mean $\delta^{34}S$ values of 0 ‰, suggesting that all pyrite was derived from the same fluid. Since all pyrite has the same $\delta^{34}S$ values (within 2σ of the mean of 0‰) it suggests that pyrite ,whether or not

associated with gold mineralization, is related to the same mineralizing event or sourced the same same sulphur reservoir.

Ideal fractionation curves for $\delta^{34}S$ values for all three sulphide phases have been plotted in a phase versus temperature fraction diagram (Fig. 6.15). This diagram shows the fractionation trend for the individual sulphide phases with respect to the temperature of formation. The diagram has two curves, one which reflects the ideal fractionation curves of pyrite and sphalerite and the other galena. If all three phases were to fractionate out of the same $\delta^{34}S$ reservoir over the temperature window interpreted for lode gold settings (200-500^{o} C; Yeates and Vanderhorn, 1998) pyrite and sphalerite would have $\delta^{34}S$ values nearing 0 ‰ $\delta^{34}S$ where as galena would be -2 ‰ $\delta^{34}S$.

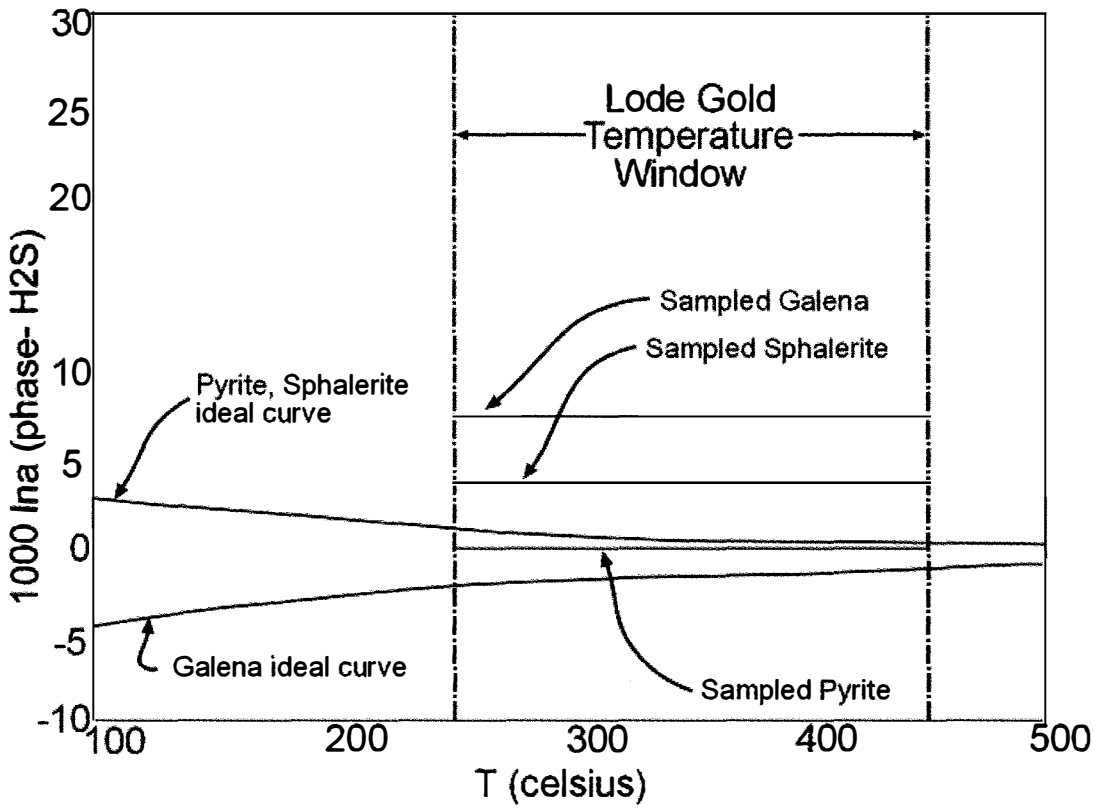

Figure 6.15. Ideal phase fractionation diagram for sulphide phases. Plotted are mean values for $\delta^{34}S$ for each sulphide phase. Fields are from Sharp (2007). Temperature of mineralisation for lode gold from Kerrich and Cassidy (1994).

The $\delta^{34}S$ values of 0 ‰ for pyrite from this study follow the ideal fraction curve for pyrite derived from a magmatic fluid (Fig. 6.12; Sharp, 2007). Therefore if the other sulphide phases, sphalerite and galena, also fractionated from the same fluid which precipitated pyrite, their $\delta^{34}S$ would also follow this ideal fractionation curve and contain $\delta^{34}S$ values of 0 ‰ and -2 ‰ respectively. However, the $\delta^{34}S$ of sphalerite (1.3-5.4 ‰) and galena (5.9-7.3 ‰) do not follow the model. This suggests that these three phases were not in equilibrium, meaning that they did not precipitate from the same fluid and that the source of $\delta^{34}S$ is changing with respect

to the speciation of separate sulphide phases (Sharp, 2007). This suggests multiple fluids in a episodic veining system.

Sulphur isotope compositions of hydrothermal sulphur bearing phases are controlled by the total sulphur isotope composition of the fluids, and by the temperature, oxygen fugacity and pH at the site of mineralization (Ohmoto and Goldhaber, 1997; McCuaig and Kerrich, 1998). The initial $\delta^{34}S$ composition of the source fluid is determined by the various sulphur reservoirs from which the fluid could have sourced sulphur. $\delta^{34}S$ values from pyrite for various gold and lode gold deposits are presented in Figure 6.16.

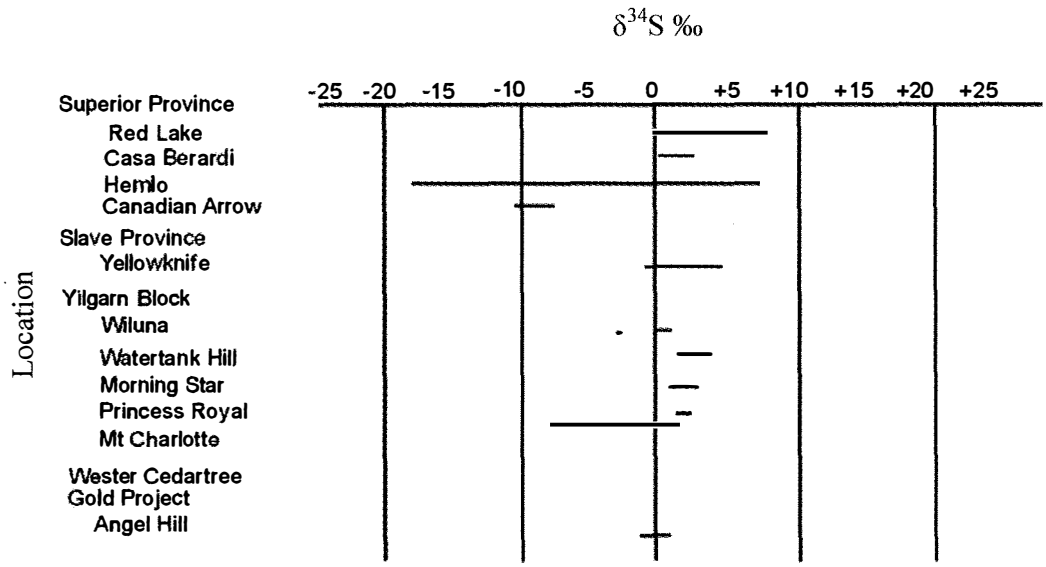

Figure 6.16. $\delta^{34}S$ values of pyrite from various Archean lode gold settings. Values from McCuaig and Kerrich (1998)

Archean settings generally have $\delta^{34}S$ values restricted to 0 to +9 ‰ which have been interpreted to indicate that the fluid redox state was below the sulphate/bisulphide boundary, and that the sulphur source was relatively isotopically homogeneous between - 1 to +8 ‰ (McCuaig

and Kerrich, 1998). $\delta^{34}S$ values such as these were likely derived either directly from magmatic sources or indirectly by dissolution or desulphidation of primary magmatic sulphide minerals (Golding et al., 1990; McCuaig and Kerrich, 1998). $\delta^{34}S$ values which vary from this norm are generally thought to be the result of sulphur inherited from the source rocks (Golding et al., 1990). For example, the turbidite-hosted deposits of the Palaeozoic Meguma Terrane contain sulphides with $\delta^{34}S$ values ranging from +9 to + 24, indicating that most sulphur was derived from the host, similarly $\delta^{34}S$ values of sulphides from the Juneau gold belt deposits correspond to the $\delta^{34}S$ values of hosting sediments (McCuaig and Kerrich, 1998). Strongly negative $\delta^{34}S$ values such as those from Wiluna, Lake View, North Kalgoorlie, Canadian Arrow and Hemlo deposits have been attributed to significant oxidation of the fluids (Fig. 6.16; McCuaig and Kerrich, 1998). The range of delta $\delta^{34}S$ values for the Angel Hill gold zone pyrite suggests that the sulphur was likely from magmatic sources.

$\delta^{18}O$ values were measured on Fe-dolomite phases found within the high grade gold zone. These carbonate phases predominantly occurred as crosscutting veins as well as alteration products of mafic phases (augite, tremolite) and within the bulk groundmass. For this study only Fe-dolomite vein material was analysed and did not include magnesite alteration of serpentine from within the less altered peridotite footwall. These analyses returned an average of $\delta^{18}O$ 15.6 ‰ and showed only little variance from sample to sample (13.6-17.9 ‰; Table 6.1). This suggests that there is one predominant phase of Fe-carbonate veining throughout.

$\delta^{18}O$ values for quartz were used to investigate genetic differences between observed quartz phases; quartz 1 (primary vein quartz; Q1) and quartz 2 (quartz overgrowths and recrystalised quartz; Q2). The values have been plotted on Figure 6.17 and show there are two separate fields for quartz mineralisation. Primary quartz (Q1) plots with a mean of $\delta^{18}O$ value of

9.1‰ whereas secondary quartz (Q2) plots with a mean $\delta^{18}O$ value of 11.8 ‰. This suggests that the secondary quartz is indeed a separate generation and has formed from a distinct fluid.

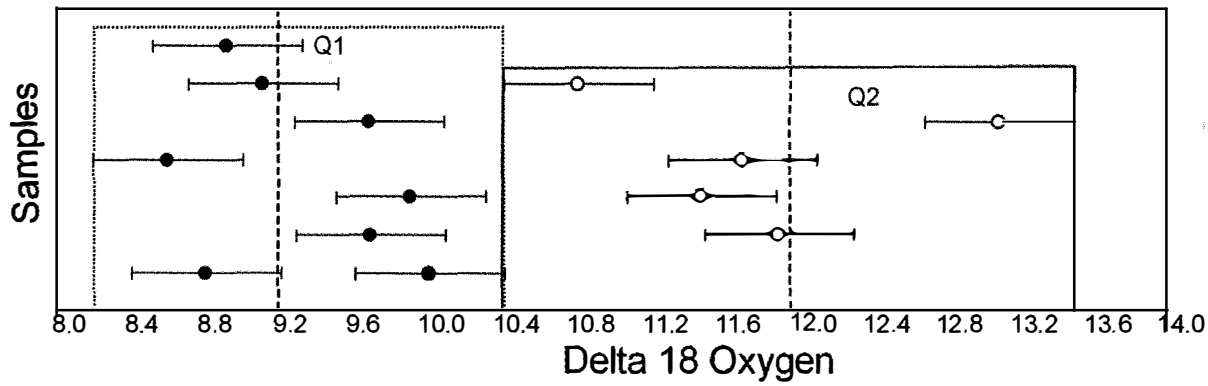

Figure 6.17. Plot of $\delta^{18}O$ samples of both phases of observed quartz. Q1 is interpreted primary quartz and Q2 interpreted as secondary quartz.

Oxygen isotope compositions of hydrothermal ore-forming fluids for lode gold settings have a narrow range of $\delta^{18}O$ values (Fig. 6.18; McCuaig and Kerrich, 1998). This range is between +6 to +11 ‰ $\delta^{18}O$ and reflects magmatic and metamorphic source waters respectively (Fig. 6.18; McCuaig and Kerrich, 1998). Quartz with $\delta^{18}O$ values greater than +8 ‰ likely reflects a mixed source of magmatic and metamorphic fluids, and values above +14 ‰ $\delta^{18}O$ likely reflect $\delta^{18}O$ enriched source reservoir such as a metasedimentary unit (Shaw et al., 1991; McCuaig and Kerrich, 1998). The analyzed $\delta^{18}O$ values of quartz 1 and quartz 2 likely represent a transition from magmatic to metamorphic fluids which suggests a history of protracted veining.

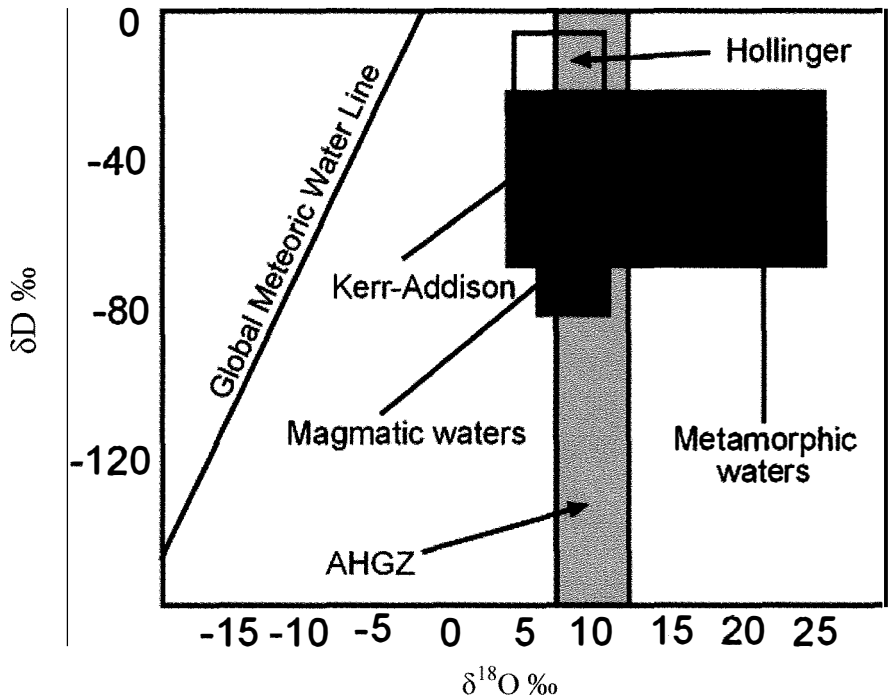

Figure 6.18 Calculated isotopic compositions of ore-forming fluids associated with Archean Lode gold deposits from McCuaig and Kerrich (1998). Grey window indicates the maximum range of sampled quartz phases for both Quartz 1 and 2. No δD values were determined in this study.

The stable isotope analyses on both sulphide and fluid phases are interpreted to represent formation from multiple fluids over a very small space suggesting multiple pulses along the same fluid pathways. Both $\delta^{18}O$ and $\delta^{34}S$ suggest ore forming fluids have a magmatic and metamorphic component. What appear to be texturally secondary phases of quartz have distinct isotopic signatures whose values suggest interaction with metamorphic fluids and an input of crustal material. Both the $\delta^{18}O$ and $\delta^{34}S$ share similar characteristics with other well documented Archean lode gold systems. The SIMS proved to be a useful tool to analyze these complex relationships as traditional techniques would have homogenised any unique isotopic signatures.

6.5 Paragenesis

The paragenesis of the Angel Hill gold zone has been broken down into three phases; regional metamorphism, mineralization, and supergene weathering. The mineral phases and relative timing have been plotted on Figure 6.19. Regional metamorphism is only preserved in the distal hangingwall and footwall. These reflect the same regional greenschist facies metamorphism observed throughout the property and include serpentine, chlorite, albite, amphibole and muscovite. Faulting occurs due to rheologic competency differences which occurred during regional scale deformation events. Faulting is episodic throughout the mineralizing event which is evident by numerous cataclastic fractures and overprinted quartz and carbonate veining.

Fluids likely propagated along these faults and included carbonate which formed magnesite after serpentine, and quartz veining. Initial sulphides include the mineralization of pyrite followed by sphalerite and galena. Gold which occurs with pyrite formed contemporaneously with barren pyrite. Quartz 1 formed first and formed coarse grained vein quartz with quartz 2 forming secondary overgrowths and recrystallised quartz. Fuchsite and muscovite formed extensively throughout the deformation and veining history of the zone. Carbonate veining cross cuts all structures and minerals and indicates the final phase.

Supergene alteration consists of hematite formation after Fe-carbonate and pyrite. This alteration is extensive and is evident by the extremely rusty weathered surface exposed over the entirety of the two strip zones.

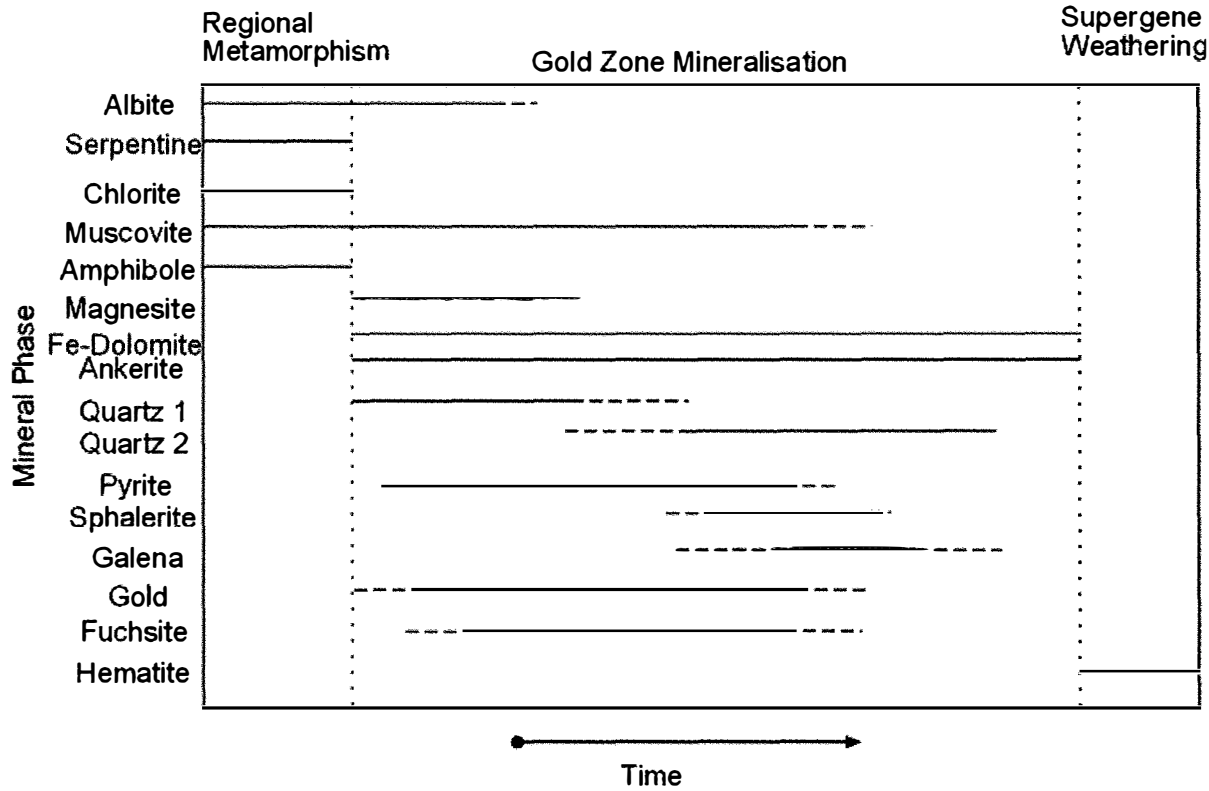

Figure 6.19. Paragenesis diagram for the Angel Hill Gold Zone.

6.6 Discussion

6.6.1 Listwanite metasomatism

Ultramafic rocks, such as these, which have been extensively altered to an assemblage of carbonate (Fe-dolomite-ankerite-magnesite), quartz and fuchsite, together with disseminated pyrite and other accessory minerals were first described by Rose (1837), who had surveyed gold deposits in the Ural mountains in an attempt to characterize mineralogical aspects of the gold mines (Ash and Arksey, 1990; Halls and Zhao, 1995; Akbulut et al., 2006). Rose described listwanites as altered rocks consisting of gold-bearing quartz-lodes with abundant carbonate quartz and fuchsite (Halls and Zhao, 1995). Since the first discoveries by Rose (1837) in the Ural

mountains more local occurrences of listwanitic rock assemblages have been recognized within the Superior Province, including the Porcupine and Kerr-Addison mines in Timmins, as well as camps in Larder Lake and Chibougamou (Halls and Zhao, 1995; Akbulut et al., 2006). However, listwanite deposits are not restricted to the Archean and occur in other more modern settings, including Urushten, north Caucasus, the Alps, Liguria, Italy, Mali, Morocco, Saudi Arabia, the Western Carpathians of the Slovak Republic, the Arac Massif, Kastamonu, in Turkey, the Cordillera in British Columbia and perhaps the best known, the Mother Lode system of California and (Ash and Arksey, 1990; Halls and Zhao, 1995; Akbulut et al., 2006; Pylusina et al., 2007).

Listwanite lode-gold localities are generally located within, or near, major fault or shear zones, many of which are terrane boundaries (Ash and Arksey, 1990; Halls and Zhao, 1995). Listwanite lode gold deposits form exclusively in packages of serpentinized and carbonatized ultramafic rocks, characteristically in tectonically disrupted accreted oceanic terranes (Halls and Zhao, 1995). These tectonic settings produce thrusted and stacked units in which ultramafic rocks are located along regional scale reverse and normal faults and shears which act as a plumbing system for metamorphic and hydrothermal fluids (Akbulut et al., 2006). For the AHGZ, peridoditic basal rocks of the Kakagi Sill are emplaced in a competency contrast against gabbro, the contact of which was faulted during regional deformation creating fluid pathways.

Listwanite deposits form by metasomatic alteration of ultramafic rocks (Ash and Arksey, 1990; Halls and Zhao, 1995; Akbulut et al., 2006). The primary result is carbonatization in the presence of K-bearing fluids. In hydrothermally-altered ultramafic rocks, the primary ferromagnesian silicate minerals (at the AHGZ these include the serpentine minerals antigorite and orthoantigorite which formed after olivine during regional metamorphism) are replaced by

an assemblage of Mg-Fe carbonate (typically Fe-dolomite and magnesite), quartz and chromian muscovite (fuchsite) with accessory minerals including pyrite and other sulphides (galena and sphalerite with in the AHGZ; Akbulut et al., 2006). To produce these listwanitic assemblages from mafic silicates requires the addition of both CO_2 and K under a mesothermal regime (Halls and Zhao, 1995). Sources of Cr for fuchsite formation come from the remobilisation of chromite, which has been observed in least altered rocks of the Kakagi Sill (Fig. 6.20), and potentially from Cr bearing silicates such as olivine. If Cr is not abundant in high enough concentrations muscovite will form instead (Halls and Zhao, 1995). Listwanites form by intermediate to low temperature metasomatic alteration of serpentine altered mafic-ultramafic rocks and are commonly located within or near major fault and shear zones (Halls and Zhao 1995).

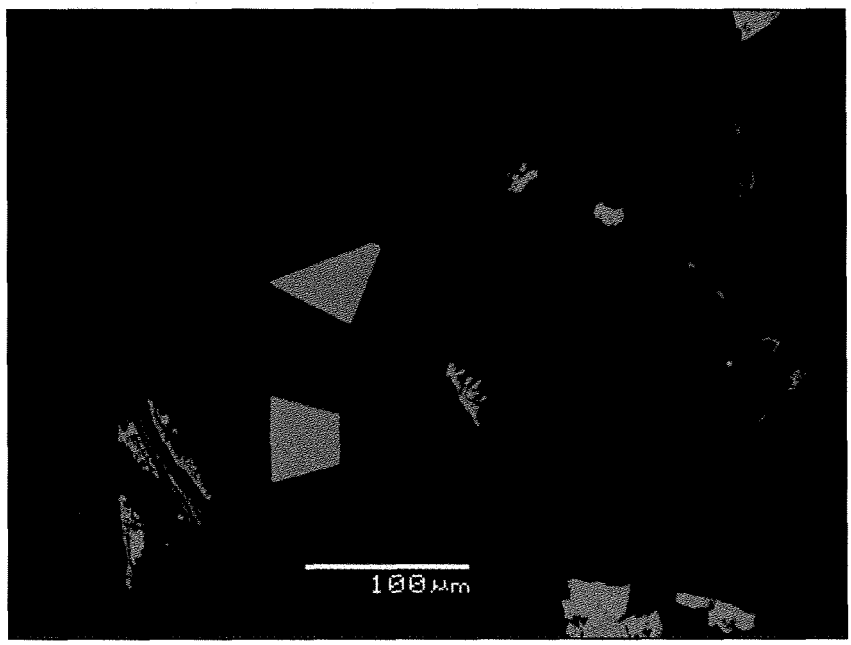

Figure 6.20. Disseminated chromite in least altered footwall peridotite of the Kakagi Sill, source for Cr in fuchsite formation.

6.6.2 Lode Gold

Listwanite deposits are among a group of structurally hosted lode gold vein systems in metamorphic terranes which constitute a single, coherent group of epigenetic precious metal deposits (Kerrich, 1993). These occurrences have been described historically as, gold only, lode gold, or Archean gold deposits. The term gold only however, does not accurately describe deposits which can contain variable to economic amounts of silver, tungsten and tellurium (Kerrich, 1993). The phrase Archean gold deposit exists because of the relative abundance of lode gold deposits in late Archean greenstone belts often with spatial association with komatiites and banded iron formations which are lithologies that are generally restricted to the Archean (Kerrich, 1993). There are, however, lode gold deposits associated with metamorphic volcanic belts within the Proterozoic and Cenozoic which share common characteristics with Archean localities, suggesting that these deposits form from a single common process (Kerrich and Cassidy, 1994). The genetic term mesothermal gold is more appropriate (whereby mesothermal refers to the implication of mid-crustal environment) to describe these deposits, since the majority of deposits occur in greenschist facies metamorphic terranes (Kerrich, 1994; McCuaig and Kerrich, 1998; Groves et al., 2003).

Mechanisms for formation of mesothermal systems center on the notion that they require gold bearing quartz veins precipitating in shear zones that focused metamorphic fluids generated at depth, all of which postdate or overprint regional metamorphism. This model therefore suggests that structurally hosted veins focused fluid advection from large source reservoirs using regional heat flow (Kerrich, 1994; McCuaig and Kerrich, 1998; Groves et al., 2003). These systems are in effect in geodynamic environments during the transpressive accretion of allochthonous terranes (Kerrich, 1993). This model also explains the global distribution of

mesothermal gold deposits with respect to periods of increased continent building such as the late Archean, lower Paleozoic and Mesozoic (McCuaig and Kerrich, 1998).

6.6.3 Gold Complexes

The mechanics of mesothermal gold systems require a gold source, fluid pathway and trap for mineralization. Aqueous ions, such as Au^{+}, in hydrothermal solution have solubilities that are far too low to account for the formation of an ore deposit (Wood and Samson, 1998). In order to facilitate the transportation of metal ions in solution, ore metal ions must form complexes. Aqueous gold bisulphide and gold chloride complexes are considered the most likely species for gold transport in hydrothermal systems due to the relative abundance and availability of reduced sulfur and chlorine ligands as well as the high thermodynamic stability of these complexes (Mikucki, 1998). The main gold complexes are Au(HS), $HAu(HS)_2$, $Au(HS)_2^-$, and Au(OH) (Mikucki, 1998; Stefansson and Seward, 2004). Complexes formed in solutions with low sulphide and abundant chloride form complexes with chlorine ions as ligands in the form of $AuCl_2^-$; however, these do not account for significant concentrations of gold in Archean lode gold systems (Roberts and Sheahan, 1988; Stefansson and Seward, 2004). Gold precipitates from hydrothermal fluids in reaction to changes in the conditions of the fluid. Changes in temperature, pressure, ligand activity, phase separation, boiling, mixing and sulphide mineral precipitation can lead to gold deposition (Phillips and Evans, 2004). These specific changes reflect changes in the geological setting. Temperature and pressure changes with respect to gold solubility are important because as a depositional mechanism it has implications on the transportation of fluids from deep sources (Mikucki, 1998, Stefansson and Seward, 2004). These fluids precipitate gold when changes in the solution cause instability in the gold complexes. These instabilities have been shown to be controlled by changes in the pressure-temperature of the system, phase

separation largely controlled by the vaporization of CO_2, and fluid-rock interaction with the wall rock during sulphide mineralization. Archean lode gold systems, like the AHGZ, are dominated by relatively simple mineralogy which includes gold associated predominantly with pyrite with accessory minerals of pyrrhotite and lesser amounts of arsenopyrite, galena and molybdenite.

6.7 Summary

In summary, the ultramafic and mafic rocks of the AHGZ, which have been strongly altered to carbonate-silica-fuchsite, have undergone extensive listwanitic metosomatism as a result of interaction with fluids generated at depth, which were channelled along the fault structure which propagated along the contact between the peridotite and gabbro subunits of the Kakagi Sill (whereby faulting resulted from competency contrasts between these units likely related to the large scale shear system of the Cameron Lake Pipestone Lake shear zone). Stable isotope geochemistry, cataclastic fault structures, and network veining textures suggest that the fault system (fluid pathway) were active for many "pulses" of fluids creating a protracted mineralizing system. Mineralization within the zone is comprised primarily of pyrite with lesser amounts of sphalerite and galena. Gold occurs as free gold and sylvanite forming small inclusions within and rimming pyrite grains generally restricted to quartz veins within the bulk of the main deformation zone. The Angel Hill Gold Zone represents a mesothermal gold system which shares common characteristics of other well documented Archean lode gold occurrences.

Chapter 7:
Conclusions

The geology of the West Cedartree Gold Project encompasses three assemblages of the Kakagi-Rowan Lakes greenstone belts. These include from east to west the mafic metavolcanic rocks of the Snake Bay Formation, mafic and ultramafic intrusive rocks of the Kakagi Sill and intermediate to felsic metavolcanic rocks of the Emm Bay Formation. The Snake Bay Formation consists of pillowed and massive basalts and fine grained tuffs which are indicative of subaqueous volcanism. Overlying these rocks are the breccias and tuff breccias of the Emm Bay Formation which are interpreted to have been deposited either subaerially or in a shallow water environment. The Kakagi Sill, intruded between these two volcanic units, consists of a medium grained gabbro roughly 1200 meters thick, with basal and intraformational coarse grained and variably textured peridotite and pyroxenite horizons up to 150 m thick. The upper contact of the sill with the intermediate to felsic rocks of the Emm Bay Formation is variable, diffuse, and displays no contact metamorphic aureole, suggesting that the country rocks were still hot when the sill intruded.

Trace element geochemistry of the Snake Bay Formation and the Kakagi Sill suggests that these rocks are contaminated island arc tholeiites. The Emm Bay Formation rocks represent subduction related arc rocks likely formed in a back arc setting. The isotopic signatures suggest these rocks formed from depleted mantle and have been metasomatised. The negative Nb anomalies observed in the island arc tholeiites and the enriched isotopic signatures likely resulted from the source melts interacting with metasomatised arc lithospheric crust. The tectonic setting for these rocks is that of the oceanic plateau like rocks of the Snake Bay Formation overlain by the subduction related

volcanic rocks of the Emm Bay Formation, which have been intruded by the mafic to ultramafic Kakagi Sills. Such an arrangement of tectonic assemblages likely formed in a back arc environment as the result of a subduction zone stepping backwards after accretion of an oceanic plateau.

The Angel Hill Gold Zone occurs as quartz and carbonate veining infilling brittle faults exposed along a portion of the contact between the ultramafic footwall and gabbro hangingwall within the Kakagi Sill. This fault, known as the master fault, displays brittle cataclastic textures as well as refaulted segments, which are suggestive of multiple episodes of deformation. The fault has been interpreted to have formed along the contact of these two units as a result of competency differences during regional deformation, possibly as a second or third order splay of the much larger Cameron Lake-Pipestone Lake shear zone. The AHGZ is characterised by rusty weathering caused by extensive weathering of Fe-bearing carbonate alteration. Alteration of the peridotite footwall includes extensive magnesite alteration after serpentine altered olivine, as well as an influx of silica. Fuchsite alteration is also extensive throughout the mineralized zone forming large green mats up to 20 m in width. Alteration within the gabbro hangingwall consists of extensive Fe-bearing carbonate and silicification. The main gold zone consists of abundant quartz and carbonate veining along the master fault, with associated pyrite, sphalerite, galena and gold mineralization. Textures suggest episodic veining with healed and cross-cutting quartz and carbonate veining. Gold mineralization consists of free gold and sylvanite both as inclusions in and rimming pyrite grains, as well as along fractures within quartz. $\delta^{34}S$ analyses on pyrite grains. This suggests that the gold was transported using bi-sulphide ligands and was likely deposited when pyrite mineralization was

induced which occured when the mineralizing fluids were reduced as a result of interaction with Fe-bearing carbonate and silicate minerals. At least two generations of quartz were observed associated with gold mineralization. Quartz 1 has been interpreted to be primary vein quartz, whereas quartz 2 has been interpreted to be secondary quartz formed as overgrowths and recrystalized subordinate grains. $\delta^{18}O$ isotope analyses from both quartz 1 and 2 confirm that these are indeed distinct phases and that quartz 1 displays a magmatic signature whereas quartz 2 displays a metamorphic signature. Both the $\delta^{34}S$ and the $\delta^{18}O$ values are consistent with published data for other Archean lode gold settings. The textural relationships and stable isotope geochemistry of the AHGZ suggest a protracted system of faulting and veining.

Ultramafic rocks associated with the AHGZ which have been extensively altered to an assemblage of carbonate (Fe-dolomite-ankerite-magnesite), quartz and fuchsite, together with disseminated pyrite, galena and sphalerite comprise a subset of mesothermal gold systems termed listwanites. Listwanite lode-gold systems are found within, or near, major fault or shear zones and form exclusively in packages of serpentinized and carbonatized ultramafic rocks. Listwanites form as a result of carbonatization in the presence of potassium bearing fluids. Fe-silicate minerals like serpentine are replaced by an assemblage of Mg-Fe carbonate, quartz and fuchsite. Although listwanite settings are not unique to the Archean, the AHGZ is the first documented occurrence of this rock assemblage in the Kakagi-Rowan Lakes greenstone belts and the Kenora mining district as a whole.

This study has significant implications for exploration within the Kakagi-Rowan Lakes greenstone belt, in which no major deposits of significant grade have yet gone into

production. All known gold occurrences in the Kakagi-Rowan Lakes greenstone belt occur in areas of competency differences. These include those near or along the transition from mafic to intermediate volcanism (Golden Sun Occurrence), those that occur in fractures in the differentiated ultramafic to mafic Kakagi sills (Angel Hill; Dogpaw; Canadian Arrow) and those that occur along shear and fault zones (Dubenski; Cameron Lake occurrence). With five intrusive sills each with extensive strike extensions, the potential for continuity of a listwanite mesothermal gold system is highly likely within the Kakagi-Rowan Lakes greenstone belt. As for the West Cedartree Gold Project it is recommended that further exploration be undertaken along strike to determine continuity of mineralization as well as test the intraformational peridotite unit, for listwanitic alteration. In addition further study of the mineralized zones within the West Cedartree property is recommended in order to test if the relationships observed in the Angel Hill Gold Zone are also present there.

References

Akbulut, M., Ozkan, P. and Ishan Karayigit, A. 2006.*The genesis of the carbonatized and silicified ultramafics known as listvenites: a case study from the Mihalıccik region (Eskisehir), NW Turkey.* Geological Journal 41. 557-580

Ash, C.H. and Arksey, R.L. 1990.*The Listwanite Lode Gold Association in British Columbia.* Geology Fieldwork 1989: Paper 1990-1

Blackburn, C.E. and Janes, D.A., 1983. *Gold Deposits in Northwestern Ontario.* Ontario Geological Survey Miscellaneous Paper 110. 1-18

Blackburn, C.E., Johns, G.W., Ayer, J., and Davis, D.W., 1991. *Wabigoon subprovince.* In Geology of Ontario. Ontario Geological Survey, Special Volume 4, Part 1. 303–381

Burnham, O.M., and Schweyer, J., 2004. *Trace Element Analysis of Geological Samples by ICP MS at the Geoscience Laboratories: Revised Capabilities Due to Improvements to Instrumentation.* In Summary of Field Work and Other Activities 2004. Ontario Geological Survey Open File Report 6145. 54-1 to 54-20.

Burwash, M. E.,1933. *Geology of the Kakagi Lake Area.* Ontario Department of Mines. Annual Report 42. 41-92

Card, K., and Ciesielski, A., 1986. *Subdivisions of the Superior Province of the Canadian Shield.* Geoscience Canada 13: 5-13.

Crowe, D. and Vaughan, R.G., 1996. *Characterization and use of isotopically homogeneous standards for in situ laser microprobe analysis of $^{34}S/^{32}S$ ratios.* American Mineralogist 81. 187-193

Cuddy, R.G.,1971. *Structural Study of Kakagi Lake Area, North western Ontario.* Unpublished Masters Thesis, McMaster University, 128p.

Cutting, D. and Anthony E., 2005. *Exploration Summary and Mineral Resource Estimate for the Angel Hill Gold Zone: West Cedartree Gold Project, Kenora Mining District Northwestern Ontario.* Houston Lake Mining Inc. 1-494

Davies, J. and Morin, J., 1972. *Cedartree Lake Area: District of Kenora.* Ontario Division of Mines Preliminary Reports in Geology. Scale ¼ mi to 1 in

Davies, J. and Morin, J., 1976. *Geology of the Cedartree Lake Area: District of Kenora.* Ontario Division of Mines. Geoscience Report 134. 1-73

Davis, D.W., and Edwards, G. R., 1982. *Zircon U-Pb Ages from the Kakagi Lake Area, Wabigoon Subprovince, Northwest Ontario.* Canadian Journal of Earth Sciences 19. 1235-1245

DePaolo, D.J., 1981. *Neodymium isotopes in the Colorado Front Range and Crust Mantle Evolution in the Proterozoic.* Nature 291. *1-193*

Fahrig, W. F., 1965. *Age Determinations and Geological Studies, K/Ar Isotopic Ages.* GSC Report 6. 65-17

Goodwin, A.M., 1965. *Preliminary Report on Volcanism and Mineralisation in the Lake of the Woods-Manitou Lake-Wabigoon Region of North Western Ontario.* Ontario Department of Mines Preliminary Report 1965-2. 1-63

Groves, D.I., Goldfarb, R.J., Robert, F. and Hart, C., 2003. *Gold Deposits in Metamorphic Belts: Overview of Current Understanding, Outstanding Problems, Future Research, and Exploration Significance.* Economic Geology 98. 1-29

Halls, C. and Zhao, R., 1995. *Listvenite and related rocks: perspectives on terminology and mineralogy with reference to an occurrence at Cregganbaun, Co. Mayo, Republic of Ireland.* Mineral Deposita 30. 303-313

Hill, R.E.T., Barnes, S.J., Gole, M.J. and Dowling, S.E., 1990. *Physical volcanology of komatiites: a field guide to the komatiites of the Norseman–Wiluna greenstone belt, Eastern Goldfields Province, Yilgarn Block, Western Australia.* Geol. Soc. Aust. (W. Aust. Div.), Excursion Guidebook

Hollings, P., 1998. *Geochemistry of the Uchi Subprovince, northern Superior Province: An evaluation of the geodynamic evolution of the northern margin of the Superior Province Ocean Basin.* Ph. D. Thesis: University of Saskatchewan, Saskatoon Saskatachewan

Hollings, P., 2002. *Archean Nb-enriched basalts in the northern Superior Province.* Lithos 64: 1-14.

Hollings, P. and Kerrich, R., 1999. *Trace element systematics of ultramafic and mafic volcanic rocks from the 3 Ga North Caribou greenstone Belt, Northwestern Superior Province.*Precambrian Research 93. 257-279

Hollings, P. and Wyman, D., 1999. *Trace element and Sm-Nd systematics of volcanic and intrusive rocktypes from the 3 Ga Lumby Lake greenstone belt, Superior Province: Evidence for Archean plume-arc interaction.* Lithos, 46. 189-213.

Jenner, G., 1996. *Trace element geochemistry of igneous rocks: geochemical nomenclature and analytical geochemistry.* In: Wyman, D. (Ed.). Trace Element Geochemistry of Volcanic Rocks: Applications for Massive Sulphide Exploration. Geological Association of Canada Short Course Notes 12. 51-77

Johns, W.G., 1986. *Kakagi Lake-Rowan Lake Regional Geology, District of Kenora.* Summary of Field Work and Other Activities 1986, Ontario Department of Mines. 1-6

Kaye, L. 1973: Rowan *Lake Area, District of Kenora; Ontario Division of Mines*. Preliminary Map P.831, Geological Series, scale I:15840. Geology I972

Kerrich, R. and Wyman, K. 1990. *Geodynamic setting of mesothermal gold deposits: An association with accretionary tectonic regimes.* Geology I8. 882-885

Kerrich, R. and Cassidy, K.F., 1994. *Temporal relationships of lode gold mineralization to accretion, magmatism, metamorphism and deformation Archean to present: A review.* Ore Geology Reviews 9. 263-310

Kerrich, R., Goldfarb, J., and Richards, J., 2005. *Metallogenic Provinces in an Evolving Geodynamic Framework.* Society of Economic Geologists, Inc: Economic Geology 100th Anniversary Volume. 1097–1136

Lawson, A.C., 1885. *Report on the Geology of the Lake of the Woods Region with Special Reference to the Keewatin Belt of Archean Rocks.* Geological Survey of Canada Annual Report. I. 1-155

Le Bas, M. J., Le Maitre, R. W., Streckeisen, A. & Zanettin, B., 1986. *A chemical classification of volcanic rocks based on the total alkali–silica diagram.* Journal of Petrology 27. 745 750

McCuaig ,T.C. and Kerrich, R., I998. *P-T-t-deformation-fluid characteristics of lode gold deposits: evidence from alteration systematics.* Ore Geology Reviews 12. 381-353

McCuaig, T.C., Kerrich, R., and Xie, Q., 1994. *Phosphorous and high field strength anomalies in Archean high-magnesian magmas as possible indicators of source mineralogy and depth.* Earth and Planetary Science Letters I24. 22I-239.

Melling, D.R., Watkinson, D., Poulsen, K. and Chorlton, L., I985. *The Geological Setting and Genesis of the Cameron Lake Gold Deposit.* Geoscience Research Grant Program Summary of Research 1984-1985, Ontario Department of Mines. 1-16

Melling, D.R. and Watkinson, D., I986. *The Geological Setting and Genesis of the Cameron Lake Gold Deposit.* Geoscience Research Grant Program Summary of Research 1985-1986, Ontario Department of Mines. 1-I0

Melling, D.R., Watkinson, D. and Taylor, R., I986. *Detailed Lithological, Structural, and Alteration Mapping of the Cameron Lake Gold Deposit, Northwestern Ontario.* Geoscience Research Grant Program Summary of Research 1985-1986, Ontario Department of Mines. 1-7

Melling, D.R., I988. *The Lithogeochemistry and Light Stable Isotope (Carbon, Oxygen, and Sulphur) Geochemistry of Hydrothermal Alteration and Breccia Veins from the*

Cameron Lake Gold Deposit, Northwestern Ontario. Geoscience Research Grant Program Summary of Research 1987-1988, Ontario Department of Mines. 1-14

Melling, D.R., Watkinson, D. and Taylor, R., 1989. *Lithogeochemical, Isotopic and Fluid Inclusion Studies of Hydrothermal Alteration and Breccia Veins from the Cameron Lake Gold Deposit, Northwestern Ontario.* Geoscience Research Grant Program Summary of Research 1988-1989, Ontario Department of Mines. 1-11

Mikucki, E., 1998. *Hydrothermal transport and depositional processes in Archean lode-gold systems: A review.* Ore Geology Reviews 13. 307-321

Pearce, J., 1996. *A user's guide to basalt discrimination diagrams. In: Wyman, D. (Ed.). Trace Element Geochemistry of Volcanic Rocks: Applications for Massive Sulphide Exploration.* Geological Association of Canada Short Course Notes 12: 79-113.

Pearce, J., 2007. *Geochemical fingerprinting of oceanic basalts with applications to ophiolite classification and the search for Archean oceanic crust.* Lithos 100: 14-48.

Pearce, J., and Peate, D., 1995. *Tectonic implications of the composition of volcanic arc magmas.* Annual Review of Earth and Planetary Sciences 23. 251-285.

Percival, J., 2003. *Orogenic framework for the Superior Province: Dissection of the 'Kenoran Orogeny.'* Geological Survey of Canada, Western Superior NATMAP abstracts.

Percival J., 2006. *Geology and metallogeny of the Superior province, Canada.* Geological Survey of Canada: http://gsc.nrcan.gc.ca/mindep/synth_prov/superior/pdf/regional_synthesis.superior.percival.pdf

Percival, J.A., Sanborn-Barrie, M. and Skulski, T. and Stott, G.M. and Helmstaedt, H. And White, D.J., 2006.*Tectonic evolution of the western Superior Province from NATMAP and Lithoprobe studies.* Canadian Journal of Earth Sciences . 1085-1117

Percival, J., Mcnicoll, V., and Bailes, A. 2006. *Strike-slip juxtaposition of ca. 2.72 Ga juvenile arc and >2.98 Ga continent margin sequences and its implications for Archean terrane accretion, western Superior Province, Canada.* Canadian Journal of Earth Sciences 43. 895-927

Phillips, G. and Evans, K., 2004. Role *of CO_2 in the formation of gold deposits.* Letters to Nature 429. 860-863.

Phillips, G.N., Groves, D.L. and Kerrich, R., 1996. *Factors in the formation of the giant Kalgoorlie gold deposit.* Ore Geology Reviews 10. 295-317

Phinney, W. C, and Morrison, D. A. 1990. Partition coefficients for calcic plagioclase: Implications for Archean anorthosites. Geochimca et Cosmochimica Acta 54. 1639-1654.

Richard, P., Shimizu, N., and Allegre, C.J., 1976. *143Nd/144Nd, a natural tracer: an application to oceanic basalts.* Earth and Planetary Science Letters 31. 269–278

Riddler, R.H.,1965. *Petrographic study of a Crow Lake ultrabasic sill, Keewatin volcanic belt, northwestem Ontario*.Unpublished MSc. thesis, Univ. Toronto

Roberts, R. and Sheahan, P., 1988. Archean Lode Gold Deposits. *Ore Deposit Models.* Geoscience Canada. 1-20

Rollinson, H., 1993. *Using Geochemical Data: Evaluation, Presentation, Interpretation.* Pearson education limited. Essex, England.

Sharp, Z., 2007. *Principles of stable isotopes (1st ed).* Upper Saddle River, N. Pearson Preston Hall.

Smith, A. D. and Ludden, J.N., 1989. *Nd isotopic evolution of the Precambrian mantle.* Earth and Planetary Science Letters 93. 14-22

Stefansson and Seward. 2004. *Gold(I) complexing in aqueous sulphide solutions to 500°C at 500 bar.* Geochemica et Cosmochemica Acta. 68, no. 20. 4121-4143

Stern, R., Syme, E.C. and Lucas, S.B., 1995. *Geochemistry of 1.9 Ga MORB- and OIB-like basalts from the Amisk collage, Flin Flon Belt, Canada: Evidence for and intra formational oceanic origin.* Geochemica et Cosmochemica Acta 19. 376-379

Stott, G., 1997. *The Superior Province, Canada.* In: de Wit, M., and Ashwal, L. (Eds.). Greenstone Belts; Oxford Monographs on Geology 35. 479-505

Stott, G.M., Corkery, T., Leclair, A., Boily, M. and Percival, J., 2007. *A revised terrane map for the Superior Province as interpreted from aeromagnetic data.* Institute on Lake Superior Geology Proceedings, 53rdAnnual Meeting, Lutsen, MN, 53, part 1, p. 74-75.

Sun, S., and Mcdonough, W., 1989. *Chemical and isotopic systematics of oceanic basalts: implications for mantle composition and processes.* In: Saunders, A., and Norry, M. (Eds.). Magmatism in the Ocean Basins. Geological Society Special Publication: 313-345.

Smith, D. R. and McNutt, R. and Clifford, P., 1973. *Nature and Origin of Salic Pyroclastic rocks at Kakagi Lake, Northwestern Ontario.* Canadian Journal of Earth Sciences 12. 90-94

Thorpe, R.I. and Franklin, J.M., 1984. *Volcanic-associated Vein and Shear Zone Gold; in Canadian Mineral Deposit Types, A Geological Synopsis, Eckstrand, O.R.* Editor, Geological Survey of Canada, Economic Geology Report 36. 1-38.

Thurston, P.C., 1991. *Archean Geology of Ontario.* Ontario Geologic Survey, special volume 4. Part 1

Tomlinson, K.Y., Stevenson, R., Hughes, D., Hall, P., Thurston, C., and Henry, P., 1998. *The Red Lake Greenstone Belt: Evidence for Plume Related Magmatism at 3Ga and Evidence of an Older Enriched Source.* Precambrian Research 89. 59-76

Tomlinson, K.Y., 2000. *Neodymium isotopic data from the central Wabigoon Subprovince, Ontario: implications for crustal recycling in the 3.1 to 2.7 Ga sequences.* Geological Survey of Canada, Radiogenic and Isotopic Studies 13. 1-12

Tomlinson, K.Y., Greg, G.M., Percival, J. A., and Stone, D., 2004. *Basement terrane correlations and crustal recycling in the western Superior Province: Nd isotopic character of granitoid and felsic volcanic rocks in the Wabigoon subprovince, N. Ontario, Canada.* Precambrian Research 132. 245-274

Tomlinson, K.Y., Hughes, D., Thurston, P., Hall, P., 2004. *Plume magmatism and crustal growth at 2.9 to 3.0 Ga in the Steep Rock and Lumby Lake area, Western Superior Province.* Lithos 46. 103-136

Valley, J.W., Eiler, J.M., Graham, C.M., Gibson, E.K., Romanek, C.S. and Stolper, E.M., 1997. *Low-temperature carbonate concretions in the Martian meteorite ALH84001: evidence from stable isotopes and mineralogy.* Science 275. 1633-1638

Winchester, J.A., and Floyd, P.A., 1977. *Geochemical discrimination of different magma series and their differentiation products using immobile elements.* Chemical Geology 20. 325 -343

Wood, S.A. and Samson, I.M., 1998. *Solubility of Ore Minerals and Complexation of Ore Metals in Hydrothermal Solutions. Techniques in Hydrothermal Ore Deposits Geology.* Reviews in Economic Geology 10. 33-77

Yeates, J. and Vanderhorn, F., 1998. *Archean Lode Gold Deposits.* Journal of Australian Geology and Geophysics 17(4). 25-258

Appendix A

Sample Descriptions

Snake Bay Formation

Mafic Meta Volcanic Rocks

Easting	Northing	Sample ID	Sample Description
435036	5464462	07-51	Fine grained tuff. Medium to light green. Mostly chloritic with some 10-15% fine grained plagioclase. Crystal tuff? Weak to moderately foliated.
435402	5464915	07-85	Highly altered fine grained mafic volcanic tuff (basalt?). Medium green. Coarse grained 15 mm thick quartz carbonate vein with localized intense alteration to iron carbonate. Highly chloritic. Trace pyrite.
434934	5464280	07-87	Altered mafic volcanic rock. Greenish with light green grey fragments. Possible flow top or tuff breccia. Blocky mafic to intermediate fragments 1-12 mm, fine grained, closely packed in a fine grained mafic groundmass. Some iron carbonate alteration visible, up to 15%, especially around fragments.
434208	5463967	07-97	Highly chlorite altered mafic volcanic lapilli tuff. Medium to light green. Coarse grained unidentified phenocrysts in a fine grained mafic matrix. Highly altered to chlorite. Visible sulphides, 3-5% coarse grained 2-4 mm.
434097	5463868	07-196	Chlorite altered mafic volcanic tuff. Medium to dark green. Medium to fine grained with small lapilli fragments up to 1-2 mm, tuff.
434233	5464020	07-99	Altered fine grained mafic volcanic tuff or fine grained basalt. Weathered surface is green to grey and fresh surface is medium to dark green. Fine grained to aphanitic groundmass with 12-15% fine grained plagioclase phenocrysts.
434547	5464185	07-132	Fine grained altered tuff. Highly chloritic fine grained groundmass. No visible sulphide. No visible fabric. (Flow?)
437193	5464268	07-138	Chlorite altered fine to medium grained basalt. Minor amphibole and feldspar phenocrysts (15%). Slight carbonate alteration (<5%). Weak to moderate foliation.
435197	5464388	07-142	Fine grained chlorite altered mafic tuff. Green colour. Weakly foliated. Trace disseminated pyrite.
434176	5461960	07-148	Fine grained mafic meta volcanic rock. Heavily chloritic groundmass. Contains up to 8% connected blebs, up to 5mm, coarse grained pyrite. Weakly foliated, tuff?
433900	5461524	07-150	Highly altered mylonitic and silicified shear. Quartz veining up to 2cm. No visible mineralization. Iron carbonate alteration of groundmass up to 15%. Elongated grains parallel to deformation (slicken fibers, dextral sense).
435297	5464498	08-111	Medium grained chlorite altered mafic volcanic tuff. Coarser grained with fine grained lapilli up to 20%.
435076	5464516	08-247	Medium to fine grained medium green tuff. Highly altered to chlorite. Minor foliation.
436448	5464558	08-096	Chlorite altered basalt proximal to contact with gabbro. Medium grained, slight carbonate alteration up to 10%. Trace pyrite, disseminated.
434961	5463301	08-144vol	Chlorite altered mafic volcanic. Medium to fine grained with small lapilli fragments up to 1-2 mm, tuff.
435453	5464863	08-121vol	Altered mafic volcanic tuff. Green to light green. Heavily chloritised, pervasive carbonate 12-15%, fine to medium grained. Pyrite fine grained to disseminated 1-5%.

Snake Bay Formation

Mafic Meta Volcanic Rocks

Easting	Northing	Sample ID	Sample Description
435099	5464222	08-241	Fine grained foliated altered mafic volcanic. Could be pillowed with well preserved vesicles up to 2 cm. Fresh surface is greenish grey and heavily chloritised. Weathered surface is dark green grey with some rusty staining.
435397	5465060	08-122	Carbonate altered sheared mafic tuff. Sample is of vein from within shear. Moderately mineralized with up to 15% pyrite, fine grained and disseminated. Silica and carbonate flooding within up to 25% proximal to contact and within shear.
435424	5465060	08-122 B	Intense carb veining within altered mafic volcanic tuff, coarse carbonate pervasive throughout (15%) . Disseminated pyrite up to 3%.
434720	5463067	08-147	Altered medium to fine grained mafic volcanic. Slight alteration to carbonate with minor carbonate veining. Trace to % very fine grained disseminated pyrite with minor associated pyrrhotite.
434631	5463216	08-194	Carbonate altered sheared mafic tuff(basalt?). Moderately mineralized with up to 15% pyrite and pyrrhotite as fine grained and disseminated. Silica and carbonate flooding up to 20%.
436160	5463485	08-253	Fine grained mafic meta volcanic rock. Heavily chloritic groundmass. Contains up to 8% connected blebs, up to 5mm, coarse grained pyrite. Weakly foliated, tuff?
436337	5463457	08-267	Chlorite altered fine to medium grained basalt. Minor amphibole and feldspar phenocrysts (15%). Slight carbonate alteration (<5%). Weak to moderate foliation
434775	5463407	08-193	Altered mafic volcanic tuff, slightly sheared with in filling of carbonate. Weathered surface shows rusty staining. Fresh surface is dark green.12% pyrite, disseminated mostly, with the occasional bleb less than 1 cm.
434457	5463325	08-211	Fine grained chlorite altered mafic tuff. Green colour. Weakly foliated. Trace disseminated pyrite.
435293	5464669	08-251	Fine to medium grained chlorite altered mafic volcanic. Either massive flow or basalt? Green to grey coloured weathered surface, fresh surface is dark to medium green.
435542	5465114	08-124	Altered typical fine grained mafic tuff. Thoroughly chlorite altered. Weakly foliated. Trace to 1% disseminated pyrite.
435856	5464931	08-66	Altered mafic tuff, medium to dark green. Fine grained, highly chloritised.
435076	5464516	08-250	Fine grained mafic tuff to basalt. Green grey weathered surface, dark to medium green fresh surface. Predominantly altered to chlorite. Weakly foliated. Trace pyrite.
435167	5463452	08-136	Fine grained chlorite altered mafic tuff. Green colour. Weakly foliated. Trace disseminated pyrite.

Emm Bay Formation

Felsic Meta Volcanic Rocks

Easting	Nothing	Sample ID	Sample Description
434097	5463869	07-96	Highly altered intermediate metavolcanics. Fine grained to aphanitic. Somewhat fractured, with fracture filling by quartz. Light greenish grey in colour. Iron carbonate alteration < 5%.
437787	5464364	07-137	Fine grained sheared (strongly foliated tuff?) felsic to intermediate metavolcanics. Abundant (15%) 1-2mm carbonate stingers.
436453	5464183	197104	Intermediate to felsic volcanic rock, tuffaceous with breccia fragments (35% 1- 8 cm). Fine grained groundmass highly altered to chlorite. Brecciated fragments are sub angular.
433989	5463278	08-186	Altered fine to medium grained felsic volcanic tuff. Heavily altered to chlorite some minor carbonate alteration up to 10%, pervasive. Blebs of pyrite up to 5mm, 3-5%.
436447	5463743	08-1207	Intermediate to felsic tuff, fine grained, Light green colour. Strongly foliated.
436696	5464144	08-224	Intermediate to felsic tuff with felsic breccia fragments. Fragments are sub rounded up to 5cm. Tuff is fine grained and highly altered to chlorite.
437050	5464933	08-085	Intermediate felsic volcanic breccia. Heavily chloritised fine grained groundmass with sub angular coarse grained rhyoltitic fragments upwards of 8 cm (35%).
436193	5462120	08-248	Intermediate to felsic volcanic rock, tuffaceous with breccia fragments (30% 1- 5cm). Fine grained groundmass highly altered to chlorite. Brecciated fragments are sub angular.
436193	5462120	197106	Intermediate to felsic tuff, fine grained, Light green colour. Strongly foliated.
436337	5463457	197107	Altered intermediate volcanic tuff with breccia with copper staining, up to 15% blebs of chalcopyrite, possible cuprite or bornite. Brecciated fragments are sub angular up to 4cm (30%).
435618	5462171	08-254	Intermediate to felsic volcanic rock, tuffaceous with breccia fragments (35% 1- 5cm). Fine grained groundmass highly altered to chlorite. Brecciated fragments are sub angular.
436293	5462430	197155	Intermediate to felsic volcanic rock, tuffaceous with breccia fragments (35% 1- 5cm). Fine grained groundmass highly altered to chlorite. Brecciated fragments are sub angular. Ground mass is strongly foliated
436443	5463880	07-93	Medium grained altered felsic volcanic. Groundmass is predominantly fine grained tuff with fine grained feldspar phenocrysts, up to 20%. Trace pyrite.
436399	5464107	07-89	Altered felsic volcanic. Fine grained, mostly chloritic. Visible feldspars up to 2 mm, 8%. Strongly foliated. Trace to 2% disseminated sulphide.
436465	5464265	07-139	Fine grained chloritic feslic volcanic tuff (flow?). Some visible fine grained plagioclase feldspars (<15%). Some visible fine grained amphibole (<5%).
436272	5464280	07-141	Felsic volcanic tuff. Fine grained, chloritic. Sample contains carbonate stringers. Trace very fine grained pyrite.
436339	5462309	197190	Highly altered intermediate metavolcanic rocks. Fine grained to aphanitic. Somewhat fractured, with fracture filling by quartz. Light greenish grey in colour.

Kakagi Sill

Gabbro

Easting	Northing	Sample ID	Sample Description
435406	5463590	07-30	Medium grained gabbro. 35% clinopyroxene (augite?) 35% 2-4mm plagioclase. 40% amphibole, sub rounded. 25% chlorite, fine grained. No visible sulphides. No visible Structure. Trace to no carbonate alteration.
435590	5463641	S1	Medium grained gabbro. Medium green grey weathered surface, dark green fresh surface. 40% amphibole, 40% plagioclase. Plagioclase is subhedral medium to fine grained laths. Chlorite up to 20%, fine grained. No sulphide. Weakly foliated. Poorly carbonate altered (<5%).
435492	5463638	S2	Medium grained gabbro. Medium to dark green grey weathered surface, dark green grey on fresh surface. 25% amphibole (hornblende), 20% chlorite. 40% plagioclase. 2% possible epidote. Minor quartz < 3%. No visible sulphide. No visible fabric.
435550	5463506	S3	Medium grained gabbro. Light to medium green colour on weathered surface and dark green on fresh surface. 20% plagioclase, heavily altered to chlorite. Anhedral amphibole 50%, fine grained chlorite 30%. Trace pyrite.
435636	5463481	S4	Medium grained gabbro. Green-grey weathered surface, dark green fresh surface. Mostly coarse to medium grained amphibole 60% with chlorite 20%. 20% medium grained subhedral plagioclase. Very weakly carbonate alterated (<5%). Trace pyrite, fine grained and disseminated. No fabric.
435467	5463904	07-27	Medium grained gabbro. Light to dark green grey weathered surface, dark green fresh surface. 50% subhedral amphibole. 30% chlorite. 20% subhedral plagioclase. Trace fine grained pyrite. Weakly silicified (2-3%).
435409	5463796	07-28	Carbonate altered mafic medium grained gabbro. Grain fining where in proximity of a small "shear" (2cm) with pervasive carbonate alteration (up to 15% up to 80% infilling shear). No visible sulphides. 35% amphibole. 25% chlorite. 30% plagioclase, sub to euhedral laths.
435271	5463321	07-32	Medium grained gabbro. Light to medium green (with up to 3% rusty staining) surface and dark green fresh surface. 40% amphibole, 15% chlorite. 2% quartz. 43% plagioclase. No sulphide, no fabric.
435131	5464098	07-39	Medium grained gabbro. 35% amphibole, 15% chlorite. 50% plagioclase, anhedral. Very minor carbonate alteration (<5%). Weakly silicified (<3%). No sulphide. No foliation.
436188	5464745	J1107	Visible mineralization in quartz vein, abundant copper staining. Visible chalcopyrite, pyrite very coarse blebs up to 5cm. Possible cuprite, possible pentlandite, possible bornite. Gabbro is medium grained light green. Contacts with quartz vein are sharp.
436188	5464745	J1107-1	Contact between medium grained gabbro and quartz vein. 70% coarse to medium grained amphibole with 30% plagioclase. Contact within proximity of quartz vein is intense quartz flooding, making a pervasive contact. Quartz is fine to medium grained, with epidote alteration up to 15% on wall rock margins.
436188	5464745	J1107-2	Coarse grained (blocky) quartz vein (8-12cm) within medium grained gabbro. Quartz is white to light grey and contains very little wall rock inclusions. Gabbro is medium grained light green. No visible mineralization in either quartz or wall rock.
435353	5464142	07-65	Medium to coarse grained gabbro. 35% subhedral plagioclase. 35% amphibole. 30% fine to medium grained chlorite. Trace pyrrhotite.

Kakagi Sill

Gabbro

Easting	Northing	Sample ID	Sample Description
435814	5465023	07-74	Medium grained slightly altered gabbro. 40% subhedral amphibole. 35% chlorite. 25% plagioclase. Trace fine grained pyrite.
435889	5465034	07-70	Medium grained mafic gabbro. 60% plagioclase found as isolated medium grained randomly oriented laths as well as in cumulates up to 2 cm (12%). Amphibole 30%, chlorite 30%. Trace sulphides. No fabric.
435559	5464674	07-79	Coarse to medium grained gabbro. Groundmass strongly altered to chlorite up to 50%. Subhedral amphibole phenocrysts up to 35% and plagioclase up to 15%. Moderate foliation. Trace pyrite.
435559	5464674	07-79B	Pegmatitic gabbro. 40% coarse plagioclase 2-18mm. 30% coarse amphibole. 25% Chlorite. Carbonate alteration and silicification up to 10%.
436278	5464182	07-88	Highly carbonate altered mafic gabbro. 40 % amphibole, 10% chlorite, 10% plagioclase, 40% carbonate. Carbonate appears to be replacing plagioclase as well as forming small veinlets up to 1.5cm.
435495	5462883	07-124	Fine grained medium to dark green gabbro. Amphibole 35%, chlorite 15%. Plagioclase 50%. Trace to 1% pyrite. No visible fabric.
436166	5464228	07-140	Gabbro, medium to fine grained. Strongly altered to chlorite up to 35%. Some visible amphibole, 25%, as well as plagioclase, 25%. Trace disseminated pyrite.
435415	5464255	07-144	Medium grained gabbro. Weathered surface is green to grey-green and fresh surface is dark to medium grained. 40% amphibole. 20% chlorite. 40% plagioclase. Weakly foliated.
435051	5462570	07-160	Medium to coarse grained gabbro. Green to medium grey green weathered surface, light to medium green fresh surface. 40% subhedral plagioclase. 30% amphibole. 30% fine to medium grained chlorite. Trace disseminated pyrrhotite.
435409	5464318	07-146	Coarse grained gabbro. 45% subhedral 1-5mm amphibole, hornblende, with 35% subhedral plagioclase laths. Chlorite is found as part of the finer grained groundmass up to 15%. Carbonate alteration is visible rimming plagioclase, 5%.
433127	5460980	07-165B	Carbonate altered coarse grained gabbro. Light to medium grey-green on weathered surface, light green on fresh surface. 20% subhedral amphibole. 40% plagioclase, 15% quartz, 20% carbonate, 5 % chlorite.
435925	5463960	07-112	Medium grained gabbro. 30% amphibole, 20% chlorite. 48% plagioclase, 2% epidote. Trace sulphide.
435560	5464279	07-167B	Coarse grained, heavily carbonate altered gabbro. 30% mafic groundmass, 40% carbonate alteration, 10% fuschitic alteration, 10% chloritic alteration, 10% silicification. Weakly foliated.
435269	5462336	07-166	Very coarse gabbro. Coarse plagioclase 15% strongly altered to chlorite 20%. Amphibole composes most of the groundmass (up to 60%), as well as forming coarse phenocrysts 30%. Locally 5% quartz. Trace pyrite, fine grained.
432849	5461136	07-162C	Highly altered medium grained gabbro. Weathered surface is rusty green grey and fresh surface is medium to dark green. Iron carbonate alteration and silicification dominate, 45% and 35%, respectively. Trace disseminated pyrite.
432849	5461136	07-162A	Highly silicified and altered gabbro. Iron carbonate alteration with quartz veining up to 8mm. Abundant sulphide, up to 10% pyrite, disseminated. Plagioclase highly altered to mica and chlorite. Some visible epidote within close proximity to vein.
432849	5461136	07-162D	Fine grained gabbro. 1cm sharp contacting quartz vein. Sample is slightly altered with abundant chlorite in the groundmass up to 40%, and amphibole up to 35%.

Kakagi Sill

Gabbro

Easting	Northing	Sample ID	Sample Description
435560	5464279	07-167A	Medium grained light to medium green gabbro. 35% plagioclase feldspar with 40% amphibole (hornblende and actinolite/tremolite), weakly micaceous up to 10%. Carbonate altered up to 10% locally and cross cut by a 12mm quartz veinlet. Weakly foliated.
432849	5461136	07-162B	Mineralised quartz vein within medium grained gabbro. Up to 15% total mineralization. Mostly disseminated pyrite with chalcopyrite up to 10% and 5%, respectively. Visible galena up to 5%, (possibly molybdenite?). Quartz is white to light grey and blocky. Up to 10% carbonate overprinting.
432856	5461088	07-164	Highly mineralized and silicified altered gabbro. Up to 18% disseminated and blebby, 1-5mm, pyrite. Cross cut by quartz veins, up to 1.5 cm. Quartz flooding is predominant within medium grained gabbro wall rock. Iron carbonate alteration is also observed to a maximum of 20%. Relict groundmass is composed primarily of fine to medium grained amphibole (35%) with chlorite (20%) and some (20%) plagioclase.
435815	5465556	08-029	Medium grained gabbro. Chlorite altered with up to 25% carbonate alteration up to 10%. Light green grey weathered surface. Dark green grey weathered surface. Trace pyrite, disseminated. Weak silicification up to 5%.
435778	5465173	08-051	Moderately altered gabbro. Medium grained with 10-15% carbonate altered. Slightly magnetic due to presence of trace to 2% pyrrhotite, with minor pyrite. 5% silicification. 40% amphibole with 40% plagioclase and <20% chlorite alteration.
435895	5465160	08-036	Medium to fine grained gabbro. Medium grained, composed chiefly of pyroxene (15%), amphibole (35%), and plagioclase feldspar (30%). Trace pyrite. Up to 5% carbonate alteration and 5-8% silica as flooding and minor veining.
435506	5464830	08-119	Medium grained gabbro. Medium to light green weathered surface and dark to medium green fresh surface. 35% amphibole as phenocrysts and as part of the groundmass. Plagioclase up to 35% as well, chlorite within the groundmass up to 30%. Minor epidote alteration (5% locally) associated with small carbonate in filled fractures. Trace pyrite. No fabric.
436407	5464577	08-095	Medium grained gabbro. 45% subhedral amphibole with 35% subhedral plagioclase laths. Chlorite is found as part of the finer grained groundmass 15%. Trace to 2% pyrrhotite with minor pyrite, slightly magnetic. 8% carbonate alteration, 5% silica flooding. Minor carbonate veining within joint sets.
435971	5463976	08-237	Medium grained gabbro. Green to grey-green weathered surface. Dark green fresh surface. 40% amphibole with 40% plagioclase and chloritic (<20%) groundmass. Weakly magnetic with up to 2 % disseminated pyrite and pyrrhotite. Weakly foliated.
436295	5464985	Peg Lens	Extremely coarse grained to pegmatitic lens of gabbro within typical medium to coarse grained gabbro. Coarse plagioclase 0.5 - 1.5 cm randomly oriented laths. Feldspar is in a matrix roughly 50-50 with coarse pyroxene and amphibole. Carbonate alteration is predominately rimming plagioclase as well as interstitially with quartz up to 5%. No visible mineralization.
434726	5462594	07-157	Medium grained gabbro. 50% medium grained plagioclase, 30% fine grained chlorite, 20% subhedral amphibole. Trace pyrite.
435478	5464828	08-120	Medium grained gabbro. Medium to light grey on weathered surface, dark green on fresh surface. Up to 40% amphibole with 40% plagioclase, 15% pyroxene (some of amphibole may be pyroxene- grain size makes it difficult to determine). Groundmass is strongly chloritic up to 25%. Up to 2% fine grained epidote.

Kakagi Sill

Gabbro

Easting	Northing	Sample ID	Sample Description
434330	5462718	08-199	Medium grained gabbro. Medium to light green weathered surface, dark to medium grained fresh surface. 35% amphibole and plagioclase phenocrysts within and groundmass of similar mineralogy except groundmass has up to 15% chlorite. Minor epidote up to 2%.
435186	5462815	08-0387	Medium grained gabbro. Dark green on the fresh surface, slightly rusty green weathered surface. Roughly 50% amphibole and plagioclase. Up to 5% carbonate alteration. Trace pyrrhotite.
435541	5462961	08-229	Medium grained gabbro. Weathered surface is medium green, fresh surface is dark to medium green. Composed of 50% subhedral amphibole, 30% chlorite, 20% subhedral plagioclase. Trace fine grained pyrite.
435287	5462961	08-218	Medium grained gabbro. Medium to light green on weathered surface, dark green fresh surface. 40% amphibole, hornblende, 40% plagioclase feldspar. Altered up to 15% chlorite, primarily in the groundmass, up to 5% muscovite. Trace carbonate alteration, trace disseminated pyrite. Weak foliation.
435795	5465454	08-30	Medium grained gabbro. Light green grey on surface and dark green grey on fresh surface. 30-35% amphibole, up to 10% visible clinopyroxene. 30% plagioclase. Groundmass contains up to 25% chlorite. Trace pyrite. No fabric.
435665	5462507	08-231	Carbonate altered medium to fine grained gabbro. 12-15% carbonate alteration with cross cutting carbonate veinlets. 30% amphibole and plagioclase phenocrysts. 25% chlorite, within the groundmass. Trace pyrite. No fabric.
435911	5463265	08-0538	Altered medium to fine grained gabbro. 40% amphibole, 30% plagioclase, 20% chlorite, 5% muscovite. Trace carbonate alteration. Slightly silicified (<5%). Trace to 3% pyrite fine grained and disseminated.
435221	5463120	08-WP0314	Medium to coarse grained grained gabbro. Medium to dark green weathered surface, dark green fresh surface. Up to 60% phenocrysts in a fine grained matrix. The matrix is composed of fine grained amphibole, plagioclase and chlorite. Phenocrysts are 30% plagioclase, 20% amphibole, 10% clinopyroxene. Trace pyrite disseminated throughout. Up to 2% carbonate alteration (primarily after feldspar).
434929	5463170	08-378	Gabbro, medium to fine grained weakly altered. Trace to 2% pyrrhotite with minor pyrite, slightly magnetic. 8% carbonate alteration, 5% silica flooding. Minor carbonate veining in joint sets.
435282	5463400	08-512	Medium grained gabbro. Medium to light green grey on weathered surface, dark green on fresh surface. 40% each plagioclase and amphibole, up to 15% chlorite within the groundmass. 2-4% pyrrhotite disseminated, magnetic, with minor pyrite. Carbonate alteration up to 5%, with carbonate quartz veining infilling fractures (10%).
436265	5464466	08-1212	Medium to fine grained gabbro. 50% amphibole (hornblende and actinolite/tremolite) with 40% plagioclase feldspar as euhedral to subhedral laths. 10% carbonate alteration. 2% disseminated fine grained pyrite.
436689	5464874	08-1033	Coarse to medium grained gabbro.40% plagioclase found as isolated medium grained unoriented laths. Amphibole 30%, chlorite 30%. Trace sulphides. No fabric.
436471	5465043	08-03	Medium grained gabbro. Chlorite altered with up to 10% carbonate alteration. Light green grey weathered surface. Dark green grey weathered surface. Trace pyrite weak silicification.
435886	5465220	08-035	Medium grained light green to grey gabbro. 40% amphibole, 35% plagioclase. 30% chlorite, 5% muscovite. Slightly magnetic. Trace disseminated pyrite and pyrrhotite.

Kakagi Sill

Gabbro

Easting	Northing	Sample ID	Sample Description
435738	5465029	08-073	Fine grained gabbro. Weathered surface is medium green and fresh surface is medium to dark green. Some (25%) elongate mostly parallel aligned chlorite within a ground mass of amphibole and plagioclase. Moderate foliation.
436051	5465377	08-23	Medium to fine grained carbonate altered gabbro. Dark green on the fresh surface, slightly rusty green weathered surface. Up to 12% carbonate alteration. Roughly 50% amphibole and plagioclase. Trace pyrite.
436094	5465243	08-021	Medium to coarse grained gabbro. Green to medium grey green weathered surface, light to medium green fresh surface. 40% subhedral plagioclase. 30% amphibole. 30% fine to medium grained chlorite. Trace disseminated pyrrhotite. with up to 2 % disseminated pyrite and pyrrhotite.
436009	5464893	08-063	Medium grained gabbro. Weathered surface is medium to light green, fresh surface is dark to medium green. Chloritic groundmass up to 25% with up to 10% carbonate alteration. 30% amphibole and 35% plagioclase. No Fabric. Trace pyrite.
436152	5464930	08-061	Medium to fine grained grained gabbro. Light to medium grey-green on weathered surface and dark green on the fresh. Trace to 2% pyrite as very small blebs and disseminations. Weakly foliated.
435555	5465299	08-058Schistose	Highly schistose gabbro (sheared?). Highly altered to carbonate with grain size reductions along foliation planes. Long parallel fractures filled with quartz and carbonate. Heavy rusty staining on weathered surface. Up to 8% observed pyrite as fine grained disseminations.
435076	5464516	08-255	Medium grained altered gabbro. Medium to light green grey on the weathered surface and dark green on fresh surface. Trace to 3% disseminated pyrite. Approximately 12 mm wide carbonate stringer crosscutting. Up to 35% carbonate alteration (pervasive). No visible mineralization within stringer.
435863	5464205	08-271	Medium grained gabbro. 30% amphibole, 20% chlorite. 48% plagioclase, 2% epidote. Trace sulphide.
434623	5462521	08-256	Medium to fine grained gabbro with abundant alteration to carbonate (12%). Slightly schistose. Weathered surface is rusty, fresh surface is green to dark green. 50% amphibole, 40% plagioclase. Up to 12% pyrite with minor associated pyrrhotite.
435624	5462673	08-169	Typical altered gabbro. Medium to fine-medium grained. Grey green weathered surface, dark green fresh surface. 40% amphibole, 40% plagioclase, 20% chlorite. Weak foliation. Trace pyrrhotite, disseminated.
435541	5462961	08-229	Medium grained gabbro. 35% clinopyroxene (augite?), 35% 2-4mm plagioclase. 40% amphibole, sub rounded. 25% chlorite, fine grained. Trace to 3% pyrite. Moderate alteration to carbonate up to 15%.
436703	5464432	08-088	Typical altered gabbro. Medium grained. Trace pyrite. No more than 10% silicification and carbonate alteration.
436453	5464183	08-093	Altered gabbro. Moderate to heavy silicification, up to 30%. Pervasive carbonate alteration throughout. Mineralization trace pyrite with pyrrhotite.

Kakagi Sill

Gabbro

Easting	Northing	Sample ID	Sample Description
434936	5462431	08-010	Silicified altered gabbro. Typical in composition though silicified up to 15%.. Pervasive carbonate alteration throughout not encompassing more than 10%. Trace to 2% pyrite as disseminations. Plagioclase is mostly rimmed with carbonate. Pyroxene weakly altered to muscovite.
435815	5465556	08-029	Medium to coarse grained gabbro. 40% amphibole, 35% plagioclase and 25% chlorite. Up to 5% silification and 8% carbonate alteration. Minor pyrite as a 1-2mm blebs and disseminations 1-3%.
435960	5464938	08-064	Moderately silicified medium grained gabbro (up to 12%). Medium to light green weathered surface, dark green fresh surface. 35% amphibole, 40% plagioclase, 15% chlorite. Trace disseminated pyrite.
435099	5464222	08-241	Fine grained gabbro. Dark blackish green grey in colour on fresh surface. Grey green on weathered surface. Total mineralogy is difficult to determine because of the grain size. Trace disseminated pyrite. Weakly foliated.
436277	5462245	08-224	Medium grained gabbro. Light to medium green grey on the weathered surface and dark green on the fresh surface. Trace pyrite. Weak silicification up to 5%. Minor carbonate alteration on fracture surfaces (5-10%).
434062	5462819	08-179	Silicified (10%), carbonate altered (10%), rusty weathered, slightly sheared gabbro. Fine grained. Pyrite visible as very small blebs and minor disseminations up to 8%.
436026	5465616	08-013	Medium grained gabbro. 35% amphibole, 15% chlorite, 50% anhedral plagioclase. Very minor carbonate alteration (<5%). Weakly silicified (<3%). Contains quartz veinlets with up to 15% carbonate over printing (primarily on margins) with trace pyrite and pyrrhotite.
435316	5464551	08-112	Slightly sheared, heavily altered carbonate with quartz veining in a fine to medium grained gabbro. Composed chiefly of pyroxene (15%), amphibole (35%), plagioclase feldspar (30%). Weathered surface is very rusty. Up to 12% disseminated pyrite.
435520	5462250	08-249	Medium grained gabbro. Weathered surface is green to grey-green and fresh surface is dark to medium grained. 35% amphibole. 15% chlorite. 35% plagioclase. Up to 15% carbonate alteration. Weakly foliated.
435362	5462345	08-162	Medium grained gabbro. Weathered surface is green to grey-green and fresh surface is dark to medium grained. 40% amphibole. 20% chlorite. 40% plagioclase. Weakly foliated.
435971	5463976	08-255	Medium grained gabbro. Light green grey on surface and dark green grey on fresh surface. 30-35% amphibole, up to 10% visible clinopyroxene. 30% plagioclase. Groundmass contains up to 25% chlorite. 5 % pyrite, disseminated.
435482	5464830	08-120	Typical medium to coarse grained gabbro though contains up to 30% quartz flooding. 30% plagioclase found as isolated medium grained randomly oriented laths. Amphibole 30%, chlorite 10%.Trace sulphide.
436016	5464569	08-257	Coarse grained gabbro. Dark to medium green weathered surface, and dark green fresh surface. 40% subhedral plagioclase. 35% amphibole. 25% fine to medium grained chlorite. Trace pyrrhotite.
435580	5465198	08-125	Medium grained gabbro. 35% subhedral plagioclase. 35% amphibole. 30% fine to medium grained chlorite. Trace pyrrhotite.

Kakagi Sills

Gabbro

Easting	Northing	Sample ID	Sample Description
437760	5466077	08-082	Altered gabbro. Medium grained, 12-15% carbonate alteration. Trace sulphides.
435628	5465295	08-056	Gabbro, medium grained. Strongly altered to chlorite up to 35%. Phenocrysts of amphibole and plagioclase up to 25% each. Trace disseminated pyrite.
435493	5465074	08-123	Medium grained mafic gabbro. 50% subhedral plagioclase. 25% subhedral amphibole with 25% fine to medium grained chlorite.
434591	5464246	08-270	Medium grained gabbro. Medium green grey weathered surface, dark green fresh surface. 40% amphibole, 40% plagioclase. Plagioclase is subhedral medium to fine grained laths. Chlorite up to 20%, fine grained. No sulphide. Weakly foliated. Weakly carbonate altered (<5%) with up to 2 % disseminated pyrite and pyrrhotite.
435888	5465053	08-59	Coarse grained gabbro. 35% pyroxene with 30-35% amphibole (hornblende with actinolite/tremolite) 25-30% plagioclase in subhedral laths up to 5 mm.10% silicified with associated trace carbonate alteration. 5% carbonate alteration trace sulphides, minor silicification.
435789	5464987	08-71	Medium to fine grained gabbro with up to 2% pyrite as fine grained disseminations and blebs, 12% carbonate alteration. Weathered surface is green to dark green with weak rusty brown patches, fresh surface is green to dark green.
435545	5462476	08-108	Coarse grained gabbro. 35% pyroxene (likely augite) with 30-35% amphibole (hornblende? actinolite?) 25-30% plagioclase in subhedral laths up to 5 mm.10% silicified with associated trace carbonate alteration. Trace to 2% disseminated pyrite.
435006	5463308	08-143	Highly altered medium grained gabbro. Heavily silicified. Rusty staining on weathered green-grey surface. Abundant pyrite, up to 20% fine grained. Carbonate alteration throughout (35%). Weakly foliated.
436326	5465481	08-1004	Medium to fine grained gabbro. Light green grey on weathered surface. Fresh surface is dark green. Individual mineralogy is difficult to determine based on grain size. Weakly altered with carbonate. Up to 2% disseminated pyrite.
436480	5465547	08-1081	Medium grained gabbro. Dark green on the fresh surface, slightly rusty green weathered surface. Roughly equal parts amphibole and plagioclase, both as phenocrysts and components of the groundmass. Up to 10% carbonate alteration. Trace pyrite.
436605	5465397	08-1022	Medium to coarse grained gabbro. Dark green to grey on fresh surface light grey on weathered. 35-40% amphibole with 25% plagioclase. Massive texture and very weakly foliated. Trace disseminated pyrite.
435999	5465116	07-68	Medium grained gabbro. Rusty green grey weathered surface and medium to dark green fresh surface. 50% subhedral plagioclase. 30% subhedral amphibole with 20% fine to medium grained chlorite. Up to 10% iron carbonate alteration.

Kakagi Sill

Ultramafic

Easting	Northing	Sample ID	Sample Description
435333	5463533	07-33	Cumulate textured peridotite. Dominated by olivine (50%) with pyroxene (20%), plagioclase (10%) and amphibole. <10 % Carbonate altered up to 5%. Very trace pyrite. Magnetic.
435245	5464355	07-57	Fine grained pyroxenite. Mostly pyroxene (35%) with some fine grained amphibole (15%) and olivine (15%). Alteration to fibrous serpentine up to 35%. Very slight carbonate alteration (<5%).
435434	5464228	07-58	Carbonate altered ultramafic. 30% pyroxene, 20% amphibole, 10% plagioclase, 28% iron carbonate alteration (ankerite?) 2% olivine. Rock is slightly magnetic, with no fabric. Trace pyrite is very fine grained and disseminated. Serpentinised groundmass.
435340	5464090	07-64	Carbonate altered olivine pyroxenite. Composed of coarse grained pyroxene (ortho and clinopyroxene), 70% with 20% carbonate alteration as round "eggs" likely after olivine. 8% amphibole and 2% plagioclase feldspar (interstitial). Weathered surface shows rusty staining (likely from iron carbonate) and fresh surface is black. Magnetic. Serpentinised groundmass.
435663	5464781	07-80	Coarse to medium grained altered ultramafic, peridotite. Dominated by pyroxene 40%, amphibole 15% and associated serpentinised olivine (40%). Up to 10 % carbonate alteration, locally. Magnetic.
435211	5464198	07-128	Altered medium grained peridotite. Composed primarily of pyroxene (40%) with amphibole (15%) and serpentinised olivine (40%). Some slight carbonate alteration, < 5%, with minor silicification < 5%.
435060	5463857	07-131	Medium grained altered peridotite. Iron carbonate alteration upwards of 12-15%. Mafic groundmass is composed primarily of altered pyroxene (30%) with amphibole (10%) and very rare, olivine though heavily serpentenised up 40%.
435416	5464259	07-143	Altered peridotite. Dark black fresh surface, black-brown rusty weathered surface. Medium grained. 60% pyroxene, 20% amphibole, 2% olivine, 18% carbonate alteration. Weakly foliated. Serpentinised groundmass after olivine.
435476	5464402	07-147	Medium grained altered peridotite. 65% pyroxene, 15% carbonate alteration, 20% amphibole. Moderately serpentinised. Weathered surface is black with brownish rusty staining. Fresh surface is black.
434868	5462346	07-149	Coarse to medium grained slightly altered ultramafic, peridotite. Composed primarily of pyroxene (45%) and amphibole (15%) groundmass with iron carbonate pseudomorphs replacing olivine (10%). Serpentinised up 30%. No visible sulphide. Magnetic.
434465	5462257	07-152	Medium grained, weakly altered ultramafic rock. 40% serpentinised groundmass, 30% pyroxene phenocrysts, 10% amphibole phenocrysts and 10% plagioclase phenocrysts. Up to 5% carbonate alteration, with very minor silicification. 5% fine grained talc. Weakly foliated.
434563	5462408	07-154	Fine to medium grained ultramafic. Relatively unaltered. Composed predominantly of serpentine, pyroxene, and amphibole groundmass 85%, with less than 5% carbonate alteration. Less than 5% relict olivine is observed as well 5% plagioclase.
434566	5462685	07-155	Medium grained pyroxenite. Fine grained, up to 2mm carbonate veinlets (10%). Slight carbonate alteration throughout sample, less than 12%, varied. Possible fuschitic alteration within veining (5-10%).

Kakagi Sill

Ultramafic

Easting	Northing	Sample ID	Sample Description
434559	5462696	07-156	Medium grained weakly altered pyroxenite. Groundmass is composed primarily of pyroxene (90%) with minor amphibole (<8%). Some slight (<5%) carbonate veining, 1-3mm, but no real sense of carbonate alteration. Non magnetic.
435546	5464259	07-169	Intensely altered ultramafic hanging wall from AHGZ. Iron carbonate, 50%, is found as coarse grained connected "eggs" as pseudo morphs after olivine within coarse pyroxene groundmass.
435732	5465280	08-056Ultra	Coarse grained peridotite. Weakly altered to carbonate. Trace to 2% pyrite. Magnetic. Very minor plagioclase, less than 5%. Serpentinised groundmass.
435492	5464737	08-118	Coarse grained, moderately altered peridotite. Weakly altered to carbonate, 2-5%. Well preserved pyroxene, olivine seems to be completely altered to serpentine (no relict olivine) and magnetite (strongly magnetic) with minor talc (5%).
434482	5462598	201 ULTRA	Coarse grained altered pyroxenite. Pyroxene dominates the groundmass and as phenocrysts with no more than 3-5% feldspar. Carbonate alteration up to 5%. Weathered surface is dark black-grey with brownish rusty staining. Fresh surface is black, dark green-black.
435030	5463319	08-143ultra	Fine to medium grained pyroxenite. Composed of pyroxene (50%) with amphibole (20%), plagioclase (10%) and biotite (5%). Carbonate altered up to 10%. Very trace pyrite. Magnetic.
435059	5463396	08-0768	Coarse to medium grained peridotite. Dominated by pyroxene 40%, amphibole 15% and associated serpentinised olivine (40%). Up to 10 % carbonate alteration, locally. Magnetic.
435506	5464830	08-119	Sheared peridotite proximal with contact to gabbro. Black with rusty brown stained weathered surface and dark black fresh surface. Fine grained with pyroxene dominated groundmass, actual percentages difficult to determine based on grain size. Brittle deformed to slightly mylonitic. Locally carbonate stringers (mm scale) up to 10%. No visible mineralization.
435732	5465280	08-056	Coarse grained, moderately peridotite. Pyroxene phenocrysts up to 50% within pyroxene dominated groundmass. 2-5% relict olivine with up to 40% serpentine (likely after olivine). Strongly magnetic. Minor talc (5%).
434086	5463068	Ultrapotential	Medium to fine grained ultramafic. Groundmass is composed primarily of pyroxene (60%) and serpentinised olivine (40%). Weathered surface is dark black with rusty staining and fresh surface is black to dark black green.
435663	5464781	07-80	Medium grained weakly altered pyroxenite. Groundmass is composed primarily of pyroxene (90%) with minor amphibole (5-10%) and olivine? (<3%). Some slight (<5%) carbonate alteration. Weakly magnetic. Weakly foliated.

Intrusive Rocks

Felsic and Lamprophyre Dikes

Easting	Nothing	Sample ID	Rock Type	Sample Description
435383	5464981	07-86	Feldspar Porphyry Dike	Highly altered feldspar porphyry dike. Silica flooded (15%) with coarse grained sub to euhedral feldspars up to 1 cm.
434413	5463977	07-135	Quartz Feldspar Porphyry Dike	Medium grained cross cutting QFP dike. Brown finer grained groundmass with some (15%) carbonate alteration. Sericitic alteration up to 15%. Trace to 3% pyrite. Fine to medium grained cubic crystals.
434264	5463910	07-136	Quartz Feldspar Porphyry Dike	Highly altered quartz-feldspar porphyry. Fine to medium grained medium brown groundmass, with subhedral feldspar phenocrysts (35%). Slight carbonate alteration observed (5-10%). Trace disseminated pyrite.
433990	5463228	Feldike30cm	Quartz Feldspar Porphyry Dike	Coarse grained quartz feldspar porphyry dike. Potassic feldspars (35%) up to 1 cm in quartz in a comparable groundmass.
Dogpaw	Vein 4	DPV4LD	Lamprophyre Dike	Coarse grained. Abundant biotite (50%) with amphibole. Groundmass is of similar composition but contains fine grained plagioclase feldspars (10-15%).
Dogpaw	Vein 4	DPV4FD	Quartz Feldspar Porphyry Dike	Coarse grained felsic dike. Slightly altered heavily weathered QFP dike. Some moderate iron staining. No carbonate. Predominantly quartz, 70% as quartz eyes.

Angel Hill Gold Zone

Diamond Drill Core Samples

Sample Id	Drill Hole	From (m)	To (m)	Sample Description
76301	WC-2004-24	76.55	76.70	10cm grey brecciated quartz-carbonate veinlet contacting with feldspar porphyry dike. Trace to 1% disseminated pyrite.
76302	WC-2004-24	74.80	74.96	Altered peridotite. Moderate to strong carbonate alteration (20%) and silicification (20%). Moderate to strong fuchsite alteration (10-15%). Numerous (20%) quartz- carbonate and carbonate veinlets (1mm-1cm). Strongly brecciated. Foliation at about 55 degrees to core axis. Trace-1+% disseminated pyrite locally.
76303	WC-2004-24	64.70	64.92	Medium dark green to grey/beige blotchy colour, fine to medium grained massive gabbro. Moderate to strong carbonate alteration (15%) with numerous irregular quartz carbonate veinlets cross cutting (1mm- 3cm). Pervasive carbonate alteration proximal to veinlets up to 3cm Sometimes (5%) veinlets have fine grained chlorite on their margins with chlorite after pyroxene up to 5% as well. Trace pyrite associated within wall rock or within veinlets. Local foliation developed at 50 degrees to core axis.
76304	WC-2004-24	81.40	81.55	Altered peridotite. Light to moderate silicification and fuchsite alteration (15% each). Strong carbonate alteration up to 25%. 3-5% pyrite locally as grains or small masses. Numerous irregular quartz carbonate veinlets cross cutting (1mm- 3cm)
76305	WC-2004-24	101.40	101.50	Least altered (relatively) ultramafic unit. Black with dark green chlorite lined fractures infillings. Medium to coarse grained massive, relatively equigranular unit. Carbonate stringers up to 0.3cm wide (10%). Very dense and strongly magnetic. Abundant serpentine.
76306	WC-2004-16	12.17	12.30	Altered peridotite. Medium to coarse grained, equigranular and massive. Pervasive carbonate up to 20% light to moderate local fuchsite (10%). Quartz-carbonate veinlet at approximately 90 degrees to core axis with very strong disseminated visible gold up to 5% associated with blebs and masses of galena (+ pyrite). Carbonate and silica flooding for approximately 10cm either side of vein within wall rock.
76307	WC-2004-16	3.66	3.81	Medium grained, massive, relatively equigranular gabbro. Medium green and light green mottled colour. Occasional (5%) hairline quartz carbonate veinlets. Nonmagnetic. Weak carbonate alteration (<5%). Typical chloritic alteration of groundmass observed through gabbro of entire sill samples.
76308	WC-2004-16	27.60	28.04	Weakly altered Ultramafic. Medium to coarse grained, massive and relatively equigranular. Medium to dark grey/black mottled colour. Strongly magnetic. Numerous (15%) irregular carbonate veinlets. Locally talc and chlorite up to 10% in addition the predominant serpentine alteration which is typical of the footwall ultramafic rocks of the Kakagi Sill. Trace pyrite.
76309	WC-2004-16	17.05	17.17	Strongly to moderately altered ultramafic footwall. Pyrite trace to 2%. Light to moderate silicification and fuchsite alteration (15% each). Strong carbonate alteration up to 25%. Numerous irregular quartz carbonate veinlets cross cutting (1mm- 3cm)
76310	WC-2004-16	9.65	9.75	Ultramafic hanging wall. Medium to coarse grained moderate to strong silicification (15%) and moderate fuchsite alteration (10%). Numerous (15%) quartz-carbonate and carbonate veinlets up to a few mm.

Angel Hill Gold Zone

Diamond Drill Core Samples

Sample Id	Drill Hole	From (m)	To (m)	Sample Description
JK 013	WC-2007-37	21.05	21.20	Medium to dark green grey gabbro. Moderate to light carbonate alteration (5-10%) with numerous (5-10%) irregular quartz-carbonate veinlets (1mm- 4cm) with carbonate and quartz flooding within wall rock associated with larger veinlets. Trace pyrite disseminated throughout. Local foliation developed 50 degrees to core axis from mica and elongate chlorite altered pyroxene and tremolite.
JK 014	WC-2007-37	67.50	67.65	Altered Gabbro. Slightly brecciated with abundant chlorite. Trace pyrite. Weakly carbonate altered (5%) with minor carbonate stringers infilling fractures (10%).
JK 015	WC-2007-37	68.35	68.50	Medium to coarse grained gabbro with increasing carbonate alteration (up to 15%) and silicification (<10%). Trace to 5% locally fuchsite alteration.
JK 016	WC-2007-37	70.55	70.65	Altered peridotite. Light to moderate silicification and fuchsite alteration (10-15% each). Strong to moderate carbonate alteration up to 20%. 3-5% pyrite locally as grains or cumulates or blebs up to 1 cm. Numerous irregular quartz carbonate veinlets cross cutting (1mm- 3cm)
JK 020	WC-2007-37	72.50	72.65	Quartz feldspar porphyry dike. Fine grained medium to light grey colour. No mineralization.
JK 021	WC-2007-37	73.20	73.30	Moderately altered peridotite. Silicified (10%) and carbonate and fuchsite altered (15% and 10%, respectively). Light brecciation with influx of carbonate and quartz stringers. Pyrite up to 5% but mostly contained in fractures.
JK 022	WC-2007-37	74.10	74.15	Moderately altered peridotite. Silicified (10%) and carbonate and fuchsite altered (15% and 10%, respectively). Light brecciation with influx and carbonate and quartz stringers and replacement by minor albite (5%). Pyrite up to 5% but mostly contained in fractures.
JK 023	WC-2007-37	74.90	74.97	Altered peridotite. Medium to coarse grained, equigranular and massive. Pervasive carbonate up to 20% light to moderate local fuchsite (10-15%). Quartz-carbonate veining infilling brittle fracturing (faulting) carbonate and silica flooding for approximately 5-8 cm either side of vein within wall rock.
JK 024	WC-2007-37	75.50	75.62	Moderately altered peridotite. Silicified up to 15% and carbonate and fuchsite altered (up to 20% and 15%, respectively). Cross cutting carbonate stringers cross cutting up to 10% with disseminated pyrite up to 3%.

Angel Hill Gold Zone

Diamond Drill Core Samples

Sample Id	Drill Hole	From (m)	To (m)	Sample Description
JK 025	WC-2007-37	75.65	75.70	Moderately altered brecciated peridotite. Quartz stringers with carbonate over printing up to 25%. Up to 12 % pyrite, disseminated. Weakly magnetic.
JK 026	WC-2007-37	76.30	76.40	Altered peridotite. Medium to coarse grained, equigranular and massive. Pervasive carbonate up to 20% with strong fuchsite (20%). Quartz-carbonate veinlets abundant with quartz and carbonate flooding within brecciated zone (20+%).
JK 027	WC-2007-37	77.50	77.60	Altered peridotite. Medium to coarse grained, equigranular and massive. Pervasive carbonate up to 30% and moderate local fuchsite (15%). Quartz-carbonate infilling brecciated zone up to 45%, carbonate and silica flooding for approximately 10cm either side of breccia (vein) up to 15%.
JK 028	WC-2007-37	80.07	80.12	Lightly altered peridotite. Weakly silicified (<10%). Moderate to weak carbonate alteration (15%) and fuchsite (<10%). No visible mineralization. Strongly magnetic. Weak to moderate brecciation in filled with carbonate stringers and quartz and carbonate stringers (10%)
JK 029	WC-2007-37	80.70	80.80	Moderately altered peridotite. Silicified up to 15% and carbonate altered (15%). Intense fuchsite alteration up to 30%. Cross cutting carbonate stringers up to 10% with disseminated pyrite up to 3%.
JK 030	WC-2007-37	83.50	83.60	Altered peridotite. Moderate to strong carbonate alteration (<20%) and silicification (15-20%). Moderate to strong fuchsite (10-15%). Numerous (20%) quartz and carbonate and carbonate veinlets (1mm-1cm) Brecciated texture. Trace-1+% disseminated pyrite locally within wall rock and veinlets.
JK 031	WC-2007-37	89.87	89.97	Altered peridotite. Light to moderate silicification and fuchsite alteration (15% each). Strong carbonate alteration up to 25%. 3-5% pyrite locally as grains or small masses. Numerous irregular quartz carbonate veinlets cross cutting (1mm- 3cm)
JK 032	WC-2007-37	92.35	92.50	Lightly altered peridotite c. Weakly silicified (<5%). Moderate to weak carbonate alteration (10-15%) and fuchsite (<10%). No visible mineralization. Strongly magnetic.
JK 033	WC-2007-37	109.30	109.40	Least altered peridotite. Black and medium to coarse grained massive, relatively equigranular unit. Carbonate stringers up to 0.3cm wide (10%). Very dense and strongly magnetic. Abundant serpentine.

Angel Hill Gold Zone

Diamond Drill Core Samples

Sample Id	Drill Hole	From (m)	To (m)	Sample Description
JK 034	WC-2007-38	34.10	34.18	Medium dark green to grey/beige fine to medium grained massive gabbro. Moderate to strong carbonate alteration (15%) with numerous (15%) irregular quartz carbonate veinlets cross cutting (1mm- 3cm). Pervasive carbonate alteration throughout. Veinlets often (5%) have fine grained chlorite on their margins with chlorite after pyroxene within wall rock up to 5% as well. Trace pyrite associated within wall rock or within veinlets. Local foliation developed at 50 degrees to core axis.
JK 035	WC-2007-38	34.45	34.53	Fracture with carbonate and quartz veining within moderately altered gabbro. Quartz is blocky textured and white. Up to 35% carbonate overprinting. Fracture is 3 cm and brittle textured. Wall rock silicified and carbonate altered up to 10 cm either side of fracture.
JK 036	WC-2007-38	40.00	40.10	Altered peridotite. Medium to coarse grained, equigranular and massive. Pervasive carbonate up to 30% light to moderate local fuchsite (15%). Quartz-carbonate veining throughout. Strong disseminated visible gold up to 3% associated with blebs pyrite (+galena). Carbonate and silica flooding for approximately 10cm within breccia.
JK 037	WC-2007-38	39.55	39.65	Moderate to strong carbonate altered (20%) and silicified (20%) ultramafic footwall. Moderate to strong fuchsite (10-15%). Numerous (20%) quartz- carbonate and carbonate veinlets (1mm-1cm). Trace-1+% disseminated pyrite locally and rutile observed fine grained up to 1%.
JK 038	WC-2007-38	44.65	44.75	Least altered ultramafic. Black medium to coarse grained massive, relatively equigranular unit. Carbonate stringers up to 1 wide (<10%). Very dense and strongly magnetic. Abundant serpentine within groundmass.

Angel Hill Gold Zone

Surface Grab Samples

Easting	Northing	Sample ID	Sample Description
435560	5464205	AHGZ-1	High grade sample. Altered quartz flooded breccia in filled Ultramafic. Medium to coarse grained, equigranular and massive. Pervasive carbonate up to 20%. Visible gold (2-3%) associated with blebs of pyrite and galena (5 %). Abundant fuchsite up to 25% locally.
435560	5464205	AHGZ-2	High grade sample. Altered quartz flooded breccia in filled Ultramafic. Medium to coarse grained, equigranular and massive. Pervasive carbonate up to 20%. Visible gold (2-3%) associated with blebs of pyrite and galena (5 %). Abundant fuchsite up to 25% locally.
435560	5464205	AHGZ-3	High grade sample. Altered quartz flooded breccia in filled Ultramafic. Medium to coarse grained, equigranular and massive. Pervasive carbonate up to 20%. Visible gold (2-3%) associated with blebs of pyrite and galena (5 %). Abundant fuchsite up to 25% locally.
435560	5464205	AHGZ-4	Moderately altered ultramafic. Silicified up to 15% and carbonate altered (15%) . Intense fuchsite alteration up to 30%. Cross cutting carbonate stringers up to 10% with disseminated pyrite up to 3%.
435560	5464205	AHGZ-5	Medium grained massive gabbro. Moderate to strong carbonate alteration (15%) with numerous irregular quartz carbonate veinlets cross cutting (10-15%). Pervasive carbonate alteration throughout up to 15%. Trace pyrite associated within wall rock or within veinlets.
435560	5464205	AHGZ-6	Medium grained, massive, relatively equigranular gabbro. Few hairline quartz carbonate veinlets (<5%). Weak carbonate alteration (<5%). Typical chloritic alteration of groundmass.
435560	5464205	AHGZ-P-1	Least altered ultramafic unit. Black fresh surface, rusty brown weathered surface. Medium to coarse grained massive, relatively equigranular unit. Carbonate stringers10%, locally. Very dense and strongly magnetic. Abundant serpentine throughout.
435560	5464205	AHGZ-P-2	Moderately altered ultramafic. Silicified up to 15% and carbonate altered (15%) . Intense fuchsite alteration up to 30%. Cross cutting carbonate stringers up to 10% with disseminated pyrite up to 3%.
435560	5464205	AHGZ-P-3	High grade sample. Altered quartz flooded breccia in filled Ultramafic. Medium to coarse grained, equigranular and massive. Pervasive carbonate up to 20%. Visible gold (2-3%) associated with blebs of pyrite and galena (5 %). Abundant fuchsite up to 25% locally.
435560	5464205	AHGZ-P-4	Medium grained massive gabbro. Moderate to strong carbonate alteration (15%) with numerous irregular quartz carbonate veinlets cross cutting (10-15%). Pervasive carbonate alteration throughout up to 15%. Trace pyrite associated within wall rock or within veinlets.
435560	5464205	AHGZ-P-5	Medium grained, massive, relatively equigranular gabbro. Few hairline quartz carbonate veinlets (<5%). Weak carbonate alteration (<5%). Typical chloritic alteration of groundmass.

Angel Hill Gold Zone

Surface Grab Samples

Easting	Northing	Sample ID	Sample Description
435560	5464205	AHGZ-P-6	Moderately altered ultramafic. Silicified up to 15% and carbonate altered (15%). Intense fuchsite alteration up to 30%. Cross cutting carbonate stringers up to 10% with disseminated pyrite up to 3%.
435560	5464205	AHGZ-GC	High grade sample. Altered quartz flooded breccia in filled Ultramafic. Medium to coarse grained, equigranular and massive. Pervasive carbonate up to 20%. Visible gold (2-3%) associated with blebs of pyrite and galena (5 %). Abundant fuchsite up to 25% locally.

Appendix B

Drill Core Logs

Note: The following drill holes were originally logged by D.R Cutting (Cutting and Anthony, 2005) but were reviewed and relogged for the purpose of this study by the author. The logs presented are a simplified version of the completed logs and are syntheses of the observations and conclusions of both workers.

Hole: WC-2004-024
Location: 5464213 m N 435603 m E
Depth: 104.55 m Dip: -45°

From (m)	To (m)	Description
0.00	0.91	Casing
0.91	53.00	Medium grained equigranular, massive gabbro (typical hangingwall). Slightly fractured with minor carbonate infilling of fractures. Unit mostly medium grey-green in colour, though some of the veinlets have a distinct pinkish tinge. Some of the carbonate has yellow/green tint. Mafic phases have slightly altered to chlorite. Roughly 60/40 for feldspars/mafics. Traces of disseminated pyrite as grains & small masses locally in unit.
53.00	74.75	Medium dark grey to grey/beige blotchy colour, fine to medium grained massive unit typical for immediate hangingwall. Moderate to strong carbonate alteration along with numerous irregular quartz-carbonate veinlets up to 2.5 cm wide. Few veinlets have a more greenish tint, which is either chlorite or fuchsite. Trace pyrite associated within wallrock and veinlets.
74.75	76.70	Altered peridotite. Medium to coarse grained with abundant carbonate alteration with strong fuchsite alteration and trace pyrite. Beginning of mineralized zone
76.70	77.55	Felsic dyke. Beige-buff in colour. Fine grained and contains 2-5% very fine disseminated pyrite. Both contacts are sharp with upper at 50 degrees and the lower at 60 degrees to core axis. Quartz carbonate veinlets on both wall rock contacts and within dike. Dyke contains small xenoliths of peridotite (3-8 cm, <12%).
77.55	82.30	Altered peridotite. Similar to 74.75-76.70 section except less intense silicification and fuchshite alteration, however, still intense carbonate altered with 3-5+% disseminated pyrite
82.30	93.50	Altered peridotite. Strongly altered to chlorite and serpentine. Sample contains dark green grey to black colour. Abundant quartz-carbonate and carbonate veinlets. Trace disseminated pyrite.
93.50	96.30	Altered peridotite with coarse grained plagioclase phenocrysts (ultramafic gabbro deformed contact). Moderate carbonate alteration with light silica overprinting. Less fuchsite with up to 3-5% disseminated pyrite.
96.30	101.15	Altered peridotite chlorite-serpentine footwall transition unit.
		Typical footwall peridotite transition zone. Unit very rubbly & fractured with numerous fault, fault/fracture or fracture zones. Fractures are and infilled by carbonate. Light to moderate chlorite and serpentine alteration, carbonate alreration is decreasing in abundance. Carbonate replacement after olivine is still predominant. Trace disseminated pyrite.
101.15	104.55	Typical least altered (relatively) peridoite unit. Black or dark green with abundant chlorite and serpentine Coarse grained and massive and equigranular. Locally relict pyroxene and olivine.

Hole: WC-2004-16

Location: 5464264 m N 435562 m E

Depth: 28.04 m Dip: -48°

From (m)	To (m)	Description
0.00	4.00	Least altered gabbro. Medium grained, massive, relatively equigranular gabbro- typical hanging wall. Medium green and light green mottled colour. Occasional small fractures with veinlets of quartz-carbonate. Little or no carbonate alteration though predominant alteration of mafic phases to chlorite.
4.00	6.97	Gabbro to Ultramafic (Altered) (Transition Zone). Unit generally medium to coarse grained relatively massive and equigranular. Increasing in coarse grained mafic content and decreasing in phenocrystic felsic phases as well as interstitial felsic phases- Olivines become gradually more visible through unit with the associated beige blotchy carbonate, bottom of unit has altered ultramafic precursor to AHGZ with moderate chlorite and carbonate alteration.
6.97	11.50	Beginning of Gold Zone: Altered Ultramafic. Medium to coarse grained, equigranular relatively massive peridotite. Moderately carbonate altered. Generally moderately magnetic. Many fractures have rusty staining over carbonate infilling. Beginning of stockwork veining zone. Trace disseminated pyrite grains.
11.50	12.90	Altered Ultramafic. Medium to coarse grained, equigranular and massive. Variably mottled with increasing carbonate alteration, silicification and fuchsite. At 12.20 2cm wide quartz-carbonate vein at ~ 90 degrees to core axis with very strong disseminated visible gold associated with blebs and masses of galena (+pyrite). This veinlet is the expression of the master fault.
12.90	13.80	Felsic Dyke. Fine grained, massive beige/grey.
13.80	14.15	Moderately altered ultramafic. Typical of footwall alteration. Trace disseminated pyrite. Weak to moderate fuchsite and chlorite alteration. Veinlets and flooding of quartz-carbonate.
14.15	14.36	Felsic Dyke. Fine grained, massive beige/grey.
14.36	16.25	Altered Ultramafic (Moderate to Strong). Medium to coarse grained, massive, and equigranular. Moderate carbonate alteration and silicification, moderate fuchsite as well. Numerous irregular quartz-carbonate veinlets. 3-5% disseminated pyrite as grains or small blebs.
16.25	16.90	Felsic Dyke. Fine grained, massive beige/grey.
16.90	17.65	Altered Ultramafic (Moderate to Strong). Same as 14.36-16.25. Pyrite trace-2%.
17.65	17.90	Felsic Dyke. Fine grained, massive beige/grey.
17.90	24.00	Altered Ultramafic (Moderate to Strong). Medium to coarse grained massive, relatively equigranular. Carbonate, silica and fuchsite alteration intensity drops off to end of AHGZ. Unit locally magnetic.
24.00	28.08	Least altered ultramafic (footwall). Medium to coarse grained, massive and relatively equigranular. Medium to dark grey/black mottled colour. Strongly magnetic. Numerous irregular carbonate veinlets. Typical highly serpentinsed and chlorite altered. Trace pyrite. EOH

Hole: WC-2004-022
Location: 5464248 m N 435622 m E
Depth: 101.19 m Dip: -55°

From (m)	To (m)	Description
0.00	2.44	Casing
2.44	68.70	Medium green grey colour, medium to fine grained least altered gabbro hangingwall. Numerous irregular white to light greenish carbonate and quartz-carbonate veinlets hairline to 3cm wide. Pervasive carbonate alteration is associated with larger or an increase in concentration of veinlets. surrounding gabbro; these carbonate intervals are up to 1m wide & quite discontinuous. Dark green chlorite associated with some veinlets others lighter green (fuchsite?) Occasional pyrite grains associated with some carbonate veinlets. Unit is non-magnetic. Moderate chlorite alteration of mafic minerals.
68.70	72.08	Strongly carbonate altered peridotite (possibly gabbro?). Difficult to determine based on carbonate alteration. Medium grained and cross cut by intense carbonate veining. Carbonate is predominantly ankerite with lesser amounts of dolomite and magnesite. Carbonate is medium to dark green beige mottled in colour. Mottling forms pseudomorphs after olivine.
72.08	77.15	Variably altered peridotite. Medium to fine grained. Locally relict serpentinsed olivine preserved though generally replaced magnesite pseudomorphs. Locally silicified and carbonate altered up to 20% with moderate to strong fuchsite. Abundant secondary fractures in filled with quartz and carbonate. Disseminated pyrite throughout up to 12% and locally blebby up to 1cm.
77.15	77.46	Felsic Dyke. Fine grained massive beige/grey.
77.46	89.10	Continuation of previous altered peridotite.
89.10	95.00	Medium green colour, generally massive leucogabbro. Locally plagioclase (albite) feldspar up to almost 1cm in length. Moderately chlorite altered groundmass throughout. Cross cut by numerous (15%) carbonate and quartz veinlets.
95.00	97.30	Altered Ultramafic (Moderate). Medium to coarse grained, massive, and equigranular. Moderate carbonate alteration and silicification, weak fuchsite alteration. Numerous irregular quartz-carbonate veinlets. 3-5% disseminated pyrite as grains or small blebs.
97.30	101.90	Least altered ultramafic (footwall). Medium to coarse grained, massive and relatively equigranular. Medium to dark grey/black mottled colour. Strongly magnetic. Numerous irregular carbonate veinlets. Typical highly serpentinsed and chlorite altered. Trace pyrite disseminated. EOH

Hole: WC-2004-018
Location: 5464226 m N 435550 m E
Depth: 46.02 m Dip: -46°

From (m)	To (m)	Description
0.00	1.22	Casing
1.22	10.90	Medium Grained gabbro typical of distal hangingwall. Medium grey-green in colour. 15-20% carbonate filled fractures. Roughly 60:40 ratios of mafic phases to felsic phases. Mafic phases have been slightly altered to chlorite though are predominantly amphibole and clinopyroxene. Traces of disseminated pyrite as grains & small masses locally in unit.
10.90	15.20	Upper contact zone between the gabbro and peridotite of Kakagi Sill. Medium grained massive and relatively equigranular with moderate chlorite and carbonate alterations. Local appearance of carbonate altered olivine (<5%). Numerous irregular stockwork veinlets. Trace to 2% disseminated pyrite. Local foliation poorly developed at 50 degrees to core axis.
15.20	17.60	Moderately altered peridotite. Medium grained and massive, as well as relatively equigranular. Dark green or black/beige mottled colour. Numerous irregular quartz veinlets. Locally fuchsite up to 10%. Weakly silicified. Trace pyrite disseminated.
17.60	18.15	Felsic Dyke. Fine grained, massive beige/grey.
18.15	19.50	Strongly altered peridotite. Brecciated (master fault?) with infilling by quartz veining. Abundant carbonate, silica, and fuchsite throughout. Trace to 2% disseminated and blebby pyrite.
19.50	19.90	Felsic Dyke. Fine grained massive beige/grey.
19.90	41.65	Altered Ultramafic (Moderate). Medium to coarse grained, massive, and equigranular. Moderate carbonate alteration and silicification, weak to locally moderate fuchsite alteration. Numerous irregular quartz-carbonate veinlets. 3-5% disseminated pyrite as grains or small blebs.
97.30	46.02	Least altered ultramafic (footwall). Medium to coarse grained, massive and relatively equigranular. Medium to dark grey/black mottled colour. Strongly magnetic. Numerous irregular carbonate veinlets. Typical highly serpentinsed and chlorite altered. Trace pyrite disseminated. EOH

Hole: WC-2004-020
Location: 5464188 m N 435537 m E
Depth: 30.78 m Dip: -47°

From (m)	To (m)	Description
0.00	1.52	Casing
1.52	10.85	Medium Grained gabbro typical of distal hangingwall. Medium grey-green in colour. 15-20% carbonate filled fractures. Slightly altered to chlorite. Traces of disseminated pyrite as grains & small masses locally in unit.
10.85	11.65	Altered Ultramafic (peridotite). Medium grained, massive, relatively equigranular. Medium green grey with beige mottling. Minor irregular quartz carbonate veinlets. Strongly carbonate altered olivine, or rather carbonate alteration after serpentine after olivine.
15.20	17.60	Moderately altered peridotite. Medium grained and massive, as well as relatively equigranular. Dark green or black/beige mottled colour. Numerous irregular quartz veinlets. Locally fuchsite up to 10%. Weakly silicified. Trace pyrite disseminated.
17.60	18.15	Felsic Dyke. Fine grained, massive beige/grey.
18.15	19.50	Strongly altered peridotite. Brecciated (master fault?) with infilling by quartz veining. Abundant carbonate, silica, and fuchsite throughout. Trace to 2% disseminated and blebby pyrite.
19.50	19.90	Felsic Dyke. Fine grained, massive beige/grey.
19.90	41.65	Altered Ultramafic (Moderate). Medium to coarse grained, massive, and equigranular. Moderate carbonate alteration and silicification, weak to locally moderate fuchsite alteration. Numerous irregular quartz-carbonate veinlets. 3-5% disseminated pyrite as grains or small blebs.
97.30	46.02	Least altered ultramafic (footwall). Medium to coarse grained, massive and relatively equigranular. Medium to dark grey/black mottled colour. Strongly magnetic. Numerous irregular carbonate veinlets. Typical highly serpentinsed and chlorite altered. Trace pyrite disseminated. EOH

Appendix C

Thin Section Descriptions

Note: Presented in this section are representative simplified thin section descriptions of each host rock and alteration assemblage observed within the property and Angel Hill Gold Zone.

197104

Composition:

40% Plagioclase
40% Chlorite
10% Quartz
5% Muscovite
5% Carbonate

Chlorite altered felsic volcanic tuff with brecciated andesitic-rhyolitc strongly chlorite altered subrounded to rounded fragments. Medium to light green. Fine grained and poorly foliated. Plagioclase occurs as anhedral grains which have been weakly to moderately altered to muscovite. Chlorite is abundant throughout, and is the major component of the fine grained to aphanitic groundmass.

07-27

Composition:

10 % Pyroxene (diopside)
5 % Plagioclase (albite)
2 % Olivine
10 % Talc
40 % Serpentine
5 % Quartz
20 % Amphibole
10% Calcite
18 % Chlorite
3 % Pyrite
2% Mica

Sample is composed primarily of highly serpentinised olivine. Olivine (relict) is medium to medium-fine grained (up to 1 mm) and euhedral. Though predominantly altered to serpentine some relict cores still exist. Pyroxene is observed as poorly preserved diopside which has been primarily altered to chlorite with minor talc. Amphibole is observed mostly as actinolite/tremolite. Interstitial to the mafic phases is plagioclase and fine grained serpentine talc and chlorite. Quartz is observed as later stage inclusions overprinting original textures. Calcite is observed within the groundmass as well as pseudomorphs after olivine and replacing serpentine. The groundmass is composed chiefly of fine grained serpentine, chlorite, talc, amphibole, mica, calcite, quartz, and muscovite. Pyrite is observed as small disseminated sub- to anhedral grains.

07-28

Composition:

40% Calcite
20% Quartz
15 % fine grained groundmass
10% Feldspar
10 % Chlorite
5% Mica

Brecciated, banded and network texture of carbonate and quartz within altered gabbro. Shows cataclastic texture with coarse (up to 2 mm) calcite crystals with coarse quartz in a fine grained matrix composed chiefly of chlorite, feldspar, calcite and quartz with limited sericite. Calcite veins are observed within the section up to 2 cm in thickness with minor interstitial quartz. Most feldspar (albite plagioclase) has undergone brittle deformation and is weakly altered to sericite along grain boundaries.

07-32

Composition:

40% Amphibole
20% Chlorite
15% Feldspar
5% Quartz
5% Muscovite
<5 % Epidote
<5% Pyroxene

Sample is primarily composed of coarse grained amphibole (tremolite-actinolite) within a matrix of feldspar and quartz. Several porphyroclasts of plagioclase feldspar (albite) are observed with euhedral laths with defined crystal twins. Interstitial chlorite and muscovite and quartz are observed within the groundmass. Rarely observed is interstitial clinopyroxene (augite) and small (less than ½ mm) clino-zoisite. Amphibole is shown with predominant alteration to chlorite along grain boundaries and cleavage planes. Feldspar has been extensively altered to muscovite. Primary textures have been well preserved. No visible sulphide mineralization is observed.

07-33

Composition:

60% Serpentine
15% Olivine
10% Talc
5% Feldspar
5% Clinopyroxene
<5% Quartz
<3% Carbonate
<2% Mica
Trace Pyrite
Trace Magnetite

Sample is composed of cumulate textured serpentine altered peridotite. Serpentine alteration is predominant and fully alters olivine except where relict cores are preserved. Relict igneous textures are well preserved. Altered olivine crystals have magnetite rims and magnetite along cleavage planes. Interstitial to the serpentinised olivine is augite, talc and muscovite altered plagioclase feldspar. Quartz is seen as fine grained quartz eyes as well as a very fine grained component of the interstitial ground mass. A few fine grained sub- to euhedral pyrite grains were observed. Carbonate phases (magnesite) were observed partially replacing serpentine and along grain boundaries.

07-39

Composition:

35% Amphibole
30% Plagioclase feldspar
15% Quartz
15% Chlorite
5% Muscovite
Trace Clinopyroxene
Trace Pyrite
Trace Pyrrhotite

Typical "least altered" Kakagi gabbro. Composed of coarse grained amphibole (hornblende with minor actinolite-tremolite) and albite plagioclase feldspar. Plagioclase forms well defined euhedral laths with interstitial quartz. Amphibole shows alteration to chlorite and feldspar to muscovite both along cleavage planes and grain boundaries. Trace augite is observed interstitial to amphibole grains. Pyrite and pyrrhotite exist as disseminated grains.

07-51

Composition:

40% Plagioclase
25% Mica
25% Chlorite
5% Quartz
3-5% Pyrite
Calcite veinlet

Mafic volcanic rock (basalt) typical of the Snake Bay Formation. Composed chiefly of mica altered plagioclase feldspar. Poorly foliated. Abundant alteration to chlorite. Pyrite is observed is sub- to anhedral blebs up to 1.5 mm across. Calcite vein cross cuts every other phase in the sample. It is composed of coarse grained calcite 50 mm in width and has sharp contacts with little to no wall rock replacement.

07-57

Composition:

70% Amphibole
10% Plagioclase
5% Quartz
8% Chlorite
12% Mica
~3% Talc
2-5% Calcite
3% Epidote

Amphibole is dominantly coarse grained oikocrystic up to 3 mm. Amphibole is composed primarily of hornblende (90 %), with associated actinolite (~ 10%) and possible tremolite (up to 2%). Fine grained plagioclase is observed interstitially between amphibole and shows weak polysynthetic and albite twins. Fine grained groundmass is dominated by anhedral quartz, chlorite, and talc. Calcite is not commonly observed but is found as fine to medium grained crystals within the groundmass. Muscovite is common as very fine grained laths within the groundmass and within feldspar. Observed epidote is clinozoisite and forms small subhedral crystals.

07-58

Composition:

30% Plagioclase feldspar
30% Amphibole
15% Carbonate
15% Chlorite
5% Clinopyroxene
5% Muscovite
0-3% Quartz
Trace Pyrite

Coarse grained gabbro. Plagioclase feldspar form large coarse grained subhedral crystals which have been weakly altered to muscovite along grain boundaries and cleavage planes. Coarse amphibole (hornblende) has been extensively altered to very fine grained carbonate (calcite-ankerite). Chlorite provides a weak foliation. Very little interstitial material exists but does include a small amount of quartz. Pyrite occurs as disseminated fine grained crystals. Clinopyroxene is observed as a few very anhedral crystals.

07-64

Composition:

50% Chlorite altered orthopyroxene
20% Clinopyroxene
10% Muscovite
5% Talc
5% Serpentine
5% Carbonate
3% Quartz
2% Plagioclase feldspar

Coarse grained pyroxenite. Sample is composed of nearly entirely of chlorite altered hypersthene with interstitial augite. The groundmass contains fine grained serpentine with talc. Minor felsic phase have been as very minor interstitial components. The plagioclase feldspar has been replaced by very fine grained muscovite (sericite). Quartz forms fine grained anhedral crystals within the ground mass. Carbonate (ankerite-calcite) is observed replacing along the cleavage of pyroxene. Of note for pyroxenite is the lack of olivine or replaced olivine.

07-65

Composition:

50% Plagioclase feldspar
20% Amphibole
15% Chlorite
10% Muscovite
5% Quartz
Trace Biotite
Trace Pyrite

Very coarse grained gabbro. Well defined highly twinned albite (up to 1.5 cm) with hornblende (1 cm). Sample contains much more feldspar as compared with most samples of gabbro. Minor amounts of interstitial quartz are observed but the groundmass is composed of finer grained plagioclase and chlorite. Muscovite is observed as fine grained inclusions within the feldspar. Unlike most samples this sample contains fine to medium grained biotite proximal though not necessarily associated with amphibole.

O7-68

Composition:

35% Amphibole
20% Plagioclase
20% Chlorite
5% Quartz
5% Muscovite
3% Clinopyroxene
3% Carbonate
2% Epidote
2% Serpentine

Medium to coarse grained gabbro. Amphibole is composed chiefly of actinonlite-tremolite as fibrous mats with well-to-poorly defined cleavage as well as minor amounts of hornblende. Amphibole has been extensively altered to chlorite with minor carbonate. Plagioclase feldspar occurs as anhedral poorly defined laths and blocky crystals. Plagioclase has been altered slightly to muscovite. Interstitially to amphibole feldspar is augite which shows alteration to calcite on grain boundaries and along cleavage up to 5%. The groundmass is comparable to the primary mineralogy except it contains minor amounts of serpentine. Epidote occurs as fine grained subhedral clinozoisite crystals.

07-70

Composition:

30% Amphibole
20% Plagioclase
20% Chlorite (within groundmass and after pyroxene)
15% Muscovite
10% Quartz
5% Carbonate

Typical altered gabbro. Medium grained with abundant chlorite alteration. Chlorite altered pyroxene as phenocrysts and as a main component of the groundmass. Relict igneous textures are well preserved. Plagioclase feldspar has been altered to muscovite, along cleavage and grain boundaries. Quartz is observed interstitial to amphibole and plagioclase as well small inclusions within the groundmass.

07-71

Composition:

35% Plagioclase feldspar
30% Chlorite
20% Amphibole
10% Muscovite
5% Quartz

Coarse grained gabbro. Highly altered to chlorite pervasively along grain boundaries as well as along cleavage planes of both feldspar and hornblende. Muscovite is predominantly observed within the ground mass as well as in inclusions within the feldspars. Quartz is found interstitially along with chlorite.

07-74

Composition:

40% Chlorite altered pyroxene and amphibole
30% Plagioclase
15% Amphibole
10% Muscovite
5% Quartz
Trace Pyrite
Trace Magnetite
Trace Calcite
Trace Epidote
Trace Serpentine

This sample is composed of chlorite altered hornblende, actinolite-tremolite, and pyroxene (augite). Almost all original mineralogy has been replaced, however relict cores and igneous textures survived. Plagioclase, when visible as phenocrysts, is extensively altered to muscovite. The groundmass is composed primarily of serpentine, with chlorite and quartz and plagioclase. There is very slight carbonate alteration rimming some amphibole and plagioclase grains.

07-79

Composition:

60% Chlorite altered amphibole and pyroxene
20% Plagioclase feldspar
10% Muscovite
10% Quartz

Extensively chlorite altered medium to coarse grained gabbro. Almost all of the amphibole (actinolite-tremolite) has been altered to chlorite or is partially altered to chlorite as well as relict fine to medium grained pyroxene (augite). Interstitial and phenocrystic plagioclase display only weak alteration to muscovite along grain boundaries. Muscovite however does make up a significant portion of the ground mass and could reflect plagioclase destruction. Quartz is relatively unaltered and forms interstitial crystals up to 1mm.

07-80

Composistion:

80% Serpentine
10% Pyroxene
10% Amphibole
8% Plagioclase
6% Chlorite
5% Quartz
3% Mica
3% Talc

Sample is composed almost entirely of fine grained mats of serpentine. Relict igneous textures dominate the structure of the sample with relict sub to euhedral pyroxene up to 4 mm, with euhedral olivine up to 2 mm. Serpentine is observed completely replacing olivine and pyroxene though some crystal cores are preserved. Pyroxene, though highly altered, is observed as diopside, augite, and hypersthene. Plagioclase occurs as fine grained laths, often altered to muscovite and calcite. Amphibole is observed replacing pyroxene. Groundmass is composed chiefly of quartz, fine grained plagioclase, mica, talc, serpentine and chlorite.

07-85

Composition:

40% Chlorite
25% Plagioclase
20% Quartz
15% Muscovite
Trace Pyrite

Medium grained chlorite, carbonate and quartz altered basalt. Mafic phases have been extensively altered to chlorite and feldspar phases to mica. Large veinlets (1cm) of quartz are observed cross cutting sample as well as pockets of carbonate alteration in the form of medium subhedral calcite grains. The groundmass has been extensively altered to fine grained chlorite.

07-86

Composition:

60% Plagioclase
30% Quartz
10% Chlorite
Trace Muscovite

Sample of quartz feldspar porphyry dike with large coarse grained well defined plagioclase phenocrysts (up to 2 cm, 25%) within a groundmass of finer grained plagioclase and quartz. The sample has been weakly altered to chlorite with very minor amounts of muscovite. Massive, non foliated.

07-87

Composition:

30% Chlorite
20% Plagioclase
20% Quartz
15% Calcite
10% Muscovite
5% Amphibole

Medium grained chlorite altered mafic flow with breccia. Brecciated fragments are sub rounded to angular and have been extensively altered to chlorite and show moderate deformation. Infilling of calcite is predominant. Primary mineralogy includes quartz, feldspar and amphibole, though mostly they comprise the groundmass. Muscovite is prevalent through most of the sample but not defining a distinct foliation.

07-88

Composition:

25% Plagioclase
20% Amphibole
15% Carbonate
15% Chlorite
15% Quartz
5-10% Muscovite
5% Pyrite

Medium grained altered gabbro. The sample has amphibole (actinolite-tremolite) which has been heavily altered to chlorite and carbonate. Extensive carbonate alteration has overprinted primary textures. Plagioclase feldspar has also been carbonate altered and muscovite altered. Relict igneous textures are visible though the mineralogy is highly altered. Plagioclase feldspars which clearly have formed large phenocrysts are now broken down to much finer components of comparable composition. Local flooding of quartz is commonly observed up to 2 cm, as well as a fine grained component of the groundmass. Pyrite occurs as fine grained anhedral grains.

07-89

Composition:

40% Plagioclase
30% Quartz
20% Chlorite
10% Muscovite

Medium to fine grained crystalline tuff. Well defined coarse plagioclase phenocrysts visible growth zonation within a matrix of finer grained to aphanitic plagioclase and quartz. The sample has been altered to chlorite with much of the feldspar phases being replaced by muscovite.

07-93

Composition:

35% Plagioclase
35% Quartz
20% Chlorite
10% Muscovite
Trace Pyrite

Medium to fine grained tuff. Predominantly composed of an aphanitic groundmass of chlorite altered plagioclase and quartz with abundant muscovite defining a weak to moderate foliation. Some smaller phenocrysts of quartz and plagioclase are observed (<0.5 cm). Some infilling and replacement by calcite is observed. Trace pyrite is fine grained and disseminated.

07-96

Composition:

40% Plagioclase
40% Chlorite
10% Quartz
10% Muscovite

Chlorite altered felsic volcanic tuff. Medium to dark green. Fine grained and strongly foliated. Plagioclase occurs as fine grained laths which have been weakly to moderately altered to muscovite. Chlorite is abundant throughout, and is the major component of the fine grained to aphanitic groundmass.

07-97

Composition:

30% Chlorite
30% Plagioclase
20% Quartz
5% Calcite
5% Muscovite
5% Amphibole
5% Biotite

Sample of medium to fine grained chlorite altered lapilli tuff. Sample weakly muscovite and biotite altered plagioclase feldspar within a ground mass of predominanly chlorite and feldspar. Plagioclase phenocrysts are fine to medium grained and subhedral and unoriented. Lapilli

fragments are strongly deformed (flattened) and show alteration to calcite and biotite. There are no more than 20% lapilli fragments observed.

07-99

Composition:

40% Plagioclase
40% Chlorite
10% Quartz
10% Muscovite
Trace Carbonate

Chlorite altered basalt. Fine to medium grained and weakly foliated. Plagioclase occurs as fine to medium grained laths which have been weakly to moderately altered to muscovite. Chlorite is abundant throughout, and along with plagioclase occurs as a major component of the fine grained to aphanitic groundmass. Quartz is only observed as very fine grained component within the groundmass and carbonate is seen weakly replacing some (<5%) of plagioclase phenocrysts along grain boundaries.

07-112

Composition:

40% Chlorite altered pyroxene
25% Plagioclase feldspar
15% Amphibole
10% Relict pyroxene
5% Muscovite
5% Quartz
Trace Pyrite

Chlorite altered medium to coarse grained gabbro. Sample is composed of plagioclase and augite phenocrysts with in a ground mass of interstitial plagioclase and augite and amphibole. Augite has been extensively altered to chlorite, strongest on grain boundaries and along cleavage, though core of augite and a few weakly altered grains exists (10%). Phenocrystic of plagioclase display only weak alteration muscovite along grain boundaries. Quartz is relatively unaltered and forms interstitial crystals up to 1mm as well as a being a fine grained component of groundmass. Pyrite is disseminated and fine grained.

07-124

Composition:

50% Chlorite altered amphibole and pyroxene
30% Plagioclase (albite)
5% Relict amphibole (hornblende and actinolite/tremolite)
5% Relict pyroxene (augite)
5% Biotite
5% Muscovite
Tr Carbonate
Tr Pyrite

Sample is composed of fine grained gabbro. Phenocrysts of hornblende and actinolite/tremolite, and augite have been extensively altered to fine grained chlorite. Not all amphibole and pyroxene have been completely altered, and relict cores, predominantly of larger grains, are still preserved. Plagioclase forms fine to medium grained anhedral laths (interstitial to mafic phases and well as independent crystals) as well as a large component of the fine grained groundmass. Muscovite occurs as alteration on grain boundaries of plagioclase. Biotite occurs as fine grained needles within the groundmass and rimming some amphibole. Trace fine grained disseminated pyrite. Trace carbonate as calcite or dolomite within the groundmass.

07-131

Composition:

25% Serpentine
25% Hypersthene
20% Augite
10% Amphibole
10% Plagioclase
5% Carbonate
5% Olivine
Trace Pyrite
Trace Magnetite

Moderately altered cumulate textured peridotite. Olivine is almost entirely altered to serpentine and rimmed with magnetite with only relict cores preserved. Igneous textures preserved. Hypersthene occurs as phenocrysts with interstitial augite, both of which have been weakly altered to tremolite/actinolite and carbonate. Trace pyrite as euhedral fine grained crystals.

07-136

Composition:

Plagioclase feldspar: 50%
Muscovite: 20%
Quartz: 20%
Amphibole 5%
Chlortie: Trace
Carbonate: up to 5% locally

Highly altered quartz feldspar porphyry. Predominantley composed of subhedral plagioclase feldspar phenocrysts which have been altered to muscovite along grain boundaries and cleavage. Quartz is observed generally interstitial to plagioclase phenocrysts though also as small fine grained phenocrysts. Amphibole is observed as fine grained tremolite patches and show alteration to chlorite. Slight carbonate alteration observed (5-10%) of mafic phases and carbonate. Trace disseminated pyrite.

07-138

Composition:

45% Plagioclase
40% Chlorite
10% Quartz
5% Muscovite
Trace Carbonate

Sample of chlorite altered basalt composed of plagioclase phenocrysts up to 5 mm within a groundmass of chlorite and plagioclase and quartz. Plagioclase phencocrysts are subhedral and porphyritc and are weakly altered to chlorite on margins and along grain boundaries.

07-139

Composition:

40% Plagioclase
40% Chlorite
10% Quartz
5% Muscovite
5% Carbonate

Sample of chlorite altered felsic to intermediate metavolcanic tuff or possibly flow. Sample contains up to 20% subhedreal randomly oriented phenocrysts of plagioglase but is generally

composed of fine grained to aphanitic chlorite altered plagioclase groundmass. Phenocrysts have been altered to muscovite/sericite along grain boundaries and crystal defects. Quartz forms individual micrograins and the occasional phenocrysts interstitial to plagioclase grains. Locally carbonate is observed within the groundmass or as fine grained inclusions within the larger plagioclase grains.

07-140

Composition:

30% Amphibole
25% Chlorite
18% Plagioclase feldspar
10% Pyroxene
5% Biotite
5% Muscovite
5% Quartz
1-2% Epidote
3-5% Pyrite

Sample of chlorite altered gabbro. Sample composed predominantly of coarse subhedral tremolite which has been strongly altered to chlorite forming fiberous mats along grain boundaries and cleavage. Plagioclase forms large coarse grains which have been weakly altered to muscovite. Small interstitial clinopyroxene forms between plagioclase and tremolite. Epidote alteration along with biotite is noted within the bulk groundmass. Locally there is silicification with associated disseminated pyrite.

76306

Composition:

35% Quartz
30% Carbonate
25% Fuchsite
1% Galena
5% Pyrite
1% Sphalerite
Tr Gold

Quartz and carbonate flooding of brecciated fault zone. Cataclistic fractures with rehealed quartz veins throughout. Carbonate cross cuts all units. Two generations of quartz observed; primary coarse grained vein quartz and secondary overgrowths as well as recrystalised quartz along the margins of other grains. Pyrite forms small blebs and contain trace inclusions of visible gold.

Sphalerite and galena form single small blebs locally. Fuchsite forms mats of greenish alteration throughout.

76302

Composition:

35% Quartz
30% Carbonate
15% Muscovite
2% Talc
2% Pyrite
10% Fuchsite
3% Pyroxene
3% Amphibole

Proximal gabbro hangingwall which has been highly altered to carbonate though primary gabbroic texture is still intact. Amphibole is almost totally altered to carbonate and very minor chlorite. What appears to be pyroxene is altered to chlorite and talc. Feldspars (30%) are totally altered to muscovite and locally fuchsite. Locally pyrite forms disseminated euhedral grains.

76303

Composition:

35% Quartz
40% Carbonate
15% Muscovite
2% Talc
10% Fuchsite

A sample of highly altered wall rock gabbro. Amphibole is totally altered to chlorite and minor carbonate. Augite is totally altered to carbonate. Plagioclase is extensively altered to muscovite and chlorite, but relics of plagioclase are still present.

76307

Composition:

30% Amphibole
20% Plagioclase
20% Chlorite
10% Muscovite
10% Carbonate

Medium grained, massive, relatively fresh and equigranular gabbro. Sample from the distal hangingwall. Amphibole and plagioclase form roughly equal amounts with only minor alteration to carbonate and muscavite. Locally there is trace disseminated pyrite.

76308

Composition:

40% Serpentine
20% Magnesite
5% Fuchsite
5% Plagioclase
10% Pyroxene
5% Quartz
10% Carbonate
5% Talc

Least altered distal footwall peridotite. Composed of weakly to moderately magnesite altered serpentine. Magnesite forms pseudomorphs after serpentine. Serpentine had formed after olivine, maintaing round igneous textures such that these pseudmorphs form small round carbonate eggs. Increased abundance in magnesite alteration is also coeval with increase development in fuchsite formation. All phases are cross cut by stringers and zones alteration fro of Fe-dolomite and ankerite.

Appendix D

Geochemistry Results

Snake Bay Formation

Mafic Metavolcanic Rocks

Sample Id	07-150	07-51	07-96	07-85	07-132	07-57	07-87	07-97
Al_2O_3	4.04	14.38	13.28	3.89	12.82	9.11	11.82	23.08
CaO	4.6	6.92	3.84	9.03	6.35	7.36	9.4	9.54
Fe_2O_3	9.55	16	8.3	4.44	15.72	12.52	16.55	8.78
K_2O	0.06	0.07	0.89	0.04	0.03	0.32	0.56	0.84
LOI	27.01	3.44	5.89	14.32	6.39	4.08	13.53	3.88
MgO	18.72	6.1	1.74	7.57	4.56	19.88	4.51	3.64
MnO	0.19	0.22	0.14	0.08	0.19	0.21	0.29	0.13
Na_2O	1.37	2.89	3.84	0.28	3.15	0.76	1.31	3.94
P_2O_5	0.01	0.16	0.18	0.07	0.19	0.03	0.15	0.08
SiO_2	33.38	48.73	60.81	61.19	49.49	46	40.04	45.89
TiO_2	0.23	1.68	1.57	0.19	1.96	0.34	1.68	0.94
Total	99.16	100.6	100.48	101.1	100.85	100.6	99.84	100.73
Ba	20.6	29.4	160.1	5	32	33.9	108.3	246.8
Be	0.38	0.72	0.65	0.19	0.69	0.16	0.65	0.33
Bi	0.155	0.012	0.015	0.068	0.01	0.009	0.028	
Cd	0.03	0.08	0.04	0.05	0.07	0.08	0.08	0.04
Ce	2.1	17.4	13.8	3.8	19	4.2	13.4	7.9
Co	81.7	40.6	33.5	27	36.9	79.5	54.9	24.4
Cr	>600	154	89	42	67	2232	177	86
Cs	0.092	0.912	0.745	0.163	0.197	3.808	0.931	2.187
Cu	44	60	47	12	88	44	73	45
Dy	0.9	5.5	4.4	0.7	6.5	1.3	5.4	2.3
Er	0.55	3.29	2.55	0.39	3.97	0.87	3.16	1.43
Eu	0.153	1.284	1.009	0.192	1.271	0.299	1.094	0.712
Ga	4.4	19.83	16.26	3.88	19.3	8.04	18.42	20.71
Gd	0.63	4.56	3.86	0.7	5.29	1.02	4.06	1.98
Hf	0.41	2.79	2.6	0.85	3.28	0.64	2.4	1.26
Ho	0.192	1.198	0.929	0.136	1.412	0.3	1.144	0.494
La	0.87	6.86	4.79	1.63	7.51	1.71	5.16	3.05
Li	5.7	16.5	14	11.8	20.4	19.6	41.8	34.1
Lu	0.091	0.547	0.38	0.073	0.627	0.15	0.484	0.226
Mo	0.1	0.42	0.36	0.12	0.25	0.34	0.44	0.18
Nb	0.53	4.88	4.74	0.77	6.05	0.8	4.29	2.15
Nd	1.57	12.75	11.64	2.39	14.37	2.45	9.71	5.46
Ni	564	65	46	72	37	571	114	52
Pb	1.2	3.2	1	1.6	1.4	0.7	2	2.1
Pr	0.32	2.53	2.17	0.53	2.83	0.53	1.95	1.09
Rb	1	2	25.7	0.6	0.7	11	15.2	24.5
Sb	0.23	0.35	0.23	0.32	0.29	0.08	0.63	0.51
Sc	17.8	35.1	33.6	7.1	37.2	31.8	33	17.5
Sm	0.48	3.89	3.31	0.66	4.44	0.75	3.07	1.72
Sn	0.17	1.96	0.95	1.38	1.86	0.29	0.77	0.29
Sr	77	178	66	221	163	21	124	375
Ta		0.4	0.3		0.4		0.3	
Tb	0.122	0.813	0.674	0 11	0.949	0.181	0.774	0.353
Th	0.13	0.65	0.59	0.64	0.78	0.29	0.5	0.28
Ti	1171	7785	7806	881	9631	1515	7804	4246
Tl	0.005	0.024	0.095		0.006	0.094	0.099	0.138
Tm	0.085	0.538	0.387	0.063	0.626	0.145	0.494	0.221
U	0.04	0.16	0.16	0.12	0.19	0.08	0.14	0.07
V	114	289	241	55	297	159	318	177
W	11.1		16.4	22.5	5.3			
Y	5.39	34.42	24.45	3.59	40.68	8.55	33.26	14.54
Yb	0.548	3.403	2.48	0.417	3.995	0.943	3.073	1.413
Zn	51	127	69	61	112	116	146	64
Zr	14	104	93	33	125	22	89	45
$(La/Yb)_{cn}$	1.13830	1.44538	1.38485	2.80266	1.34785	1.30018	1.20394	7.61613
$(La/Sm)_{cn}$	1.17088	1.13922	0.93485	1.59542	1.09267	1.47288	1.08579	2.33224
$(La/Y)_{cn}$	0.96048	1.42002	1.29771	2.69928	1.30911	1.25856	1.13933	6.59640
Nb/Nb*	0.54838	0.67289	1.06319	0.41070	0.76007	0.42852	0.80517	0.19821
Zr/Zr*	1.11645	1.02232	1.03723	1.81897	1.08336	1.12355	1.12848	0.91443
Ti/Ti*	1.15325	1.12619	1.13673	0.69127	1.14123	1.05317	1.10300	0.46252

	Snake Bay Formation		Emm Bay Formation				
	Mafic Metavolcanic Rocks		*Felsic Metavolcanic Rocks*				
Sample Id	**07-99**	**07-142**	**197104**	**197106**	**197107**	**197155**	**197190**
Al_2O_3	12.62	12.94	13.05	14.11	14.44	14.81	13.39
CaO	9.59	4.69	5.72	4.72	4.41	4.83	6.78
Fe_2O_3	17.24	17.05	5.46	5.21	4.97	7.39	9.32
K_2O	0.03	0.09	0.64	0.93	0.95	0.16	0.56
LOI	9.96	4.7	5.69	5.76	5.61	5.76	7.78
MgO	4.39	4.49	2.36	2.61	2.69	5.53	4.16
MnO	0.29	0.19	0.09	0.11	0.11	0.13	0.16
Na_2O	2.01	3.98	4.6	4.74	4.94	4.93	3.54
P_2O_5	0.13	0.22	0.12	0.19	0.2	0.13	0.18
SiO_2	42.03	49.68	60.9	60.72	61.37	56.26	53.52
TiO_2	1.71	2.09	0.7	0.57	0.52	0.44	0.89
Total	100.01	100.11	99.31	99.67	100.2	100.37	100.27
Ba	11	34.5	116.6	299.7	344.5	77.8	197
Be	0.36	0.77	0.61	0.95	1.05	0.81	0.78
Bi	0.028	0.024	<0.009	0.067	0.066	0.097	0.015
Cd	0.06	0.05	0.05	0.08	0.09	0.06	0.08
Ce	27.3	22.4	21.8	46.3	51.8	38.5	39.1
Co	53.7	35.1	20.5	20.6	20.4	34.6	31.3
Cr	136	91	111	110	108	125	95
Cs	0.15	0.614	0.611	1.051	1.174	0.235	0.706
Cu	141	45	38	20	12	14	62
Dy	5.5	6.7	2.3	2.2	2.1	2.7	3.4
Er	3.2	4.04	1.31	1.15	1.11	1.58	1.97
Eu	1.409	1.417	0.879	1.159	1.255	1.022	1.208
Ga	18.6	20.81	12.8	15.98	17.44	18.29	17.54
Gd	5.47	5.8	2.53	3.01	3.19	3.29	3.71
Hf	2.55	3.56	2.16	2.73	2.94	3	2.78
Ho	1.152	1.436	0.454	0.403	0.395	0.539	0.685
La	10.84	8.58	9.56	22.33	25.24	18.19	18.65
Li	22.7	20.5	9.2	11.9	12.8	20.1	16.4
Lu	0.503	0.642	0.19	0.161	0.152	0.238	0.276
Mo	0.22	0.65	0.57	0.37	0.29	0.22	0.38
Nb	4.58	6.78	2.89	3.51	3.48	2.54	3.83
Nd	18.98	16.34	11.8	21.98	24.58	20.3	20.01
Ni	78	38	30	30	34	98	45
Pb	1.4	2.3	1.1	2.4	2.8	1.6	1.9
Pr	3.94	3.28	2.85	5.7	6.28	4.91	4.89
Rb	1.7	1.9	17.7	26.9	28.8	2.9	15.9
Sb	0.09	0.72	0.16	0.22	0.23	0.17	0.18
Sc	30.1	38.3	15.3	14.8	16.3	30.1	23.7
Sm	5.3	4.83	2.63	4.02	4.27	3.95	4.03
Sn	1.15	0.76	0.68	0.76	0.78	0.74	0.96
Sr	35	165	267	262	281	408	179
Ta	0.3	0.4	0.2	0.2	0.2	0.2	0.3
Tb	0.901	1.026	0.38	0.404	0.4	0.458	0.547
Th	0.9	0.85	1.34	3.66	4.13	2.34	2.87
Ti	7454	9665	4281	3685	3479	2699	5693
Tl	0.024	0.012	0.058	0.089	0.102	0.013	0.058
Tm	0.511	0.648	0.189	0.16	0.158	0.232	0.276
U	0.19	0.23	0.31	0.79	0.9	0.52	0.61
V	279	331	122	118	122	116	183
W	4.8	0.5	14.9	11	7.4	6.3	6.2
Y	32.32	41.2	12.57	11.13	10.96	14.92	17.84
Yb	3.248	4.268	1.247	1.053	1.008	1.528	1.83
Zn	220	115	44	53	58	138	82
Zr	88	136	83	107	116	125	104
$(La/Yb)_{cn}$	2.39294	1.11667	5.49681	15.20476	17.95345	8.53549	7.30713
$(La/Sm)_{cn}$	1.32125	0.96182	2.34820	3.58835	3.81851	2.97487	2.98955
$(La/Y)_{cn}$	2.47601	1.16792	5.03782	13.28966	15.25454	8.07577	6.92475
Nb/Nb*	0.39682	0.93550	0.25708	0.12154	0.10553	0.11022	0.16056
Zr/Zr*	0.60741	1.06344	1.03144	0.78802	0.78386	0.96638	0.80175
Ti/Ti*	0.93182	1.14285	0.68822	0.41292	0.35203	0.31292	0.60550

	Emm Bay Formation				Kakagi Sills		
	Felsic Metavolcanic Rocks				*Gabbro*		
Sample Id	**07-93**	**07-139**	**07-141**	**07-89**	**07-112**	**07-124**	**07-28**
Al_2O_3	16.74	17.02	12.1	16.29	16.54	16.02	5.98
CaO	3.95	3.59	5.63	4.17	11.89	9.11	11.94
Fe_2O_3	3.5	3.91	16.73	7.27	10.19	11.48	7.31
K_2O	0.65	1.02	0.02	1.03	0.28	0.28	0.01
LOI	3.8	2.09	7.76	3.6	2.66	3.46	14.42
MgO	2.44	3.3	5.72	4.67	6.71	5.91	12.94
MnO	0.06	0.05	0.15	0.08	0.18	0.22	0.26
Na_2O	6.64	6.9	2.24	4.84	2.2	2.39	0.04
P_2O_5	0.09	0.16	0.19	0.2	0.03	0.04	0.01
SiO_2	61.78	62.8	47.96	58.17	50.25	50.94	47.63
TiO_2	0.45	0.45	1.99	0.55	0.56	0.53	0.21
Total	100.1	101.28	100.5	100.87	101.49	100.38	100.75
Ba	187.7	399.4	8.2	210.6	47.5	85.3	4.1
Be	0.65	0.95	0.78	0.63	0.18	0.25	<0.06
Bi	0.029	0.018	0.019	0.025	0.012	0.021	0.009
Cd	0.03	0.04	0.06	0.05	0.03	0.03	0.03
Ce	13.3	27.8	18.4	27.4	4.8	5.9	2.1
Co	20.4	13.9	35.8	23.5	81.8	312.6	51
Cr	130	64	89	166			>600
Cs	0.66	0.78	0.217	0.927	0.459	0.398	1.064
Cu	4	6	143	4	46	119	4
Dy	1.1	1.6	6.9	2	1.8	1.7	0.7
Er	0.58	0.77	4.22	1.04	1.15	1.08	0.44
Eu	0.54	0.839	1.405	0.853	0.404	0.481	0.135
Ga	17.25	17.02	19.2	19.19	14.15	14.57	5.52
Gd	1.38	2.32	5.59	2.76	1.32	1.36	0.55
Hf	2.19	2.46	3.36	2.45	0.78	0.87	0.31
Ho	0.22	0.292	1.501	0.38	0.402	0.378	0.153
La	6.48	11.96	6.7	11.95	2.08	2.66	1.04
Li	10.2	7.7	31.9	17.4	5.2	11.9	15.2
Lu	0.087	0.121	0.655	0.171	0.186	0.182	0.073
Mo	0.15	0.28	0.77	0.13	0.16	0.34	0.1
Nb	2.1	2.47	6.12	2.77	1.09	1.32	0.34
Nd	6.79	15.52	14.48	16.63	3.43	3.77	1.44
Ni	45	55	31	63	58	50	249
Pb	3.4	1.8	1	2	0.5	0.8	1.3
Pr	1.62	3.54	2.83	3.62	0.72	0.81	0.3
Rb	13.8	22	0.3	27.4	6.1	5.3	1.4
Sb	0.12	0.23	0.44	0.23		0.16	0.2
Sc	9.7	12.1	37.4	20.7	44.1	44.4	25.1
Sm	1.58	3.04	4.5	3.31	1.05	1.08	0.42
Sn	0.54	0.95	0.64	0.56	0.25	0.48	0.1
Sr	492	518	136	375	141	162	26
Ta	0.2	0.2	0.4	0.2	0.2	1	
Tb	0.202	0.293	1.002	0.359	0.249	0.244	0.101
Th	0.99	2.01	0.79	2.4	0.34	0.34	0.13
Ti	2199	2110	9081	2579	2715	2827	1019
Tl	0.062	0.067		0.08	0.024	0.023	0.006
Tm	0.086	0.121	0.674	0.164	0.181	0.172	0.072
U	0.28	0.44	0.25	0.52	0.09	0.09	0.04
V	75	81	314	120	221	234	88
W	46.2		3.7		>120	>120	2.1
Y	6.26	8.63	41.58	11.68	11.3	10.96	4.42
Yb	0.55	0.793	4.302	1.125	1.178	1.12	0.475
Zn	34	21	124	37	48	58	45
Zr	82	99	124	98	27	33	10
$(La/Yb)_{cn}$	8.44756	10.81377	1.11667	7.61613	1.26601	1.70288	1.56985
$(La/Sm)_{cn}$	2.64942	2.54150	0.96182	2.33224	1.27970	1.59107	1.59962
$(La/Y)_{cn}$	6.13193	8.80256	1.16792	6.59640	1.21928	1.60765	1.55859
Nb/Nb*	0.24805	0.17902	0.93550	0.19821	0.45099	0.41048	0.24618
Zr/Zr*	1.73314	0.99778	1.06344	0.91443	0.98493	1.13218	0.89018
Ti/Ti*	0.74946	0.41313	1.14285	0.46252	1.23966	1.17236	1.12397

Kakagi Sills

Gabbro

Sample Id	07-65	07-146	07-162C	07-166	SJ 11-07-1	S4	07-27	07-30
Al_2O_3	14.85	14.98	13.18	12.75	12.6	14.26	12.04	17.7
CaO	13.8	12.06	6.42	7.74	12.65	8.11	7.62	14.56
Fe_2O_3	9.22	11.01	8.99	9.47	8.63	8.49	9.22	6.63
K_2O	0.22	0.18	0.5	0.48	0.14	0.28	0.1	0.18
LOI	2.97	2.5	13.66	7.77	0.76	1.59	4.48	2.25
MgO	9.04	8.49	6.24	10.31	13.53	2.23	16.65	9.1
MnO	0.18	0.18	0.14	0.17	0.17	0.11	0.18	0.13
Na_2O	1.52	1.4	5.2	2.21	0.84	4.3	0.83	1.12
P_2O_5	0.03	0.05	0.11	0.05	0.02	0.05	0.03	0.01
SiO_2	48.55	49.13	44.12	49.18	51.42	59.74	49.52	49.28
TiO_2	0.48	0.73	1.81	0.71	0.25	0.98	0.32	0.23
Total	100.86	100.71	100.37	100.84	101	100.14	100.98	101.18
Ba	67.3	29.5	321	73.9	76.3	23.2	19.5	21
Be	0.18	0.22	1.23	0.43	0.36	0.11	0.12	0.11
Bi	0.041	0.011	0.027	0.012	0.02	0.009	0.01	0.044
Cd	0.04	0.04	0.03	0.03	0.04	0.03	0.05	0.03
Ce	4.3	5.7	29.7	7.8	12	3	3.4	2.5
Co	45.3	50.8	40.3	44.9	27.8	46.3	57.8	34.4
Cr	215	73	29	>600	61	1289	1633	488
Cs	1.14	0.712	0.288	0.547	0.281	0.814	1.185	0.649
Cu	40	50	7	4	8	27	52	21
Dy	1.7	1.9	5.1	2.3	3	1	1	0.9
Er	1.08	1.23	3.04	1.46	2.04	0.63	0.63	0.55
Eu	0.351	0.456	1.502	0.414	0.753	0.212	0.223	0.215
Ga	11.83	13.21	15.68	13.14	15.52	8.99	8.71	11.62
Gd	1.34	1.49	4.51	1.77	2.45	0.69	0.73	0.66
Hf	0.69	0.94	2.14	1.22	2.77	0.39	0.53	0.36
Ho	0.375	0.427	1.1	0.508	0.685	0.218	0.216	0.2
La	1.88	2.45	14.43	3.2	5.5	1.22	1.4	1.04
Li	12.2	6.7	45.3	20.9	2.6	3.2	10.4	6.2
Lu	0.179	0.207	0.449	0.24	0.359	0.109	0.111	0.093
Mo	0.17	0.16	0.38	0.1	0.38	0.18	0.21	0.15
Nb	0.93	1.6	3.74	2.2	1.37	0.43	0.7	0.4
Nd	3.06	3.89	16.16	5.18	7.17	1.77	1.9	1.51
Ni	106	96	152	157	19	156	204	103
Pb	1.2	0.6	5.2	0.6	0.6		0.5	
Pr	0.66	0.82	3.75	1.1	1.51	0.38	0.41	0.32
Rb	3.9	2.8	7.9	8.1	5.7	3.4	2.2	3.1
Sb	0.18	0.06	0.87	0.11	0.07		0.55	0.08
Sc	49.3	43.3	43.3	42.8	31.6	45.7	37	40.1
Sm	0.98	1.21	3.92	1.47	1.98	0.55	0.56	0.51
Sn	0.57	0.38	1.72	0.57	0.28	0.12	0.17	0.12
Sr	103	81	300	57	312	69	45	122
Ta			0.2	0.2				
Tb	0.241	0.277	0.746	0.323	0.457	0.137	0.132	0.123
Th	0.24	0.27	0.92	0.64	1.52	0.39	0.24	0.13
Ti	2416	3663	8757	3901	4567	1174	1420	1027
Tl	0.019	0.016	0.033	0.029	0.027	0.018	0.013	0.013
Tm	0.172	0.194	0.482	0.244	0.323	0.105	0.104	0.093
U	0.08	0.09	0.99	0.14	0.41	0.05	0.08	0.04
V	207	234	471	229	99	161	145	126
W	7.9	31.7	6.1	9.5				
Y	10.79	12.06	29.87	14.54	20.74	6.38	6.2	5.82
Yb	1.112	1.277	2.94	1.53	2.186	0.689	0.704	0.59
Zn	51	54	61	50	29	50	49	36
Zr	24	33	81	45	99	13	18	13
$(La/Yb)_{cn}$	1.21219	1.37561	3.51915	1.49961	1.80398	1.26958	1.42585	1.26386
$(La/Sm)_{cn}$	1.23927	1.30802	2.37801	1.40626	1.79444	1.43295	1.61500	1.31733
$(La/Y)_{cn}$	1.15414	1.34567	3.20001	1.45783	1.75661	1.26666	1.49574	1.18367
Nb/Nb*	0.42195	0.56662	0.19894	0.62495	0.20268	0.32322	0.45284	0.34479
Zr/Zr*	0.95945	1.05300	0.70454	1.12894	1.81897	0.91213	1.20805	1.02554
Ti/Ti*	1.08762	1.44233	1.13512	1.15277	0.29169	4.12380	1.29982	0.99613

Kakagi Sills

Gabbro

Sample Id	07-32	07-39	07-58	07-66	07-68	07-70	07-74	07-79
Al_2O_3	15.29	15.94	7.7	13.98	14.5	14.33	12.9	7.52
CaO	13.52	13.53	7.93	10.45	11.57	13.14	7.05	8.83
Fe_2O_3	7.55	8.13	12.23	113 4	10.34	9.07	11.26	9.48
K_2O	0.07	0.11	0.13	0.17	0.06	0.3	0.11	0.05
LOI	4.5	2.95	2.51	4.97	3.12	3.52	4.42	5 35
MgO	10.36	9.7	20.94	6.28	10.13	9.7	14.38	18.33
MnO	0.16	0.16	0.2	0.18	0.19	0.18	0.19	0.19
Na_2O	1.32	1.08	0.44	1.28	1.41	0.58	1.98	0.6
P_2O_5	0.01	0.02	0.02	0.06	0.02	0.02	0.01	0.02
SiO_2	47.73	49.06	48.74	51.24	49.37	49.65	48.5	50.03
TiO_2	0.24	0.31	0.29	0.7	0.39	0.35	0.22	0.31
Total	100.75	101	101.14	100.65	101.12	100.84	101.02	100.7
Ba	11.5	17.6	18.3	32.8	15	26.9	41.8	5,3
Be	0.12	0.13	0.11	0.3	0.17	0.15	0.15	0.16
Bi	0.042	0.015		0.011	0.03	0.031	0.021	0.04
Cd	0.02	0.04	0.04	0.02	0.03	0.04	0.03	0.04
Ce	2.4	3.4	2.7	7.8	3.7	3.6	2.2	2.2
Co	41.9	41	80.8	35.9	46.4	44.6	62.2	56.7
Cr	743	995	1784	82	94	137	1074	1618
Cs	0.266	0.718	0.361	0.305	0.961	0.448	1.247	0.799
Cu	38	40	37	6	16	42	39	15
Dy	0.9	1.2	0.9	2.5	1.5	1.3	0.7	1
Er	0.64	0.74	0.62	1.55	0.9	0.82	0.46	0.65
Eu	0.226	0.264	0.188	0.501	0.322	0.279	0.517	0.172
Ga	10.8	11.44	6.62	13.38	11.33	11.09	9.07	6.3
Gd	0.69	0.87	0.66	1.94	1.08	0.96	0.46	0.72
Hf	0.58	0.51	0.38	1.23	0.58	0.48	0.26	0.42
Ho	0.223	0.262	0.211	0.546	0.336	0.281	0.157	0.235
La	0.99	1.46	1.03	3.2	1.52	1.36	0.83	0.7
Li	9	14.2	2.4	17.8	9.7	8.3	16.6	15.6
Lu	0.104	0.128	0.103	0.257	0.152	0.136	0.081	0.106
Mo	0.15	0.22	0.18	0.41	0.2	0.38	0.21	0.2
Nb	0.33	0.67	0.56	1.76	0.67	0.65	0.29	0.51
Nd	1.52	2.16	1.6	5.05	2.49	2.21	1.17	1.42
Ni	129	135	435	68	98	102	164	254
Pb		0.6	0.5	3.2	0.4	0.7	0.5	
Pr	0.34	0.46	0.35	1.04	0.5	0.47	0.26	0.29
Rb	0.8	1.5	3.7	3.9	1.1	7.9	3	1
Sb	0.13	0.09	0.04	0.35	0.07	0.35	0.24	0.34
Sc	47.3	43.1	34.8	44	55.4	49	41.2	41.8
Sm	0.54	0.65	0.54	1.51	0.81	0.74	0.35	0.53
Sn	0.12	0.17	0.12	0.27	0.19	0.19	0.08	0.15
Sr	95	79	56	212	111	96	63	18
Ta								
Tb	0.128	0.167	0.121	0.342	0.197	0.175	0.093	0.141
Th	0.11	0.21	0.12	0.45	0.23	0.21	0.09	0.17
Ti	1093	1528	1221	3163	1685	1566	889	1302
Tl	0.005	0.009	0.022	0.026	0.006	0.04	0.022	0.01
Tm	0.1	0.127	0.096	0.246	0.149	0.13	0.076	0.112
U	0.03	0.06	0.04	0.13	0.06	0.06	0.03	0.05
V	161	181	143	274	210	184	149	162
W								
Y	6.24	7.72	5.95	15.38	9.21	8.27	4.49	6.7
Yb	0.652	0.808	0.65	1.613	0.95	0.867	0.535	0.696
Zn	36	45	63	45	51	45	54	51
Zr	23	18	13	42	19	18	9	15
$(La/Yb)_{cn}$	1.08870	1.29557	1.13617	1.42244	1.14720	1.12471	1.11236	0.72112
$(La/Sm)_{cn}$	1.18433	1.45102	1.23219	1.36901	1.21225	1.18724	1.53194	0.85321
$(La/Y)_{cn}$	1.05092	1.25273	1.14668	1.37821	1.09321	1.08932	1.22448	0.69206
Nb/Nb*	0.30136	0.39854	0.53150	0.49996	0.40014	0.47181	0.34537	0.85393
Zr/Zr*	1.75749	1 05165	0.96821	1.05293	0.92618	0.97441	0.97364	1.19699
Ti/Ti*	1.00457	1.05590	1.30081	1.09356	1.09385	1.07729	1.45743	1.31255

	Kakagi Sills	Kakagi Sills					
	Gabbro	*Ultramafic*					
Sample Id	**07-140**	**07-128**	**07-147**	**07-64**	**07-80**	**07-154**	**07-155**
Al_2O_3	12.83	9.16	8.84	9.23	5.74	6.39	5.33
CaO	10.39	6.53	10.59	6.13	4.26	1.88	5.03
Fe_2O_3	17.68	12.11	10.85	12.48	14.94	12.05	12.7
K_2O	0.12	0.15	0.08	0.07	0.07	0.05	0.07
LOI	2.05	5	1.64	6.49	7.29	8.35	12.34
MgO	4.12	19.97	16.89	17.42	25.75	25.32	24.68
MnO	0.21	0.22	0.21	0.17	0.17	0.14	0.28
Na_2O	2.3	0.84	0.58	0.39	0.18	0.13	0.1
P_2O_5	0.07	0.04	0.01	0.01	0.03	0.03	0.02
SiO_2	49.23	45.31	51.03	47.44	41.85	45.44	39.87
TiO_2	2 02	0.39	0.25	0.25	0.29	0.3	0.23
Total	101.00	99.72	100.97	100.08	100.58	100.07	100.64
Ba	37.7	41.8	9	6.4	8.3	5.2	8
Be	0.43	0,17	0.07	0.11	0.13	0.15	0.14
Bi		0.033	0.057	0.01	0.034		0.014
Cd	0.02	0.07	0.04	0.03	0.03	0.05	0.05
Ce	8.4	4.5	1.8	1.5	3.4	2.6	3.1
Co	51.1	88.1	66.1	89.6	117	97	99
Cr	67	>600	>600	>600	1935	3251	2532
Cs	0.314	1.273	0.746	1.991	1 098	0.853	3.542
Cu	7	63	26	58	54	9	34
Dy	2.9	1.5	0.9	0.7	1	0.7	0.9
Er	1.81	1.03	0.6	0.52	0.6	0.46	0.66
Eu	0.763	0.402	0.189	0.186	0.179	0.083	0.137
Ga	17.57	8.2	6.87	7.37	5.74	6.45	5.36
Gd	2.39	1.19	0.67	0.52	0.73	0.54	0.69
Hf	1.31	0.73	0.34	0.26	0.43	0.5	0.39
Ho	0.649	0.356	0.211	0.177	0.211	0.152	0.218
La	3.33	1.95	0.81	0.66	1.35	1.1	1.29
Li	5.9	25.5	4.2	13.8	0.8	3.7	11.4
Lu	0.312	0.173	0.101	0.099	0.097	0.088	0.114
Mo	0.28	0.16	0.15	0.1	0.18	0.11	0.12
Nb	2.16	0.91	0.33	0.31	0.55	0.68	0.49
Nd	6.13	2.92	1.43	1.19	2.08	1.49	1.84
Ni	12	667	236	545	718	851	697
Pb	0.4	1.9	0.5	0.6	1		1.6
Pr	1.19	0.62	0.28	0.23	0.42	0.32	0.39
Rb	1.6	3.1	2.5	2.5	2.6	3	3.8
Sb	0.11	0.1	0.07	0.75	0.15	0.17	0.11
Sc	60.5	34.1	48.1	40.2	23.4	24.4	26.7
Sm	1.88	0.88	0.49	0.38	0.6	0.44	0.52
Sn	0.27	0.31	0.12	0.14	0.16	0.17	0.15
Sr	112	24	42	24	6	19	78
Ta							
Tb	0.405	0.219	0.129	0.104	0.136	0.101	0.134
Th	0.7	0.33	0.11	<0.09	0.2	0.24	0.19
Ti	9252	2026	1262	1256	1225	1287	981
Tl	0.016	0.02	0.021	0.018	0.032	0.021	0.048
Tm	0.292	0.165	0.093	0.09	0.093	0.077	0.106
U	0.17	0.09	0.03	0.02	0.05	0.06	0.06
V	389	169	161	139	132	146	113
W		4.8	6.3	1.6			
Y	18.87	10.03	5.85	5 01	5.87	4.33	6.12
Yb	1.983	1.042	0.607	0.567	0.625	0.532	0.722
Zn	51	109	57	67	74	67	68
Zr	45	26	11	9	15	17	13
$(La/Yb)_{cn}$	1.20404	1.34179	0.95679	0.83460	1.54872	1.48252	1.28107
$(La/Sm)_{cn}$	1.14424	1.43148	1.06788	1.12200	1.45350	1.61500	1.60258
$(La/Y)_{cn}$	1.16894	1.28782	0.91717	0.87262	1.52341	1.68277	1.39624
Nb/Nb*	0.61020	0.40162	0.33763	0.39810	0.38265	0.54491	0.34041
Zr/Zr*	0.91767	1.12285	0.90972	0.92653	0.92954	1.45349	0.92006
Ti/Ti*	2.72453	1.03953	1.15082	1 53821	1.23073	1.67946	1.05699

	Kakagi Sills	Intrusive Rocks		
	Ultramafic	*Feldspar Porphyry Dike*		
Sample Id	**07-156**	**07-86**	**07-136**	**07-135**
Al_2O_3	6.39	16.13	15.95	15.14
CaO	4.46	1.17	2.23	2.52
Fe_2O_3	15	3.46	3.46	2.24
K_2O	0.05	0.27	2.8	2.12
LOI	9.22	1.99	4.05	2.79
MgO	24.63	1.62	1.15	0.77
MnO	0.19	0.02	0.05	0.03
Na_2O	0.21	8.3	5.14	5.99
P_2O_5	0.02	0.26	0.27	0.1
SiO_2	39.68	67.32	65.35	66.53
TiO_2	0.23	0.53	0.53	0.32
Total	100.09	101.07	100.98	98.55
Ba	17	916.9	851.7	877.2
Be	0.14	1.06	2	1.77
Bi		0.079	0.133	0.165
Cd	0.06	0.04	0.07	0.06
Ce	3	135.6	133.4	52.1
Co	115.5	15	11.3	5.1
Cr	3043			38
Cs	2.503	0.417	4.118	2.786
Cu	7	3	15	10
Dy	1.2	2	2.1	1.2
Er	0.82	0.73	0.76	0.51
Eu	0.189	1.929	2	0.908
Ga	7.34	21.53	21.65	20.9
Gd	0.84	5.18	5.31	2.28
Hf	0.33	4.25	4.15	3.26
Ho	0.286	0.323	0.331	0.201
La	1.31	66.67	65.75	27.36
Li	12.2	7.1	6.2	6.1
Lu	0.126	0.096	0.1	0.069
Mo	0.27	0.07	0.12	0.11
Nb	0.51	5.09	5.07	4.49
Nd	1.86	57.17	58.23	22.62
Ni	934	16	16	12
Pb	1	4.5	7.3	5.5
Pr	0.39	15.51	15.48	5.91
Rb	2 1	7.5	90	72.9
Sb	0.2	0.42	0.23	0.17
Sc	23.8	4.3	5	3.4
Sm	0.63	8.47	8.37	3.56
Sn	0.23	0.99	0.98	0.74
Sr	39	310	352	262
Ta		0.4	0.4	0.3
Tb	0.17	0.575	0.57	0.281
Th	0.17	12.01	12.66	6.44
Ti	945	2823	2807	1532
Tl	0.026	0.041	0.613	0.376
Tm	0.127	0.106	0.106	0.077
U	0.08	2.18	2.98	2.2
V	121	49	49	31
W		36.5	18.5	
Y	8.35	9.34	10.04	6.39
Yb	0.833	0.642	0.689	0.478
Zn	90	23	66	44
Zr	13	164	167	129
$(La/Yb)_{cn}$	1.12758	74.45855	68.42199	41.04000
$(La/Sm)_{cn}$	1.34327	5.08487	5.07461	4.96476
$(La/Y)_{cn}$	1.03921	47.28288	43.37928	28.36192
Nb/Nb*	0.33249	0.05791	0.05834	0.11654
Zr/Zr*	0.83138	0.51594	0.52368	0.99518
Ti/Ti*	0.89763	0.19460	0.19368	0.27685

The West Cedartree Gold Project
Kenora Mining District, Ontario

Houston Lake Mining Inc.
and Lakehead University

By: Scott Secord
And:

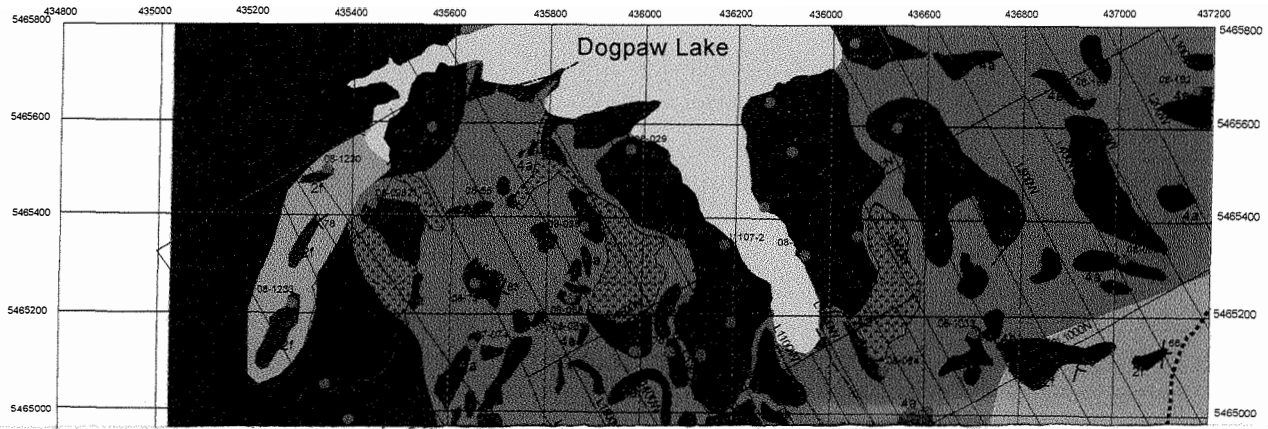

Vertical Exageration: 6.6:1